SEISMIC ANISOTROPY AND MANTLE DEFORMATION: WHAT HAVE WE LEARNED FROM SHEAR WAVE SPLITTING?

M. K. Savage[1]
Institute of Geophysics
Victoria University of Wellington
New Zealand

Abstract. Shear wave splitting measurements now allow us to examine deformation in the lithosphere and upper asthenosphere with lateral resolution <50 km. In an anisotropic medium, one component of a shear wave travels faster than the orthogonal component. The difference in speed causes the waves to separate; this phenomenon is called shear wave splitting. The polarization of the fast component and the time delay between the components provide simple measurements to characterize the anisotropy. Strain aligns highly anisotropic olivine crystals in the mantle, which is the most likely cause of splitting measured from records of distant earthquakes. The seismic community is in the fundamental stages of determining the relations between strain and anisotropy, measuring anisotropy around the world, and determining how much is formed by past and present lithospheric deformation and how much is formed by crustal and asthenospheric sources. The mantle appears isotropic between 600 km depth and the D″ layer at the top of the core-mantle boundary. Shear wave anisotropy of up to 4% is ubiquitous in the upper 200 km of the crust and mantle. Evidence for stronger and deeper anisotropy is less common. Anisotropy in the transition zone between 400 and 600 km and in the D″ layer may be patchy. Transcurrent deformation at plate boundaries appears to be one of the best mechanisms for causing splitting on nearly vertically traveling waves by aligning foliation planes and the fast axes of olivine within the lithosphere parallel to the boundary and in the most favorable orientation for splitting. Similar deformation may also contribute to anisotropy observed at convergent margins. Shear wave splitting data are challenging conventional beliefs about mantle flow. Simple models of asthenosphere diverging at spreading centers and flowing downward beneath subduction zones appear to be only part of the story, with significant components of flow parallel to ridges and trenches. Parallelism between fast polarizations of waves passing through the deep mantle beneath cratons and surficial geological strain indicators has been used to suggest that the mantle at depths of several hundred kilometers beneath the cratons may have been stable since the initial deformation in the Archean. New paths of investigation include testing a wider range of anisotropic symmetry systems and more complicated models by examining variations in splitting as a function of earthquake arrival angle and distance and by numerical modeling of waveforms and of proposed deformation scenarios.

1. INTRODUCTION

Within the last 10 years a proliferation of measurements of *shear wave splitting* from teleseismic phases has allowed us to map seismic anisotropy in the mantle. Seismic anisotropy occurs when elastic waves vibrating or traveling in one direction travel faster than another. When shear waves travel in an anisotropic medium, the component polarized parallel to the *fast direction* begins to lead the orthogonal component (Figure 1). This phenomenon, termed "shear wave splitting," is a seismological analog to optical *birefringence*. Routine measurements of shear wave splitting yield high-lateral-resolution estimates of the *polarization* of the fast wave (ϕ) and of the *delay time* (δt) between fast and slow waves. Mantle anisotropy is believed to result from strain-induced, preferred orientation of mantle minerals (mainly olivine), and thus shear wave splitting measurements can characterize the orientation and depth extent of mantle strain fields. This allows us, for the first time, to examine the structural geology within the mantle. The seismic community is in the initial stages of determining the relation between strain and anisotropy and of mapping the strain and determining how much of it is caused by past and present lithospheric deformation and how much of it is caused by crustal, asthenospheric, and lower mantle sources.

All materials are anisotropic, and the line between

[1]Also at Seismological Laboratory, University of Nevada, Reno.

Reviews of Geophysics, 37, 1 / *February 1999*
pages 65–106
8755-1209/99/98RG-02075$15.00
Paper number 98RG02075

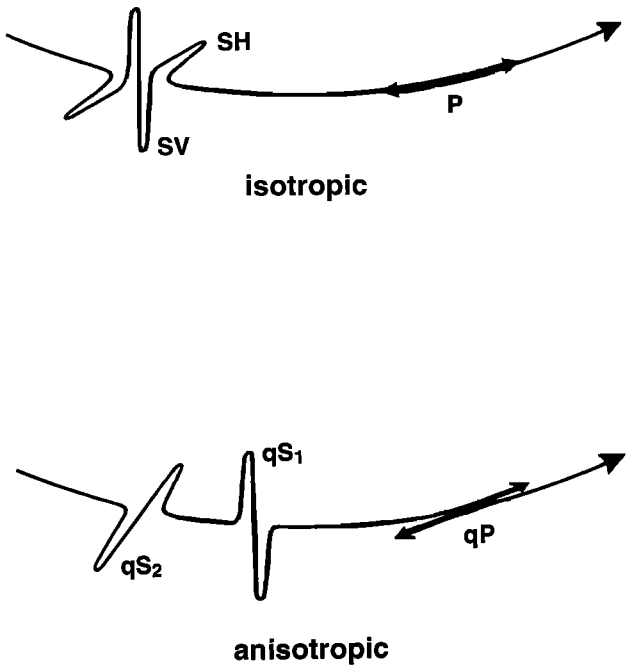

Figure 1. Schematic comparison of isotropic and anisotropic wave propagation, in three dimensions. Isotropic propagation has linear *P* wave particle motion parallel to the propagation direction and *S* wave particle motion perpendicular to propagation, with two components arbitrarily defined as oriented horizontally (*SH*) and in the vertical plane (*SV*). Anisotropic propagation has a quasi-*P* wave with linear particle motion that is not quite parallel to the propagation direction, and two quasi-*S* waves (qS_1 and qS_2) with polarizations parallel and perpendicular to the fast direction for the propagation direction in question. The quasi-*S* waves are separated by a time δt. See the appendix for a detailed explanation of the terms.

anisotropy and isotropy is one of the resolution of available instrumentation. Theoretical study of anisotropy preceded observations for many years because instrumentation was inadequate. Theoretical wave propagation in anisotropic media was first investigated in connection with light. Because light was originally thought to propagate through an elastic ether, there was no difference between the study of light and seismic waves. The study of seismic anisotropy began with a long theoretical treatise by *Christoffel* [1877] and was further advanced by *Lord Kelvin* [1904] in his Baltimore lectures and by *Love* [1944]. In the 1950s, when experiments with ultrasonic waves began in earnest, rapid progress was made by physicists and theoretical seismologists. *Musgrave* [1959] provided a review of the theory and showed some of the practical applications to experimental studies of crystals. Seismologists realized that rocks have fabric and orientations that are obviously anisotropic; much of the field of structural geology is devoted to studying orientations of crystal fabric. Yet despite the strides in theoretical and laboratory studies and the knowledge of preferred mineral fabric orientations, observational seismologists were able to explain all their field data with isotropic mantle models until the early 1960s.

Radial anisotropy (the appendix and the glossary) explained discrepancies in velocities determined for *Love waves* and *Rayleigh waves* [*Anderson*, 1961]. The early observations of *azimuthal anisotropy* were based on variations of velocity from *Pn* refraction data and were limited to characterizing upper mantle anisotropy [e.g., *Hess*, 1964] (Figure 2). Analyses of *surface waves* that travel across the Pacific [*Forsyth*, 1975] are also consistent with azimuthal anisotropy in the upper mantle [*Smith and Dahlen*, 1973]. Once the existence of crustal anisotropy due to cracks was realized and found to characterize fracture alignments within the crust [e.g., *Christensen*, 1966a, b; *Nur and Simmons*, 1969; *Crampin*, 1977, 1981], the field was concentrated on crustal anisotropy. Several reviews of crustal anisotropy are available [e.g., *Crampin*, 1977, 1981, 1994; *Garmany*, 1989; *Helbig*, 1993]. The advent of numerous broadband seismometers and the use of portable seismometers to study shear wave splitting in *S* and *SKS* phases has brought

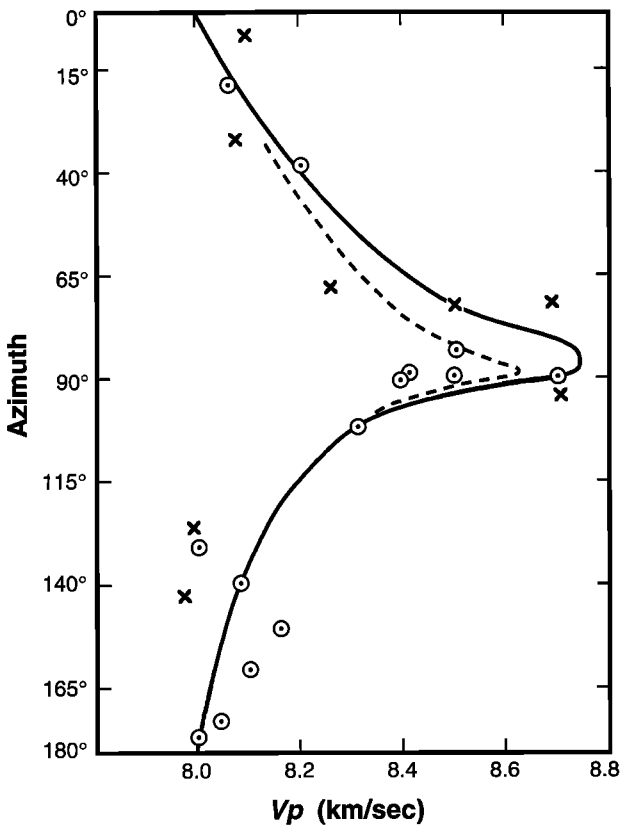

Figure 2. Variation of seismic V_p velocity with azimuth for refraction surveys near the Mendocino fracture zone area off California. The E-W fast direction parallels the fracture zones in the region and was the first evidence that olivine *a* axes may align parallel to spreading. Circles, Mendocino area; crosses, Maui area; dashed curve, model for Mendocino; solid curve, model for both areas combined. (Reprinted with permission from *Nature* Copyright 1964 Macmillan Magazines Limited.) [*Hess*, 1964].

mantle anisotropy to the fore again; *Silver* [1996] provides a review of results from *SKS* phases received at continental stations. While seismologists studying the crust can usually ignore mantle anisotropy, the fact that seismic recorders are based on the surface means that crustal anisotropy must always be considered in mantle studies. Thus, while this paper concentrates mainly on mantle anisotropy, crustal anisotropy must be considered as a possible contaminant of the signal.

Most results published to date have been interpreted with a classical anisotropic layer approach to interpreting shear wave splitting results. Other approaches such as including slowly varying anisotropy, dipping layers, lateral variations in anisotropy, and possible frequency-dependent anisotropy have the potential to change some of the interpretations derived from these studies.

2. INTERPRETING SHEAR WAVE SPLITTING MEASUREMENTS

Anisotropy causes shear wave splitting, and shear wave splitting measurements are now reasonably routine. Interpreting the splitting parameters in terms of tectonic processes is still controversial. The appendix contains a tutorial on *S* wave splitting and on the main causes of anisotropy. It shows that the major cause of shear wave splitting of teleseismic phases such as *S* and *SKS* is probably the preferred orientation of mantle minerals, primarily olivine. The fast polarization ϕ tends to align parallel to the olivine *a* axes, and mantle xenoliths yield *percent anisotropy* of up to 7%. Here we discuss the deformation mechanisms thought to be causing the preferred orientation and the tectonic processes postulated to control anisotropy in the mantle. Further detail and historical references are given by *Babuška and Cara* [1991].

2.1. Relation Between Anisotropy and Deformation

Rocks deform by a wide variety of mechanisms, depending on mineral type and conditions of deformation. Deformation is often complicated by recrystallization occurring simultaneously. Two deformation types are important in upper mantle conditions; *diffusion creep* and *dislocation creep*. Diffusion creep is solid-state diffusion between grain boundaries or across a crystal lattice [e.g., *Nicolas*, 1984; *Karato and Wu*, 1993]. Preferred mineral orientation is not developed, and thus the deformed material is isotropic [e.g., *Karato and Wu*, 1993]. Diffusion creep occurs at relatively low stress, small grain size, or both; the strain rate increases linearly with stress but decreases significantly with grain size [e.g., *Karato and Wu*, 1993]. Dislocation creep is the motion of crystalline dislocations within grains; it causes preferred mineral orientation and therefore anisotropy [e.g., *Nicolas and Christensen*, 1987; *Karato*, 1987; *Karato and Wu*, 1993]. It occurs with high stress, large grain size, or both; the strain rate increases nonlinearly with stress and is insensitive to grain size [e.g., *Karato and Wu*, 1993].

Anisotropic fabric depends on both the type and extent (or history) of strain. For example, theoretical models predict different fabric develops for simple shear, pure shear, and axial compression [*Wenk et al.*, 1991]. Both theoretical [*Ribe and Yu*, 1991; *Wenk and Christie*, 1991] and experimental studies [*Nicolas et al.*, 1973; *Mainprice and Nicolas*, 1989; *Zhang and Karato*, 1995] suggest that mineral preferred orientation in the mantle forms in polycrystalline aggregates due to alignment of slip planes and directions with the shear plane and direction, respectively, during progressive rotational deformation. In addition, for large strains, dynamic recrystallization via subgrain rotation enhances effects of the deformation [e.g., *Zhang and Karato*, 1995]. For large (>150%) strain by progressive simple shear, experimental and theoretical studies suggest that olivine *a* axes align within the foliation plane, nearly parallel to the lineation direction and parallel to [*Ribe*, 1989; *Zhang and Karato*, 1995] or within 30° of [*Wenk et al.*, 1991] the direction of ductile shear (Figure 3). However, measurements of anisotropy in olivine crystals deformed in simple shear suggest that small strains orient olivine *a* axes parallel to the minimum principal stress, at about 45° to the flow plane [e.g., *Zhang and Karato*, 1995]. Thus the relation between strain and mineral preferred orientation is complicated, and maximum strain is expected to align parallel to asthenospheric flow only for large strain by progressive simple shear [*Ribe*, 1989; *Wenk et al.*, 1989].

Other forms of deformation may yield different anisotropic properties. Uniaxial compression tends to orient the slip plane normal to the compression axis [e.g., *Ida*, 1984]. For more general strain in olivine aggregates, the *a*, *b*, and *c* axes tend to align with the extension, compression, and intermediate axes of the strain ellipse, respectively [*McKenzie*, 1979; *Ribe and Yu*, 1991; *Ribe*, 1992]. Many natural mantle samples, from kimberlite nodules, Alpine massifs, ophiolites, or xenoliths such as basaltic nodules from oceanic islands, have a basic similarity: the olivine *a* axis concentrations are within the foliation plane and parallel to the lineation direction [*Christensen and Salisbury*, 1979; *Toriumi*, 1984; *Mainprice and Silver*, 1993; *Kern*, 1993a, b; *Ji et al.*, 1994] (Figure 3). Olivine *b* axes and *c* axes are more variable: sometimes the *b* axes form a single-point maximum approximately perpendicular to the foliation plane, forming orthorhombic symmetry, whereas at other times the *b* and *c* axes form a complete girdle approximately normal to the lineation, causing *hexagonal symmetry* with the *a* axis concentrations as the (fast) axis of symmetry. However, axially deformed specimens of ultramafic rock sometimes have olivine oriented with *b* axes normal to foliation and *a* and *c* axes forming a girdle in the foliation plane. This causes hexagonal symmetry with the slow axis of symmetry in the direction of *b* axis concentration [*Christensen and Crosson*, 1968]. Some rock sam-

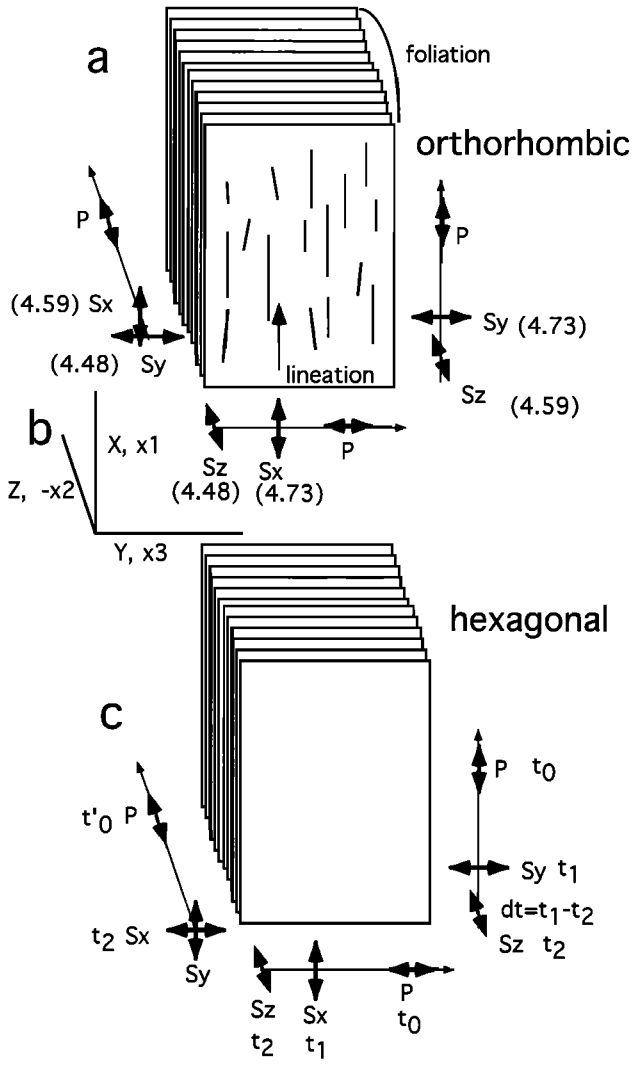

Figure 3. Definitions of foliation and lineation and *S* wave splitting in orthorhombic and hexagonal media. (a) Schematic examples of splitting for propagation in three orthogonal directions in an orthorhombic medium. *S* wave speeds in kilometers per second in parentheses are for the mantle xenolith defined by the elasticity tensor given in section A3 (the appendix explains the meaning of the elasticity tensor). (b) The *X*, *Y*, *Z* coordinate system used in most literature is shown, with the lineation direction often defined as the lineup of olivine *a* axes. The $x1$, $x2$, and $x3$ coordinate system described in the appendix is given by *X*, $-Z$, and *Y*, respectively. (c) Schematic splitting for propagation in a hexagonal medium.

ples exhibit this symmetry (e.g., lherzolitic xenolith from France [*Kern*, 1993a]). Such rocks yield maximum splitting for *S* waves propagating at 45° to the lineation within the foliation plane, and the maximum *S* wave velocity and splitting are not parallel to the maximum *P* wave velocity [*Kern*, 1993a] (Figure 4a, 45°).

In summary, the popular conception that ϕ from splitting is parallel to olivine *a* axis orientations and subparallel to the horizontal flow direction or to the extension direction in the upper mantle and that for simple shear and large strains the maximum extension is approximately parallel to shear [e.g., *Silver and Chan*, 1991; *Nicolas*, 1993] appears to be valid for many, but not all, cases.

2.2. Factors Affecting Anisotropy

2.2.1. Temperature and pressure. Laboratory measurements of mantle xenoliths exhibit only a slight increase in V_S anisotropy for isothermal conditions (20°C) with pressure from 200 to 600 MPa, and only a slight decrease in V_S anisotropy for isobaric conditions (600 MPa) with temperature between 100°C and 600°C [*Kern*, 1993a]. However, higher temperatures and pressures affect preferred orientation. At high temperatures, diffusion and grain boundary mobility help to select favorably oriented grains and enhance preferred orientation [*Mainprice and Nicolas*, 1989]. Below a critical temperature of 900°C, deformed olivine crystals may not easily be reoriented [e.g., *Goetze and Kohlstedt*, 1973; *Estey and Douglas*, 1986]. Thus regions deformed at temperatures above 900°C and then cooled below 900°C may be considered to have their anisotropy "frozen in" from a past tectonic episode [*Silver and Chan*, 1988; *Vinnik et al.*, 1992]. For example, shallow regions may only reflect current deformation in hot areas such as rifts, while in other areas, shallow anisotropy evidences past deformation and only regions deeper than about 200 km may reflect current deformation [e.g., *Ishikawa*, 1984]. However, current deformation in regions deeper than 200 km may be isotropic if they deform by diffusion creep [*Karato*, 1992].

2.2.2. Partial melt. Partial melt might prevent the formation of preferred orientation by promoting a transition from dislocation creep to diffusion creep [*Cooper and Kohlstedt*, 1986; *Dell'Angelo and Tullis*, 1988] or by causing embrittlement [*Van der Molen and Paterson*, 1979; *Davidson et al.*, 1994]. Alternatively, because the presence of melt increases the efficiency of mineral preferred orientation, it may increase the grain size and therefore increase splitting by increasing alignment or by increasing the depth interval over which dislocation creep predominates [e.g., *Nicolas*, 1992; *McNamara et al.*, 1994; *Hirn et al.*, 1995]. Stress-controlled, melt-filled fractures might explain splitting measurements in the asthenosphere [e.g., *Ando et al.*, 1983; *Kendall*, 1994; *Ji et al.*, 1994; *Blackman and Kendall*, 1997] (the appendix, section A6).

2.2.3. Strain history. Minerals cannot reorient instantaneously, and the preferred orientation is a complicated function of the strain history, depending on how the response varies with time and with the amount of strain, in addition to other factors such as temperature, strain rate, and initial conditions [e.g., *Ribe*, 1989, 1992; *Ribe and Yu*, 1991; *Wenk and Christie*, 1991]. Experimental results are conclusive that increasing axial strain in uniaxial shortening of up to about 60% yields increasingly highly oriented fabric in dunite [e.g., *Nicolas et al.*, 1973; *Mainprice and Silver*, 1993]. Numerical simulation

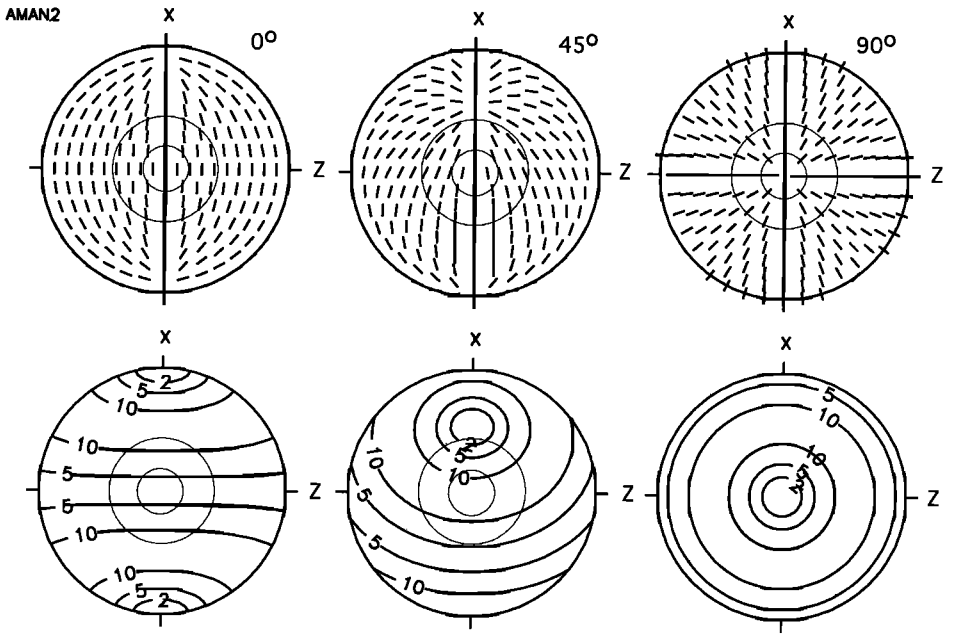

Figure 4a. Examples of shear wave splitting parameters for hexagonal and orthorhombic symmetry systems, calculated with the ANISEIS processing code [*Taylor*, 1987]. (top) Equal-area stereoplots with lines oriented parallel to ϕ for propagation along the path with back azimuth and incidence angle given by the center of the line. Large and small inner circles represent the shear wave window (see the appendix) and an incidence angle of 15°, about equal to the average *SKS* incidence angle. (bottom) Equal-area stereoplots with contours of δt, with units of 1 s through a thickness of 1000 km of material. The top right-hand corner of each diagram gives the dip angle of the fast axis measured downward from the X direction. Transversely isotropic material based on model 2 of *Keith and Crampin* [1977] consists of 1/3 transversely isotropic olivine (b and c crystallographic axes randomly distributed about the a axis) and 2/3 isotropic medium (ρ = 3300 kg/m^3, V_P = 7.6 km/s, V_S = 4.4 km/s). Strike of axis of symmetry is in the X direction.

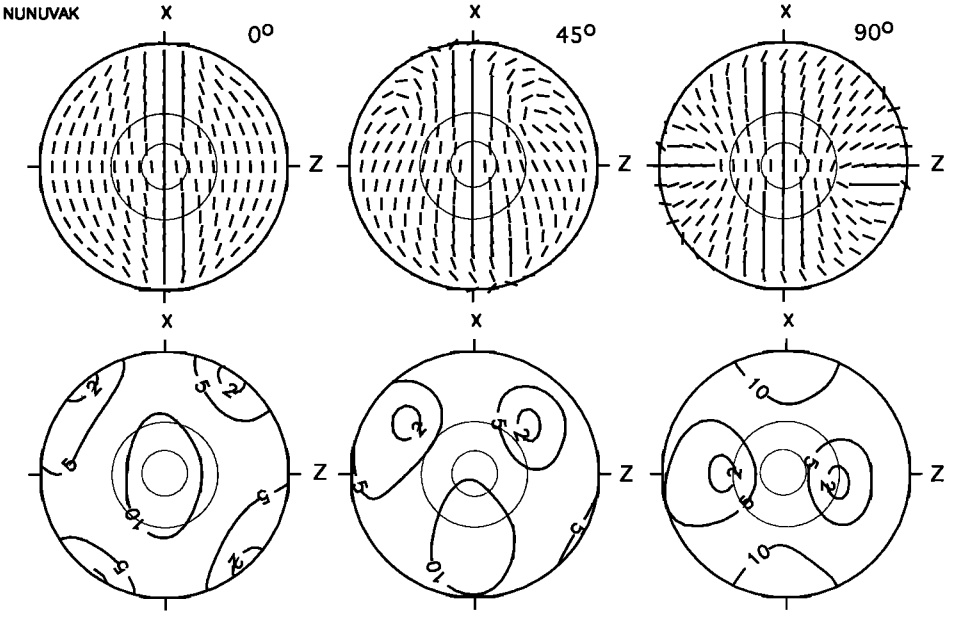

Figure 4b. Same as Figure 4a, except for nearly orthorhombic material, with the elastic tensor C_{ijkl} determined for a xenolith in Nunuvak, Canada, by *Ji et al.* [1994] (Table 1 and Figure 3). For dips of 0°, X, Y, Z are as in Figure 3.

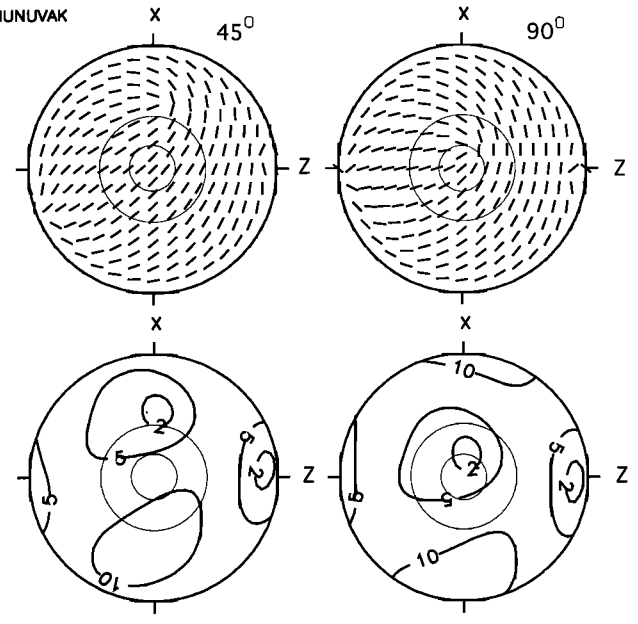

Figure 4c. Same as Figure 4b, except that the strike of the fast axis is oriented 45° to *X*.

of fabric development also suggests increasing alignment with increasing strain [e.g., *Wenk et al.*, 1991; *Mainprice and Silver*, 1993], although there may be a saturation of the fabric strength, caused by postdeformational grain boundary migration [*Mainprice and Silver*, 1993; *Kern et al.*, 1996]. Thus increasing strain tends to increase anisotropy and, as outlined in section 2.1, may change its orientation [*Zhang and Karato*, 1995].

2.2.4. Composition and orientation. *P* velocity anisotropy is strongly dependent on the modal amount of olivine, with variations of the maximum anisotropy of from 6% to 13.9% anisotropy for amounts from 50% to 100% olivine, respectively. In contrast, the difference between fast and slow shear waves ranges from only 7.1% to 9.5% for the same concentrations [*Mainprice and Silver*, 1993]. Maximum anisotropy in reported quasi-shear velocities range from 3% to 7% for most types of mantle xenoliths [e.g., *Mainprice and Silver*, 1993; *Ji et al.*, 1994; *Kern et al.*, 1996] but up to 35% for some serpentinites, representing altered mantle rocks [*Kern*, 1993a]. These maximum values usually occur for propagation within the foliation plane and perpendicular to the lineation. For many samples, propagation perpendicular to the foliation or parallel to the lineation yields splitting of half or less of this value [e.g., *Mainprice and Silver*, 1993; *Ji et al.*, 1994] (Figure 4).

2.3. Proposed Relations Between Tectonic Processes and Anisotropy

Once we assume a mechanism relating deformation to anisotropy, we must determine the relationships between tectonic processes and deformation to relate the tectonic processes to the measured shear wave splitting parameters. The major hypotheses linking tectonic processes with anisotropy concern stress and fluid-filled cracks or defects, stress and strain and lithospheric deformation, coherent deformation of the mantle and crust, frozen-in orientation from past episodes, and asthenospheric flow with large-scale flow related to absolute or relative plate motion or small-scale flow and flow around barriers.

2.3.1. Stress and strain and lithospheric deformation. Anisotropy in the mantle may be caused by fluid-filled cracks that respond to the local stress regime, analogous to crustal mechanisms (the appendix, section A6) [e.g., *Ando et al.*, 1983; *Vinnik et al.*, 1992]. This is thought to be particularly likely in mid-ocean ridge spreading centers [e.g., *Kendall*, 1994; *Blackman and Kendall*, 1997]. Fast polarizations should align parallel to the maximum compressional stress for crack-induced anisotropy but perpendicular to the maximum compressional stress for olivine preferred orientation if the maximum strain is parallel to the maximum stress (section 2.1). *Hirn et al.* [1995] propose that in regions of partial melt, fluid-filled defects are aligned parallel to ductile flow directions. Such orientations would be difficult to distinguish from olivine alignment, since they produce identical fast polarizations.

In an elastic medium with infinitesimal deformation, stress and strain are linked through Hooke's law, but for finite deformation they must be considered independently. Only crack-induced anisotropy can be considered a direct indicator of present stress. Inferences of stress from mineral orientation carry an implicit assumption that the stress has been acting in the same direction over a sufficiently long time that the minerals are totally reoriented and may be based on oversimplistic notions of the relation between slip planes and stress [e.g., *Wenk and Christie*, 1991]. As related above (section 2.2), this complex, time-dependent relation varies with many factors such as temperature, strain rate, and amount of strain.

Strike-slip, or transcurrent, deformation should align foliation planes, as defined by the mineral orientation, vertically. A fast, horizontal axis should be parallel both to the lineation and to the strike-slip deformation for large deformations [e.g., *Nicolas and Poirier*, 1976; *Silver and Chan*, 1991] (Figure 3). The vertical foliation plane should cause relatively large values of splitting for near-vertical incidence (section 2.2.4).

If deformation during collisional events is caused by uniaxial compression, then the axis of symmetry is the *b* axis, the slow direction. It is parallel to the direction of shortening: thus ϕ will be parallel to the strike of structures [e.g., *Christensen and Crosson*, 1968]. However, modeling results and measurements of mantle xenoliths suggest that the dominant form of anisotropy is with the *a* axis aligned parallel to flow lines and *b* and *c* axes either orthorhombic or randomly oriented perpendicular to the *a* axes (section 2.1). Furthermore, collisional episodes commonly include a strong transcurrent component [*Vauchez and Nicholas*, 1991], so the foliation

plane may be vertical with a possibly nonhorizontal fast direction. The magnitudes of splitting expected for the most favorable propagation orientations are similar for the cases of uniaxial compression and for transcurrent motion [e.g., *Kern*, 1993a, b]. In either case, ϕ should be parallel to major structures such as present plate boundaries or mountain belts [e.g., *Milev and Vinnik*, 1991; *Nicolas*, 1993; *Silver*, 1996].

One hypothesis is that the crust and mantle lithosphere deform coherently. Then ϕ would be parallel to strain indicators in the crust, even though the major contribution to δt comes from the mantle [e.g., *Silver and Chan*, 1988, 1991; *Vinnik et al.*, 1992; *Silver*, 1996]. Anisotropy observed at shallow, cool depths may be caused by older tectonic episodes in the subcrustal lithosphere, while anisotropy at deeper, hotter depths may be caused by recent deformations in the lithosphere or asthenosphere [e.g., *Ishikawa*, 1984; *Vinnik et al.*, 1992; *Tommasi et al.*, 1996]. Anisotropy from the last significant tectonic episode might be preserved in the upper mantle. If vertically coherent deformation occurred, then the crustal geologic structure should be parallel to the fast anisotropic direction for the part of the path that traveled through the lithosphere.

Nicolas [1993] and *Vauchez and Barruol* [1996] further suggest that in some areas, past events may create a mechanically anisotropic fabric that influences subsequent mechanical behavior of the lithosphere during new tectonic events, allowing narrow anisotropic zones from each individual orogenic episode to build up in parallel and to form a more pervasive coherent anisotropy.

2.3.2. Asthenospheric flow. Asthenospheric flow has often been invoked to explain mantle preferred orientation of olivine [e.g., *Vinnik et al.*, 1989a, b; *Russo and Silver*, 1994]. When flow occurs in simple shear, the *a* axis of olivine, and therefore ϕ, tends to be parallel to the direction of flow [*Nicolas and Poirier*, 1976; *McKenzie*, 1979; *Nicolas and Christensen*, 1987; *Ribe*, 1989, 1992; *Ribe and Yu*, 1991].

One possibility [e.g., *Leven et al.*, 1981; *Vinnik et al.*, 1989a] is that passive motion of the lithosphere over the relatively stationary asthenosphere orients the fast directions and therefore ϕ parallel to the plate motion. Some suggest, however, that this mechanism will create foliation in the horizontal plane, and thus vertical propagation through the plane will yield less splitting than would vertical propagation through a lithospheric region with transcurrent deformation [e.g., *Mainprice and Silver*, 1993].

Other modeling suggests that asthenospheric flow and its associated anisotropy should be governed by relative plate motion. Plate motion is often modeled by large convection cells, caused by thermal convective flow [e.g., *Ribe*, 1989; *Gable et al.*, 1991; *Chastel et al.*, 1993; *Bunge and Richards*, 1996]. *Ribe*'s [1989] model of convective flow and preferred orientation suggests that the evolution of preferred orientation is extremely complex.

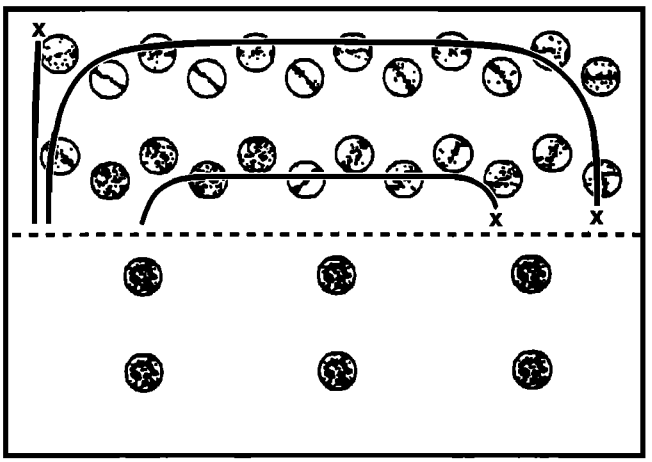

Figure 5. Model of a convection cell with stereographs of *a* axes pole figures describing the anisotropy throughout the cell. Bold line is path followed to reach position *X*. Dashed line, located at 150 km depth, separates weak anisotropic olivine aggregate above from more rigid isotropic material below, which is designed to correspond to a transformation from olivine to spinel/perovskite. Note the wide variation of *a* axis alignments throughout the upper cell. From *Chastel et al.* [1993, problem A, Figures 11 and 14].

The fast polarizations at a fast spreading ridge should be parallel to the spreading direction and anisotropy should be larger than that at a slow spreading ridge [e.g., *Ribe*, 1989]. Other models suggest that while fast polarizations greater than about 40 km from the ridge axis should be parallel to spreading, those directly below the ridge may be perpendicular to spreading and parallel to the ridge axis [e.g., *Blackman et al.*, 1996; *Blackman and Kendall*, 1997]. For corner flow at mid-ocean ridges, both the stretching lineation and the foliation plane are expected to be horizontal [e.g., *Hess*, 1964; *Silver*, 1996]. Therefore *Pn* anisotropy will be strong, but smaller amounts of splitting will occur for vertically traveling *S* waves than occurs when the foliation plane is vertical (section 2.2.4). In these models a subducting plate should entrain the surrounding asthenosphere, and therefore anisotropy ought to be observed with a dipping symmetry axis parallel to the subduction direction.

Chastel et al. [1993] use a polycrystalline theory to model the expected anisotropy of peridotite in a convection cell (Figure 5). They show that a strong texture develops during upwelling, is sustained during spreading, and is attenuated during subduction. Near the surface of the Earth, the *a* axis concentrations of olivine align roughly parallel to the spreading direction but are slightly inclined to the horizontal. The texture varies strongly with depth.

Olivine preferred orientation could be induced by larger-scale flow in the asthenosphere. The fast direction would coincide with the direction of flow but might differ from the direction of plate motion if the plate motion is decoupled from the flow beneath it [*Tanimoto*

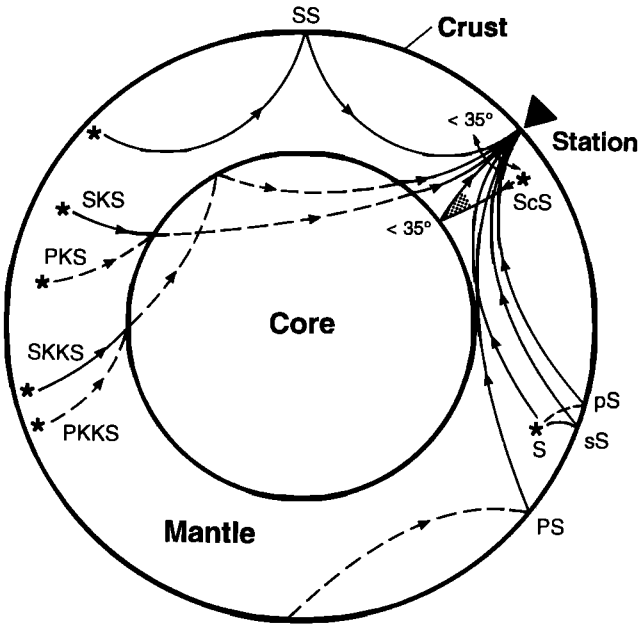

Figure 6. Phases that have been used for shear wave splitting studies. The shear wave window of 35° at the surface and at the core-mantle boundary ensures phases with smaller incidence angles will yield linear *S* wave particle motion for isotropic propagation (see glossary). Solid lines are *S* path segments, dashed lines are *P* path segments, and stars are earthquake sources.

and Anderson, 1984]. Such decoupling may occur, for instance, in the North Atlantic [e.g., *Hager and O'Connell*, 1979; *Bjarnason et al.*, 1996].

In some regions, small-scale asthenospheric flow due to localized effects that may be unrelated to surface tectonics may explain rapid variations in parameters or fast polarizations that are not parallel to directions expected from surface tectonics [e.g., *Sandvol et al.*, 1992; *Makeyeva et al.*, 1992; *Sheehan et al.*, 1997]. Such explanations are inconclusive due to the difficulty in testing.

Rather than entraining the asthenosphere within a subduction zone, slabs may act as barriers to flow within the asthenosphere [e.g., *Alvarez*, 1982; *Russo and Silver*, 1994; *Özalaybey and Savage*, 1995]. These barriers may channel flow parallel to the slab, either actively by seaward or landward progression of the subduction zone or passively by acting as a rigid barrier to flow caused by other processes.

3. WHAT CAN WE INFER FROM SPLITTING MEASUREMENTS?

Here we discuss the evidence for the vertical and lateral distribution of anisotropy and for the anisotropic symmetry systems and tectonic models just outlined.

3.1. Where Along the Path Does the Anisotropy Occur?

The shear wave splitting parameters have excellent lateral resolution but limited vertical resolution. Splitting could be caused by one or more anisotropic layers anywhere along the path between the source and receiver (Figure 6). Thus much study has focused on determining where along the path the splitting occurs.

3.1.1. Methods used. The most common technique, and the easiest, is to assume an anisotropic symmetry system and orientation, to assume the anisotropy has occurred in the upper mantle, to assume an average value for the degree of anisotropy, and then to use δt to calculate possible path lengths [e.g., *Silver and Chan*, 1988; *Vinnik et al.*, 1989b]. Alternatively, a thickness can be assumed and a percentage of anisotropy can be calculated [e.g., *McNamara et al.*, 1994]. The assumed symmetry systems and degree of anisotropy are based on the theoretical and laboratory measurements (section 2.1 and the appendix). Often 4% anisotropy and the simplest symmetry system of *transverse anisotropy* with a horizontal symmetry axis are assumed. Other methods test the assumptions.

The most straightforward method for determining the percent and the depth extent of anisotropy is to vary either the depth of the source or the depth of the receivers. In the near surface, vertical seismic profiles allow receiver depth to vary. Consequently, much progress has occurred in shallow crustal studies [e.g., *Crampin*, 1994]. For the deep crust and mantle, variation in splitting parameters for earthquake sources at different depths directly beneath a seismic station provides the best estimate of the variation of anisotropy with depth [e.g., *Shih et al.*, 1991; *Kaneshima and Silver*, 1995; *Gledhill and Stuart*, 1996; *Fouch and Fischer*, 1996; *Fischer and Wiens*, 1996] (Figure 7). Estimates of anisotropy beneath earthquake sources have been made by examining teleseismically recorded *S* waves for source-side anisotropy [e.g., *Kaneshima and Silver*, 1992, 1995; *Schoenecker et al.*, 1997]. Unfortunately, deep earthquakes are limited to subduction zones, which could have different anisotropic properties than other tectonic settings. In addition, the dip of the subduction zones usually allows a trade-off between laterally heterogeneous anisotropy and depth-dependent anisotropy. Thus alternate methods are needed as well.

Additional techniques involve comparing splitting to other measures of anisotropy such as *Pn* and surface waves that have better control on the depth distribution of anisotropy [e.g., *Savage et al.*, 1990b; *Farra et al.*, 1991], examining splitting on phases refracted at different boundaries [e.g., *Tong et al.*, 1994]; comparing splitting from *P* waves converted to *S* waves at boundaries between different depths [e.g., *McNamara and Owens*, 1993; *McNamara et al.*, 1994], comparing splitting from local or teleseismic direct *S* and *ScS* with that from *SKS* [*Kaneshima and Silver*, 1992, 1995], examining amplitudes of phases converted from *P* to *SH* or from *SH* to

P at a boundary between two anisotropic media with differing properties or between an isotropic and anisotropic medium [e.g., *Farra et al.*, 1991; *Vinnik and Montagner*, 1996; *Levin and Park*, 1997a, b; *Bostock*, 1997; *Savage*, 1998], and comparing the variation of splitting parameters between stations or between *back azimuths* at the same station with the *Fresnel zones* expected for the location in question [e.g., *Ando et al.*, 1983; *Silver and Chan*, 1988; *Gao et al.*, 1994; *Alsina and Snieder*, 1995; *Hirn et al.*, 1995; *Guilbert et al.*, 1996; *Sheehan et al.*, 1997]. (Figure 8). The evidence for the likely anisotropic structure as a function of depth is often conflicting (Table 1 and Figure 9).

3.1.2. Crustal anisotropy. *Crampin* [1994] reviews the worldwide evidence for crustal anisotropy and concludes that the vast majority of crustal anisotropy is caused by cracks and microcracks in the upper 10–15 km of the crust [e.g., *Kaneshima et al.*, 1988], which produces differences in S velocity of 1.5–4%. These average values contribute from 0.04 to 0.2 s to the splitting. However, some stations located above faults may record as much as 0.5 s splitting [*Savage et al.*, 1990a].

At pressures greater than ~200–300 MPa, corresponding to ~10–15 km depth, much of the anisotropy measured in the laboratory disappears primarily due to closure of cracks [e.g., *Kern*, 1990; *Hrouda et al.*, 1993]. Therefore any crustal anisotropy below this depth is probably caused by other phenomena, for example, minerals aligned during ductile flow of the lower crust. For teleseismic shear wave splitting, crustal rocks may contribute little to splitting because foliation planes within the crust are usually horizontal, and with vertical propagation of teleseismic phases the splitting is expected to be small (section 2.2.4) [*Barruol and Mainprice*, 1993; *Barruol and Kern*, 1996]. However, in some areas, highly anisotropic schists that were once at lower crustal depths are now upthrust, with near-vertical foliation planes (e.g., the Alpine Fault in the South Island of New Zealand). The 10 km thickness of these sheets would be enough to cause splitting of up to 1.0 s [*Okaya et al.*, 1995; *Savage et al.*, 1996a].

Phases converted from P to S at the *Moho* provide the most obvious source for isolating the lower crust from the upper mantle, yet they are often complicated by lateral heterogeneity in the crust and have not been widely examined for anisotropy. In the regions examined (Basin and Range, Tibet, Russian Urals, Canadian Shield, New Zealand), up to 0.1–0.3 s of splitting may be explained by lower crustal anisotropy ranging up to 15% [*McNamara and Owens*, 1993; *McNamara et al.*, 1994; *Levin and Park*, 1997a, b; *Savage*, 1998]. These splitting values are small compared to those usually reported for *SKS* phases. In Tibet, the Urals, and New Zealand the lower crustal splitting fast polarization is consistent with the *SKS* splitting [*McNamara et al.*, 1994; *Levin and Park*, 1997a, b; *Savage*, 1998]. In the Basin and Range

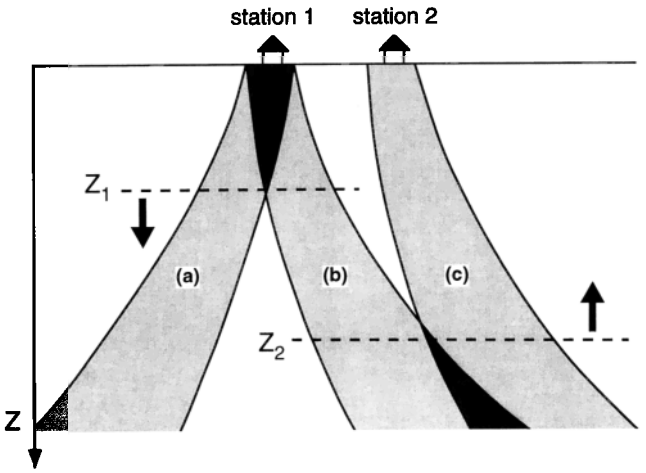

Figure 8. Schematic illustration of the Fresnel zone as a function of depth for *SKS* phases arriving nearly vertically at two neighboring stations. (Reprinted with permission from *Alsina and Snieder* [1995].) The two different back azimuths (a and b) at station 1 share a common path above Z_1, while similar back azimuths at stations 1(a) and 2(c) share a common path below Z_2. Thus, assuming a simple symmetry system in which parameters vary little with back azimuth, different results from opposite back azimuths at station 1 suggest that anisotropy occurs below Z_1. Similarly, differences in splitting between events from the same back azimuth recorded at stations 1 and 2 would be caused by differences in anisotropy above Z_2.

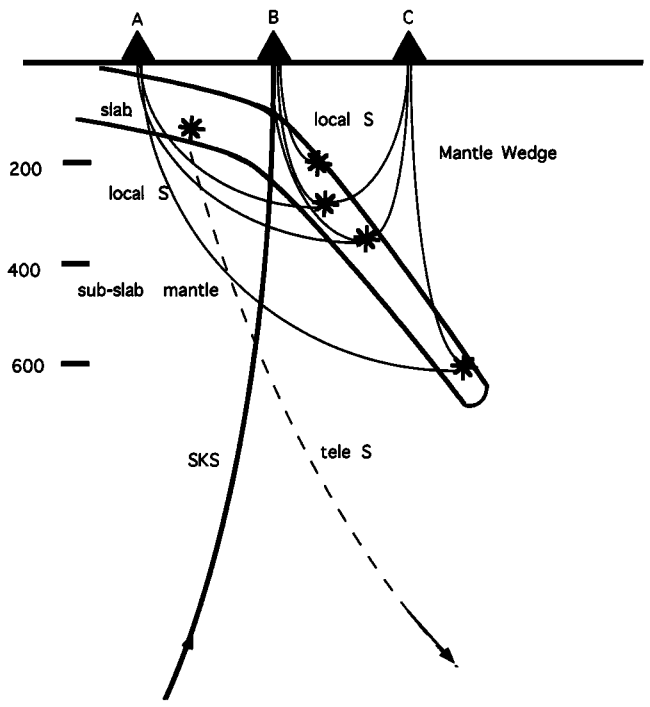

Figure 7. Schematic diagram showing use of subduction zone events to determine changing anisotropy with depth. Differences between splitting along paths shown to station A will be caused by subslab mantle anisotropy, differences to B will reflect within-slab anisotropy, and those to C relate to mantle-wedge anisotropy. Teleseismically recorded events reflect mainly subslab anisotropy.

TABLE 1. Depth Extent of Shear Wave Anisotropy Determined by Various Studies

Depth, km	*Study*	δt, s	*Percent S Anisotropy*	*Region*
		Worldwide Averages		
Crust	*Crampin* [1994]	···	1.5–4	worldwide
Crust	*Silver* [1996]	0.1–0.3	···	worldwide
100	*Montagner* [1994]	···	2.2	worldwide surface waves
Above 220	*Montagner and Kennet* [1996]	···	1.5–4.8	(radial) worldwide
220–410	*Montagner and Kennett* [1996]	···	isotropic	(radial) worldwide
410–660	*Montagner and Kennett* [1996]	···	1	(radial) worldwide
Below 410	*Silver* [1996]	0.2	···	worldwide
Lower mantle	*Montagner and Kennet* [1996]	isotropic	···	worldwide
D″	*Montagner and Kennet* [1996]	···	1	(radial) worldwide
		Continents		
Lower crust	*McNamara and Owens* [1993]	0.2	3–11	Basin and Range
Crust	*McNamara et al.* [1994]	0.19	···	Tibetan Plateau
Lower crust	*Levin and Park* [1997a, b]	0.25	15	Ural Mountains
Upper 10 km of mantle	*Mjelde and Sellevoll* [1993]	···	5–10	Norway *Sn*
27–80	*Vinnik and Montagner* [1996]	···	3	Germany
45–80	*Farra et al.* [1991]	···	5	China
75–85	*Bostock* [1997]	···	5	Canadian Shield
27–166	*Farra et al.* [1991]	···	3	Germany
160–220	*Farra et al.* [1991]	···	5	Norway
80–320	*Vinnik and Montagner* [1996]	···	3	Germany
Above 252	*Gaherty and Jordan* [1995]	···	3.3	Australian Craton
Above 250	*Gao et al.* [1994]	0.9	···	Baikal Rift
Below 100	*Sheehan et al.* [1997]	1.0	···	Basin and Range
210–410	*Tong et al.* [1994]	···	1	Australian craton *SH/SV*
Sublithosphere	*Alsina and Snieder* [1995]	0.4–1.1	···	NARS-NL array
Below 252	*Gaherty and Jordan* [1995]	···	<1	Australian Craton
580–620	*Vinnik and Montagner* [1996]	···	3	Germany
Between core and surface	*Silver* [1996]	0–2.4	···	continental compilation for *SKS*
		Subduction Zones		
Crust	*Gledhill and Stuart* [1996]	0.1	4	New Zealand
Crust above 20	*Cassidy and Bostock* [1996]	0.2	2.3	Juan de Fuca
Crust 20–70	*Cassidy and Bostock* [1996]	0.32	···	Juan de Fuca
Wedge 50–150	*Iidaka and Obara* [1995]	···	···	Japan
Wedge below 250	*Okada et al.* [1995]	···	3	East Honshu, Japan
Wedge below 250	*Okada et al.* [1995]	···	1.5	West Honshu, Japan
Wedge	*Kaneshima and Silver* [1995]	0.1–0.5	···	worldwide
Wedge	*Kaneshima and Silver* [1995]	0.15	···	Peru
Wedge above 120	*Shih et al.* [1991]	0.1	···	Colombia
Mantle wedge 120–200	*Shih et al.* [1991]	0.4	···	Colombia
Mantle wedge 50–150	*Yang et al.* [1995]	···	1	Aleutians
Mantle wedge 50–200	*Ando et al.* [1983]	···	<4	Honshu, Japan
Within slab	*Hiramatsu and Ando* [1996]	0.5–1.0	5	Japan
Within slab	*Hiramatsu et al.* [1997]	1.0	5	Japan
Slab and below	*Kaneshima and Silver* [1995]	0.8	2	Peru
Subslab 30–250	*Gledhill and Stuart* [1996]	0.3–1.2	1.4	New Zealand
>100 slab and below	*Schoenecker et al.* [1997]	2.5–3.5	···	Hindu Kush (source-side)
>200 slab and below	*Schoenecker et al.* [1997]	2.5	···	Hindu Kush (source-side)
30–300 slab and below	*Russo and Silver* [1994]	0.3–4.0	···	South America (source-side)
<400 slab and above	*Fouch and Fischer* [1996]	···	0.5–1.0	NW Pacific
<400 slab and above	*Fischer and Wiens* [1996]	···	0.8–3	Tonga
Below 400	*Vinnik and Kind* [1993]	···	several	north NW Pacific
410–520 slab and above	*Fouch and Fischer* [1996]	···	0.5–1.0	Southern Kurils
410–520 slab and above	*Fouch and Fischer* [1996]	···	<0.5	Izu-Bonin
Transition zone	*Fischer and Wiens* [1996]	···	<0.5	Tonga
>410 slab and above	*Meade et al.* [1995]	0.0	0	South America, Japan
>410 slab and above	*Fischer and Wiens* [1996]	···	<0.5	Tonga
Lower mantle	*Fouch and Fischer* [1996]	<0.2	~0	southern Kurils
		Oceans		
Mantle lid above 45	*Kawasaki* [1986]	···	2	mid-Pacific (surface waves)
Above 125	*Forsyth* [1975]	···	2	mid-Pacific (surface waves)
Periods <100 s	*Nishimura and Forsyth* [1988]	···	1.6	Pacific plate <80 Ma (surface waves)
Above 166	*Gaherty et al.* [1996]	···	3.7	Pacific between Fiji and Hawaii
D″	*Maupin* [1994]	···	1	Pacific
D″	*Matzel et al.* [1996]	3–5	1.5–3	(radial) Alaska
D″	*Kendall and Silver* [1996]	3–9	0.5–2.8	(radial) Caribbean
D″	*Garnero and Lay* [1997]	···	0–1.5	(radial) Alaska and Pacific Northwest

the fast polarization associated with the 0.2 s of splitting is parallel to the present spreading direction, perpendicular to that expected for crack alignment in the upper crust, and at a high angle to the *SKS* measurements [*McNamara and Owens*, 1993]. This suggests that mineral alignment in the lower crust causes the observed splitting, which may be a minimum measure as it is partially cancelled by splitting from the upper crust. Thus it remains possible that splitting in the lower crust is larger than 0.3 s.

3.1.3. Upper mantle anisotropy. The upper mantle probably contributes most to the delay times observed in teleseismic phases. Debate continues about whether anisotropy is confined to the upper 200 km beneath the mantle or continues through to the transition zone.

Global models of anisotropy, determined from comparisons between Love and Rayleigh waves or between *SV* and *SH waves*, are sensitive to radial anisotropy. The preliminary reference Earth model [*Dziewonski and Anderson*, 1981] includes anisotropy only in the upper 220 km. Inversions of surface and higher modes and body wave data [*Nishimura and Forsyth*, 1988; *Montagner and Tanimoto*, 1991; *Gaherty and Jordan*, 1995; *Gaherty et al.*, 1996] suggest that significant radial anisotropy is confined to the upper 200–300 km of the mantle. The boundary is probably deeper beneath continents than under ocean basins [*Gaherty et al.*, 1996]. On this basis it has been suggested that the *Lehmann discontinuity* at about 200 km depth [*Lehmann*, 1959, 1961] may be caused by a transition from dislocation creep and anisotropic material in the upper region to diffusion creep and isotropic material below [e.g., *Karato*, 1992; *Zhang and Karato*, 1995; *Gaherty and Jordan*, 1995]. If there is a lower limit to the anisotropic layer, it should be thinner where there is high heat flow, and therefore it should be thicker beneath cold cratons than beneath warm orogenic belts [e.g., *Karato*, 1992; *Ji et al.*, 1994]. This corresponds to the form of variation in depth observed for the Lehmann discontinuity [*Revenaugh and Jordan*, 1991].

The numerous results of over 1.0 s for δt are too large for anisotropy to be confined to the crust in most regions. Most studies (section 3.1.4) suggest little or no splitting in the mantle below 400–600 km [e.g., *Vinnik et al.*, 1992; *Mainprice and Silver*, 1993; *Barruol and Mainprice*, 1993; *Vinnik et al.*, 1995a, 1996]. If the splitting is distributed over 400 km, minimum values of average anisotropy are 1.1 and 2.2% for 1.0 s and 2.0 s splitting, respectively. If the splitting is confined above 250 km depth, minimum values are 3.6% for measurements of 2.0 s. This is consistent with direct measurements of mantle xenoliths from depths of 40–170 km, which yield maximum *S* wave splitting anisotropy of 3.5–4.5% [e.g., *Mainprice and Silver*, 1993; *Ji et al.*, 1994] or 7% [*Kern et al.*, 1996]. A few measurements above 2.0 s in plate boundary regions may require deeper anisotropy, larger percentage anisotropy, or both. Moho refracted phases in some areas suggest even higher anisotropy, up to

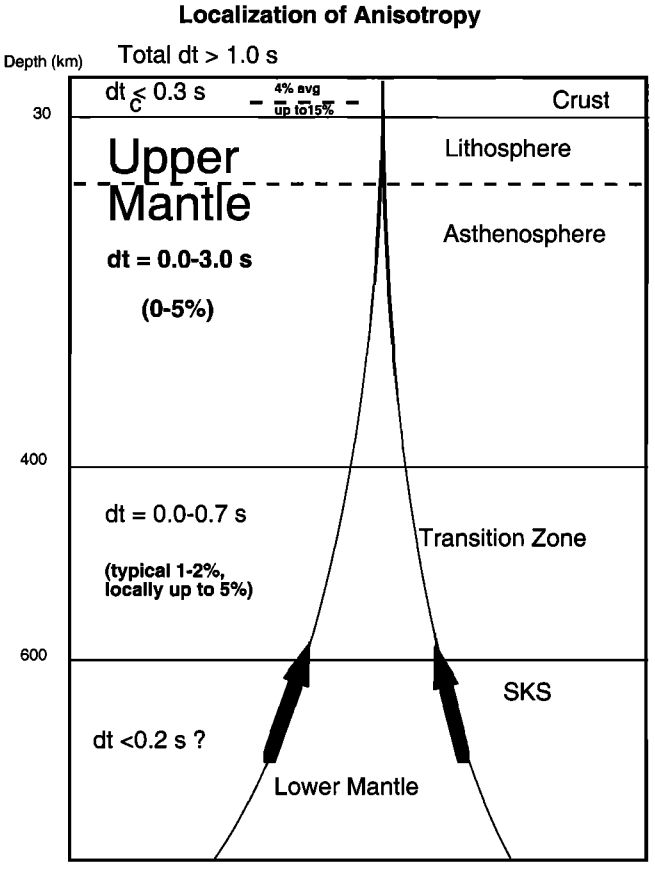

Figure 9. Summary of results in Table 2 concerning anisotropy variation with depth.

11–15% for *Pn* [*Mjelde and Sellevoll*, 1993; *Enderle et al.*, 1996] and 5–10% for *Sn* [*Mjelde and Sellevoll*, 1993]. *P-S* conversions from layers in the upper mantle suggest anisotropy of 5% in a layer lying from 75 to 85 km in the Canadian Shield, with fast direction at a high angle to nearby *SKS* ϕ measurements [*Bostock*, 1997].

Variations in splitting parameters observed between closely spaced stations suggest that anisotropy is heterogeneous in the upper mantle above 250 km [e.g., *Gao et al.*, 1994; *Alsina and Snieder*, 1995; *Hirn et al.*, 1995; *Guilbert et al.*, 1996; *Plomerovà et al.*, 1996; *Barruol and Souriau*, 1995; *Sheehan et al.*, 1997] (Figure 8). However, apparent variations between stations might occur in *homogeneous* regions if the anisotropic symmetry system were complex and the parameters were measured for different polarizations, back azimuths, or incidence angles (Figures 4c and 10). Furthermore, even though waves share a common path through a possibly anisotropic medium below, an upper layer of anisotropy could vary between observation points. Many studies using the most closely spaced stations were carried out in short-term deployments where there is not sufficient azimuthal coverage to rule out two or more layers of anisotropy [e.g., *Gao et al.*, 1994]. Therefore these studies cannot rule out anisotropy in the asthenosphere.

Several lines of reasoning suggest that at least in some regions, anisotropy continues well below 200 km. Grain

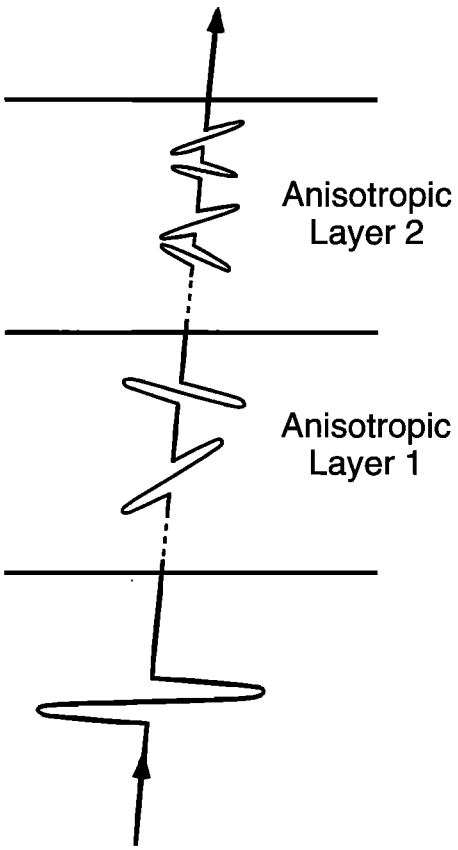

Figure 10a. Schematic diagram of shear wave splitting in the case of two anisotropic layers. The incoming shear wave is split twice, leading to four individual waves at the receiver. (Reprinted with permission from *Yardley and Crampin* [1991].) With lower frequencies, the individual arrivals are unresolved, and instead, apparent single-layer anisotropy will be observed.

size may vary with depth in the mantle. The typical geothermal gradients for orogenic zones and cratons could allow dislocation creep and therefore anisotropy down to the olivine-spinel transition zone [e.g., *Ji et al.*, 1994]. Splitting of horizontally propagating *SV* and *SH* refracted waves in northern Australia suggests anisotropy of 1% between 210 and 400 km depth, with *SH* faster than *SV* [*Tong et al.*, 1994]. Weaker evidence includes precursors to a single *S* phase received at the NORSAR array that have been interpreted as phases converted from *SH* to *P* at a boundary which lies at 220 km depth between two anisotropic media with different axis orientations [*Farra et al.*, 1991].

The only values of anisotropy that are directly measured via changes in splitting for earthquakes at different depths come from subduction zones. They suggest anisotropy of between 0.5% and 2.0% for the mantle above and below the slabs and up to 5% within the slabs [e.g., *Shih et al.*, 1991; *Kaneshima and Silver*, 1995; *Gledhill and Stuart*, 1996; *Fouch and Fischer*, 1996; *Hiramatsu et al.*, 1997] (section 3.3.4, Table 1 and Figure 11). Most comparisons of *SKS* and *S* report some splitting from the region below slabs in the asthenospheric mantle below 200 km [e.g., *Russo and Silver*, 1994; *Gledhill and Stuart*, 1996].

The presence of anisotropy of up to 2% in the asthenosphere below 200 km is incompatible with olivine deforming solely by diffusion creep in that region and must be reconciled with the apparently contradictory evidence that radial anisotropy is confined above the Lehmann discontinuity. Possible explanations are rapid changes of anisotropy with depth (e.g., convection models of *Chastel et al.* [1993]; see Figure 5), causing averaging to radial isotropy [e.g., *Gaherty et al.*, 1996], or changes in anisotropic symmetry orientation. Whatever explanation is finally invoked, it seems clear that we cannot blithely assume that the anisotropy must be above 200–250 km in any given region.

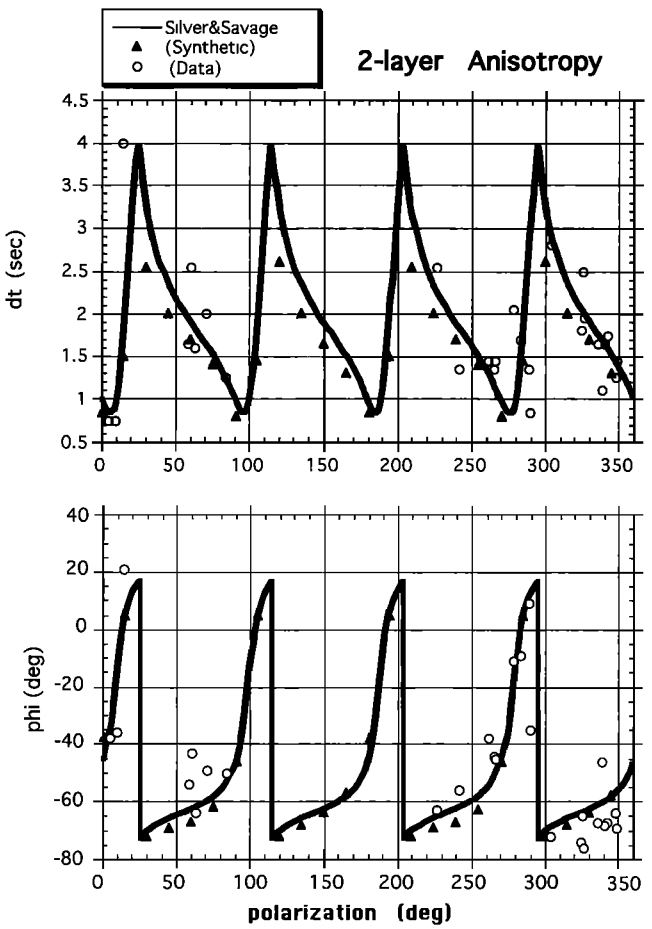

Figure 10b. The values of ϕ and δt from synthetic seismograms (solid triangles) calculated by the method of *Keith and Crampin* [1977] through a medium with two layers of anisotropy with fast axes separated by 45°, with average splitting properties given in the text and by *Özalaybey and Savage* [1995]. Real data from BKS (Berkeley) (open circles are from *Özalaybey and Savage* [1995]) plotted as a function of the incoming polarization direction. The solid line is the theoretical curve from the single-frequency analysis of *Silver and Savage* [1994] for the two-layer case determined from *Özalaybey and Savage* [1995].

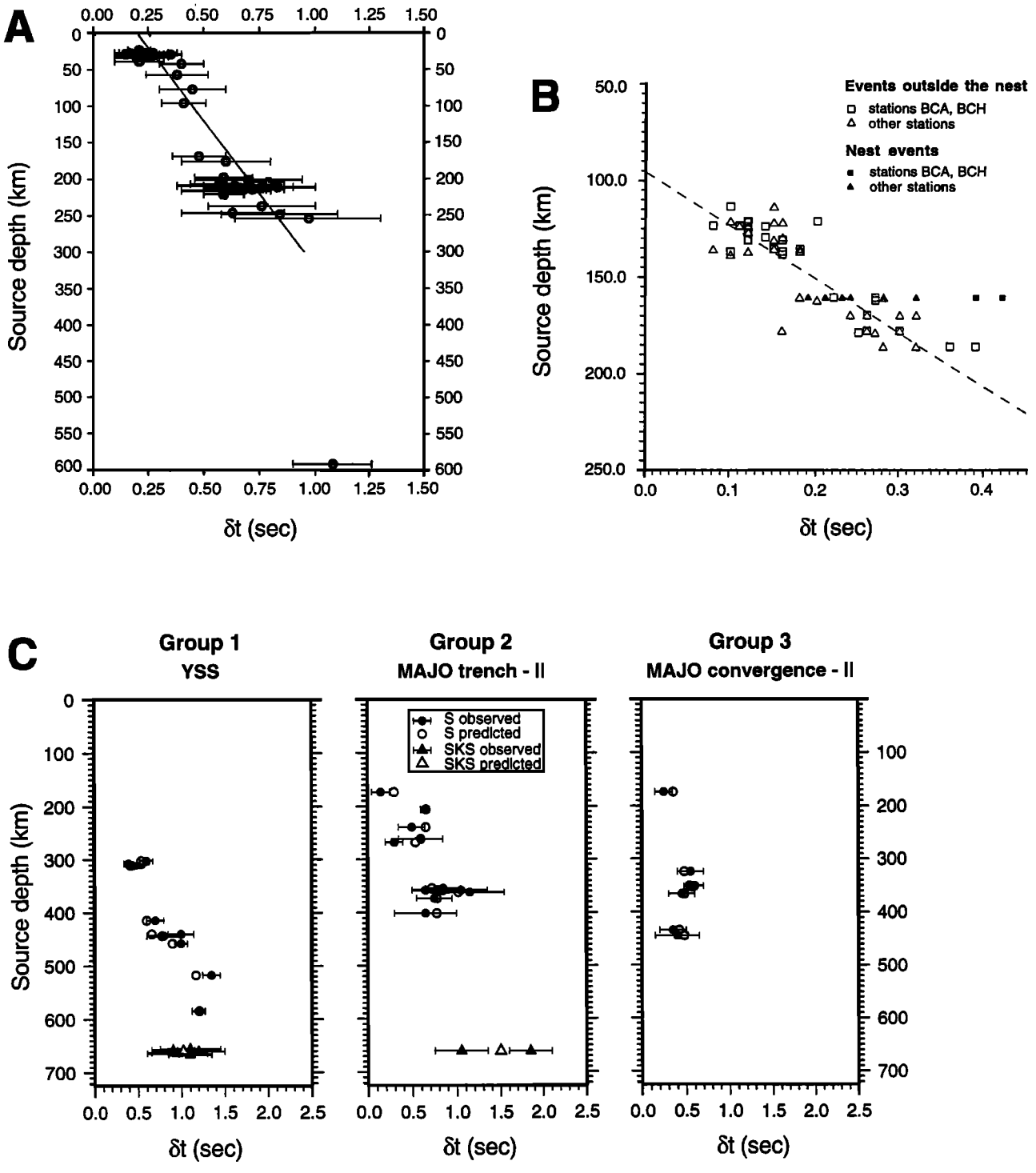

Figure 11. Examples of the variation of splitting with depth of earthquake source in subduction zones. (a) New Zealand, with differences between paths mainly subslab. (Reprinted from *Gledhill and Stuart* [1996], with permission from Elsevier Science.) (b) Bucaramanga Nest, Colombia, with differences between paths mainly due to the mantle wedge. After *Shih et al.* [1991]. (c) (left) Sakhalin Island (YSS) and Japan (MAJO), with anisotropy separated into groups whose fast polarizations are (middle) trench-parallel and (right) convergence-parallel. Paths for both stations pass mainly through the mantle wedge. After *Fouch and Fischer* [1996].

3.1.4. Anisotropy in the transition zone. Most work suggests a largely isotropic lower mantle. Comparison of *S* waveforms from events deeper than 400 km with *SKS* waveforms usually suggests they have been split by the same amount [e.g., *Kaneshima and Silver*, 1995; *Meade et al.*, 1995; *Fouch and Fischer*, 1996; *Gledhill and Stuart*, 1996]. Similarly, splitting at stations in Tonga is nearly identical for local earthquakes with

depth ranges between 400 and 600 km [*Fischer and Wiens*, 1996]. This suggests that in many regions, lower mantle minerals do not develop a strong preferred orientation. This is consistent with experimental studies that suggest deformation occurs by diffusion creep over most of the lower mantle [e.g., *Karato and Li*, 1992; *Meade et al.*, 1995].

However, in some areas, anisotropy may occur in the transition zone below 410 km (Figure 11). At station YSS at Sakhalin Island, delay times increase with source depth from about 0.7 s at 400 km to 1.2–1.4 s at 500 km and below, suggesting anisotropy of 0.5% down to at least 480 km [*Fouch and Fischer*, 1996], although other measurements with poorer resolution fail to resolve anisotropy in this region [*Sandvol and Ni*, 1997]. At one station on the Eurasian plate immediately above the Japan subduction zone, differences between *SKS* fast polarizations and those of shear waves from local earthquakes deeper than 400 km suggest anisotropy beneath 400 km [*Sandvol and Ni*, 1997]. Weaker evidence comes from comparison of *SKS* to direct *S* from subduction zone events received at the Grafenberg array (GRF) in Germany, which suggest that β spinel anisotropy of up to several percent may occur in some regions [*Vinnik and Kind*, 1993]. Similarly, *Vinnik and Montagner* [1996] find that at GRF, energy on *transverse components* from phases converted from *P* to *S* at the 660-km discontinuity cannot be explained simply by splitting of the phase if it were converted from *P* to *SV* at an isotropic boundary and later split in an anisotropic medium with the parameters given by the *SKS* results. It could be explained by the transverse energy that is generated when *P* is converted to *SH* at a boundary between an isotropic and an anisotropic medium. They model the mantle as anisotropic above 320 km, as isotropic between 320 and 580 km, and with 3% anisotropy between 580 and 620 km.

Montagner and Kennett [1996] also suggest that anisotropy in the lower transition zone is necessary to reconcile body wave and normal mode data in a reference Earth model. They suggest that a convective boundary layer may exist between the upper and lower mantle, at least in some regions, which may be caused by horizontal flow in a low-viscosity region near the base of the mantle transition zone.

3.1.5. Anisotropy in the D″ layer. The *D″* layer extending 250–300 km above the boundary between the core and mantle in some regions was only recently discovered [*Lay and Helmberger*, 1983] and is therefore just beginning to be characterized. It is extremely heterogeneous and is probably anisotropic in some areas.

Most studies suggesting anisotropy in the D″ layer have modeled it as radially anisotropic [e.g., *Lay and Young*, 1991; *Vinnik et al.*, 1995a; *Montagner and Kennett*, 1996; *Matzel et al.*, 1996; *Kendall and Silver*, 1996; *Garnero and Lay*, 1997], with shear velocity anisotropy reported between 0% and 3%, with the suggestion that the anisotropy may vary along closely spaced paths [e.g., *Vinnik et al.*, 1995a; *Garnero and Lay*, 1997]. Radial anisotropy would not cause transverse energy on *SKS* waveforms and is consistent with the lack of splitting reported on paths beneath 600 km outlined in section 3.1.4. Only preliminary results in a few places in the Pacific [*Maupin*, 1994] suggest that parts of the D″ layer could be azimuthally anisotropic.

3.2. How Is Anisotropy Best Characterized?

A single shear wave splitting measurement can characterize anisotropy beneath a station, provided that one assumes a symmetry system, orientation, and depth extent of anisotropy. However, such characterization may be misleading because in most symmetry systems and orientations, splitting parameters vary as a function of back azimuth and incidence angle. Even in the simple anisotropic system of a transversely isotropic solid with a vertical axis of symmetry, one needs wave speeds of vertically traveling *P* and *S* waves, horizontally propagating *P* and *SH* waves, and information in another direction of propagation to fully characterize the anisotropy [e.g., *Anderson*, 1989]. Similarly, fundamental mode surface waves are sensitive to only a limited number of elastic constants [*Maupin*, 1985; *Montagner and Tanimoto*, 1991]. Furthermore, changes in anisotropy either with depth or laterally can cause variations in splitting parameters with back azimuth. Therefore measurements of splitting and *P* and *S* arrival times at a wide variety of azimuths and incidence angles would be needed to completely characterize a general anisotropic medium. Limited azimuth coverage makes it difficult to distinguish one pattern from another; thus full symmetry systems have not yet been determined. Therefore assumptions are necessary to proceed from measurements to interpretations.

3.2.1. Inferring anisotropic symmetry systems. Most techniques of examining anisotropy are only sensitive to variations of velocity in two orthogonal directions. Comparisons of *SH* to *SV* data for global studies and comparisons of Love and Rayleigh wave phase velocities are only sensitive to difference between vertical and horizontal velocities. Similarly, single shear wave splitting measurements are sensitive only to variations in a horizontal plane. The simplest models used to explain variations in two orthogonal directions are hexagonally symmetric models. Therefore anisotropy in surface waves and global comparisons of *SH* to *SV* wave speeds has been interpreted in terms of radial anisotropy, and shear wave splitting is usually interpreted in terms of transverse anisotropy with a horizontal symmetry axis. These models probably average variations in other directions [e.g., *Babuška and Cara*, 1991]. For example, horizontal olivine *a* axes with varying azimuths will average over large lateral regions to a radially anisotropic model; this mechanism is considered a likely explanation for Love-Rayleigh *polarization anisotropy* [e.g., *Gaherty et al.*, 1996]. If both radial anisotropy and shear wave splitting were measured in a region, they could be combined to derive a model with orthorhombic symmetry,

but the dip of the axes would remain unresolved without careful examination of azimuthal variations.

Plotting the splitting parameters on stereonets facilitates examination of the variation as a function of back azimuth as well as incidence angle [*Crampin and McGonigle*, 1981; *Ando et al.*, 1983] (Figure 4). Splitting parameters for inclined symmetry axes have a characteristic pattern, which has been used to suggest an inclined symmetry axes in the crust near Long Valley caldera, California [*Savage et al.*, 1990a]. Variations in delay time are more pronounced than polarizations and may be more useful for distinguishing dips.

Babuška et al. [1984, 1993] suggest that anisotropy with inclined symmetry axes may be common. They argue convincingly that in Europe, simple hexagonal symmetry with an inclined symmetry axis fits teleseismic *P* delay variations and splitting better than models with inhomogeneous structures. *Guilbert et al.* [1996] report remarkably consistent results in northern Tibet with similar methods. *Levin et al.* [1997] also point out that observed splitting variations may be the cause of significant travel time anomalies, which should be considered in inversions for velocity structure. Interpretations by *Plomerovà et al.* [1996] for orthorhombic symmetry with inclined axes in the western United States are less convincing (section 3.3.3).

In a number of locations, little splitting is measured for any polarization direction. These locations are candidates for possible near-vertical orientation of *a* axes (e.g., Rocky Mountains [*Savage et al.*, 1996b], Pakistan Himalayas [*Sandvol et al.*, 1994, 1997], and Australia [*Clitheroe and van der Hilst*, 1998; S. Özalaybey and W.-P. Chen, Frequency-dependent analysis of *SKS*/*SKKS* waveforms observed in Australia: evidence for transverse isotropy, submitted to *Physics of the Earth and Planetary Inveriors*, 1997, hereinafter cited as Özalaybey and Chen, submitted manuscript, 1997].

Fortunately, despite the near-limitless possibilities for complicated anisotropic symmetry systems, most measurements and calculations of anisotropy in samples of mantle-derived rocks appear to have either orthorhombic or hexagonal symmetry (section 2.1). These two likely candidates have patterns that do not differ significantly for horizontal *a* axis alignment and near-vertical incidence angles. Furthermore, the olivine *a* axis is aligned with the extension direction or flow direction for most observed symmetry systems; therefore the distinction between orthorhombic and hexagonal symmetry may be of minimal importance in interpreting splitting measurements, as long as one symmetry axis is the *a* axis.

3.2.2. Inferring heterogeneous anisotropy. Most *S* wave splitting interpretations assume the simplest models, of a single homogeneous layer of transverse anisotropy with a symmetry axis oriented in the horizontal plane. As we have just seen, homogeneous anisotropy with certain symmetry systems and orientations can produce variations in splitting parameters. In addition, multiple layers of anisotropic material and laterally varying anisotropy can produce variations of anisotropy with back azimuth. The most general case of continuously varying anisotropic media may eventually be required to explain all the data. In the meantime, increasingly complicated systems are being examined.

Multiple layers of anisotropy with different symmetry axes can cause unusual effects on splitting parameters (Figure 10). As each split phase propagates through subsequent layers, the phases will be split again. In the top anisotropic layer, whatever shear phases arrive will again be split into fast and slow components, and the initial wave polarization will be parallel to the fast direction of the last layer of anisotropy [e.g., *Crampin*, 1981; *Yardley and Crampin*, 1991]. However, when whole waveform techniques are used, measured apparent splitting parameters depend on the period of the signal, the splitting parameters of each layer, and the polarization of the initial isotropic shear wave [*Silver and Savage*, 1994] (Figure 10). These expected patterns are valid whenever splitting parameters of each layer are only weakly dependent on the angle of incidence or back azimuth. This is valid for most xenoliths measured if the olivine *a* axis alignments are primarily horizontal and if *SKS* phases are used (e.g., Figure 4). The patterns of variation in splitting parameters from two layers of anisotropy can distinguish which layer is on top, but they cannot directly reveal where along the path each layer is located. Patterns due to multiple layers of simple anisotropic material can be distinguished from that of lateral heterogeneity and complicated symmetry systems because both of the latter patterns are functions of propagation direction, while the former is a $(\pi/2)$ function of polarization direction. Including deep sources of *S* waves, which in general have varying polarization, can help distinguish the two. These patterns have been used to model anisotropy variations with depth beneath the San Andreas Fault [*Savage and Silver*, 1993; *Özalaybey and Savage*, 1994, 1995; this paper, section 3.3.3] and beneath the German regional seismic network [*Vinnik et al.*, 1994] and to test hypothetical two-layer models [e.g., *Savage and Silver*, 1993; *Wolfe and Silver*, 1998].

To distinguish heterogeneity from complex anisotropy, results obtained at closely spaced stations are useful [e.g., *Ando et al.*, 1983; *Alsina and Snieder*, 1995], and plotting individual measurements from each earthquake-station pair in map view can be enlightening (Figure 12). Such plots allow one at least qualitatively to see whether variations in back azimuth may be caused by symmetry systems (e.g., if each station has the same pattern as a function of back azimuth) or lateral variations in anisotropy (if rays traversing a given region give the same results at different stations and other regions give different results). In the western United States, such a map suggests lateral variations in anisotropy and possibly asthenospheric flow (Figure 12).

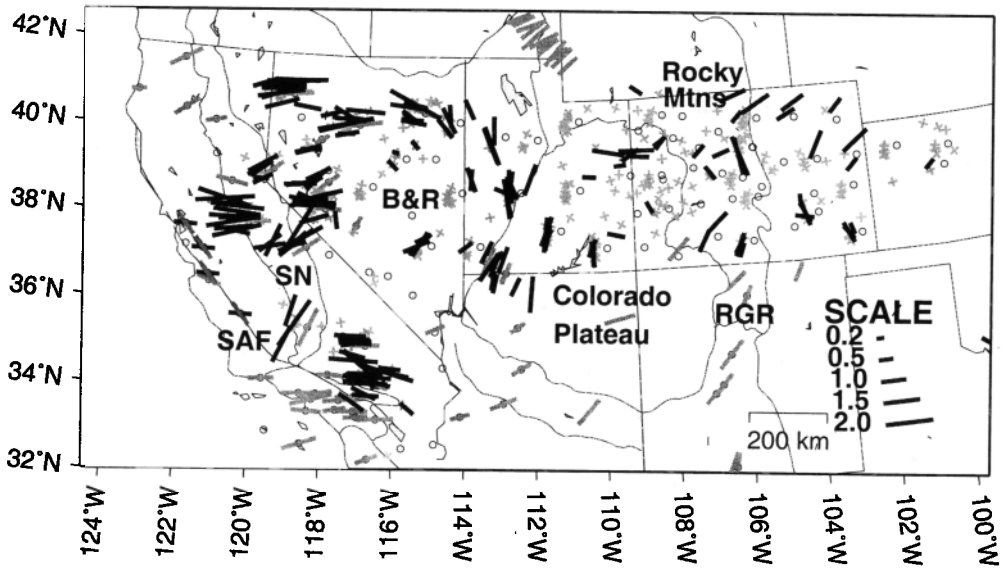

Figure 12. Compilation of shear wave splitting measurements in the southwestern United States. Single measurements are represented by one or two lines. A positive measurement is represented by a single line oriented parallel to ϕ, with length proportional to δt. Null measurements are plotted with two crossed lines with orientations equal to the allowed ϕ. Shaded measurements are station averages, which are plotted at the station location. All single measurements are plotted at the 220 km depth projection of the ray. Data sources are *Sheehan et al.* [1997], *Özalaybey and Savage* [1994, 1995], *Ruppert* [1992], *Sandvol et al.* [1992], *Savage and Silver* [1993], *Savage et al.* [1990b], E. Sandvol (personal communication, 1994), *Liu et al.* [1995], and *Schutt et al.* [1998]. Station locations are indicated by open circles. SAF, San Andreas Fault; SN, Sierra Nevada mountain range; B&R, Basin and Range province; and RGR, Rio Grande Rift.

3.3. Which Models Fit Which Regions?

Below we relate the observations made in different tectonic regions to the hypotheses outlined above (Figure 13).

3.3.1. Middle of oceanic plates. The first observations of azimuthal anisotropy were for *Pn* arrivals on marine seismic refraction lines in the Pacific [*Hess*, 1964] (Figure 2). These observations suggested that anisotropy in the oceanic crust and sub-Moho mantle were caused by fossil fabric formed at the spreading ridge, with the fast axis parallel to the spreading direction [*Francis*, 1969; *Raitt et al.*, 1969; *Shearer and Orcutt*, 1986]. Within ophiolite sequences, olivine *a* axes are usually oriented subparallel to the spreading direction, inferred by the orientation of sheeted dikes, again implying fast polarizations parallel to spreading [e.g., *Christensen*, 1984]. Early studies of Rayleigh wave propagation also confirmed the fast direction as parallel to spreading in the Nazca and the Pacific plates [e.g., *Forsyth*, 1975; *Kawasaki*, 1986]. Anisotropy inferred from long-period surface waves suggests that in the Pacific the fast axis of anisotropy is parallel to the fossil spreading at shallow depths around 100 km but parallel to the present-day flow direction of kinematic plate models at deeper locations [*Nishimura and Forsyth*, 1988, 1989; *Montagner and Tanimoto*, 1990, 1991; *Montagner*, 1994]. For the Pacific Plate the most recent spreading direction happens to coincide with the absolute plate motion direction, but that is not a general result for all spreading systems. The fast directions at 200 km depth in the Indio-Australian plate are correlated with the absolute plate motion direction but with an offset of about 30° between the fast directions and the absolute plate motion direction [*Montagner*, 1994].

Splitting results are more variable (Figure 13). *PS* splitting for waves with conversion points in the Pacific [*Su and Park*, 1994], and *SKS* and *ScS* received at stations in the South Pacific Islands [*Wolfe and Silver*, 1998] yield fast directions parallel to present absolute plate motion as well as to the most recent spreading direction. Stations in Hawaii, the North Pacific, and Ascension Island near the Mid-Atlantic Ridge yield *SKS* ϕ measurements parallel to the fossil spreading [*Kuo and Forsyth*, 1992; *Wolfe and Silver*, 1998]. The generation of quasi-Love waves near Hawaii suggests strong anisotropic gradients in azimuthal anisotropy related to hotspot flow [*Yu and Park*, 1994]. Several studies of *SS* and *SS-S* travel times in the Atlantic give conflicting results [*Kuo et al.*, 1987; *Woodward and Masters*, 1991; *Sheehan and Solomon*, 1991] and may be affected by variations of incidence angle or by faults in processing such as the lack of correction for source-side or receiver-side splitting [*Yang and Fischer*, 1994]. However, the reported splitting of *SS* phases with bounce points in the North Atlantic is consistent with *Montagner and Tanimoto*'s [1991] surface wave results [*Fischer and Yang*, 1994] and with *SKS* splitting at World-Wide Standardized Seismograph Network (WWSSN) station BEC in Bermuda [*Kuo and Forsyth*, 1992]. These are not parallel to either the fossil seafloor spreading direction or to

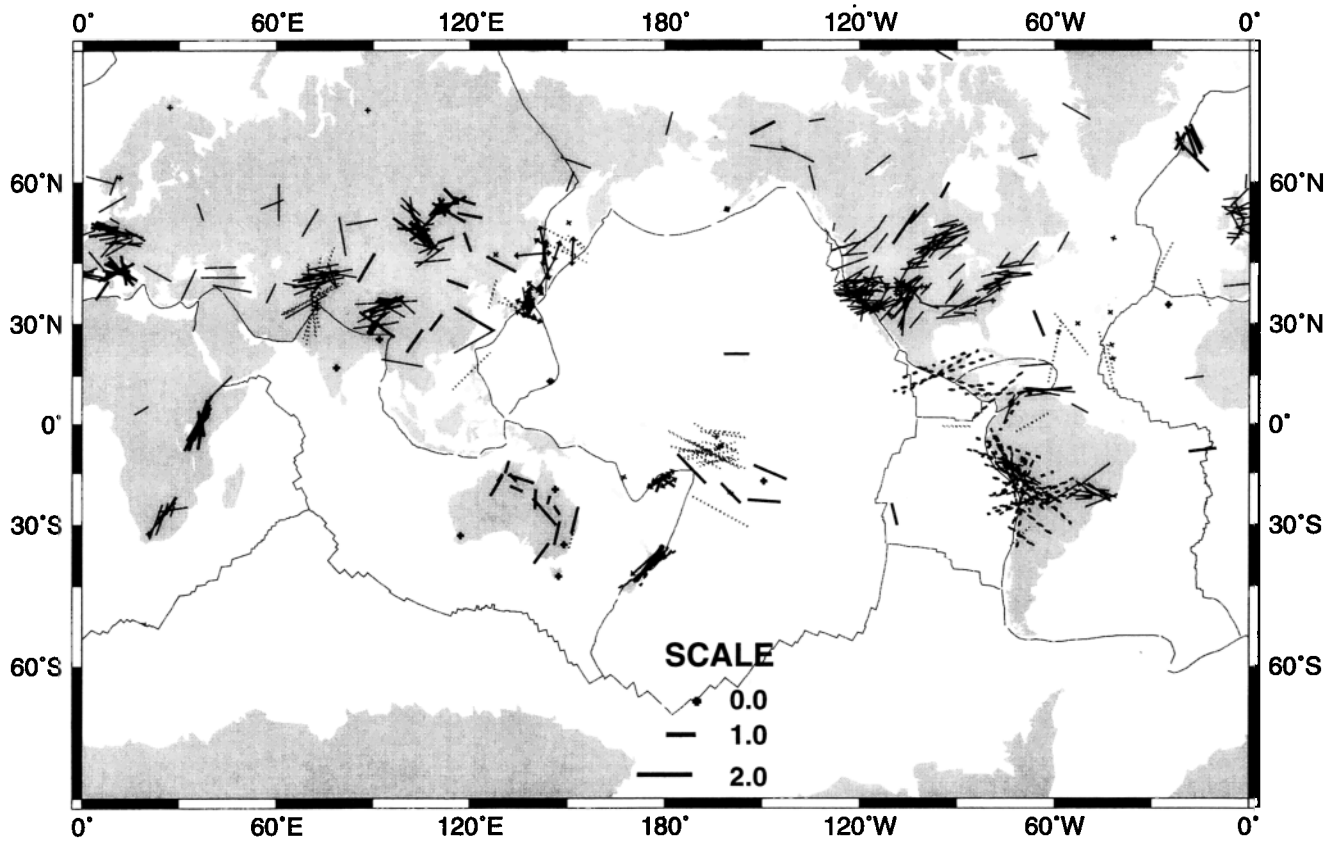

Figure 13a. Compilation of worldwide shear wave splitting measurements. Bar orientations represent ϕ, and lengths represent δt according to scale. Crosses are null measurements, as in Figure 12, with thick crosses for *SKS* data and thin crosses for *S*, *ScS*, or *SS* data. Thin solid lines are from compilation of *Silver* [1996], except that older results are deleted if later studies using more data are available. Thick solid lines are *SKS* or *SKKS* measurements not included in the work by *Silver* [1996] [*Bowman and Ando*, 1987; *Christensen et al.*, 1991; *Kuo and Forsyth*, 1992; *Alsina and Snieder*, 1995; *Bjarnason et al.*, 1996; *Menke et al.*, 1994; *Zheng and Gao*, 1994; *Díaz et al.*, 1996; *Vinnik et al.*, 1996; *Guilbert et al.*, 1996; *Margheriti et al.*, 1996; *Clitheroe and van der Hilst*, 1998; *Ellis et al.*, 1997; *Gao et al.*, 1997; *Marson*, 1997; *Sandvol et al.*, 1997; *Wolfe and Silver*, 1998; Özalaybey and Chen, submitted manuscript, 1997]. Thin dotted lines are splitting from *PS* [*Su and Park*, 1994] or *SS* [*Yang and Fischer*, 1994] phases, plotted at approximate locations of the bounce points, or local *S* waves corrected for anisotropy [*Schoenecker et al.*, 1997] or *ScS* phases [*Ando*, 1984]. Lines with arrows are splitting from *S* or *SKS* phases most probably caused by anisotropy in the mantle wedge; results from studies where data from many individual stations give similar values have been averaged and plotted at average station locations [*Ando et al.*, 1983; *Shih et al.*, 1991; *Xie*, 1992; *Fischer and Yang*, 1994, *Hiramatsu and Ando*, 1996; *Okada et al.*, 1995; *Iidaka and Obara*, 1995; *Yang et al.*, 1995; *Fouch and Fischer*, 1996; *Fischer and Wiens*, 1996; *Gledhill and Gubbins*, 1996; *Russo and Silver*, 1994; *Marson*, 1997]. Thick dotted lines are splitting from *S* or *SKS* phases most probably caused by anisotropy in the subslab mantle [*Russo and Silver*, 1994; *Kaneshima and Silver*, 1995; *Gledhill and Gubbins*, 1996; *Oda and Shimizu*, 1997; *Cassidy and Bostock*, 1996; *Fouch and Fischer*, 1996; *Marson*, 1997].

present-day plate motion. Similarly, shear wave splitting from five stations above the Mid-Atlantic Ridge in Iceland yields fast directions that are north-northwest/south-southeast, inconsistent with simple models of flow diverging horizontally in the plate spreading direction or radially from the hotspot [*Bjarnason et al.*, 1996]. These results suggest that the fast polarizations may be caused by mantle flow that is not simply coupled to surface plate motions.

In summary, some oceanic areas, particularly the Pacific Ocean, follow the "conventional wisdom" that upper layers have frozen-in fast directions parallel to past spreading (lithospheric extension) and lower layers parallel the present absolute plate motion. However, in other areas, either large-scale or small-scale asthenospheric flow may be operating to give different directions. This observation may support the modeling in which olivine *a* axes align with spreading only under fast spreading ridges [*Ribe*, 1989].

3.3.2. Rifts and oceanic spreading centers. Measurements of anisotropy within rifts do not always follow the same pattern (Figure 13). Above some rifts, ϕ is parallel to the extension direction, e.g., the Red Sea [*Vinnik et al.*, 1989a; *Hadiouche et al.*, 1989] and a few

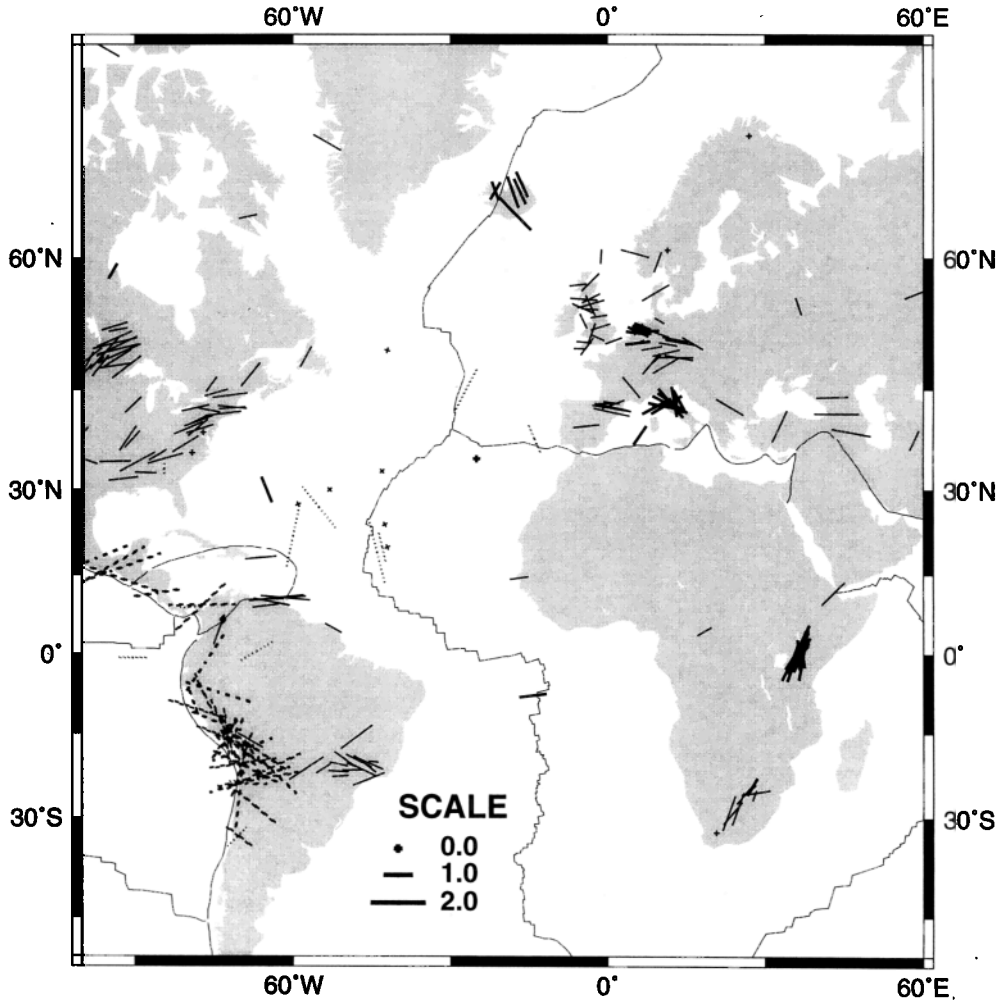

Figure 13b. Same as Figure 13a, except a closeup view of the Atlantic Ocean.

events measured above the Baikal Rift [*Gao et al.*, 1994, 1997], Ascension Island near the southern Mid-Atlantic Ridge [*Wolfe and Silver*, 1998], and the East Pacific Rise from *SKS* measurements of ocean bottom seismometer (OBS) data [*Wolfe et al.*, 1996] and from inversion of controlled-source *Pn* sources [*Dunn and Toomey*, 1997]. However, the fast direction is parallel or subparallel to other rifts, suggesting ridge-parallel flow or anisotropy controlled by fluid-filled cracks rather than olivine alignment. Examples include the Rio Grande Rift [*Sandvol et al.*, 1992], the East Pacific Rise [*Wolfe and Silver*, 1998; *Wolfe and Solomon*, 1998; *Forsyth et al.*, 1998], the proposed rifting of the French Massif Central [*Vinnik et al.*, 1992], and the East African Rift [*Gao et al.*, 1997]. Such results may be consistent with the modeling discussed in section 2.3.2, in which fast axes align with the spreading direction outside the ridge but perpendicular to spreading within the rift [e.g., *Blackman and Kendall*, 1997]. Still other regions of rifting yield ϕ neither parallel nor perpendicular to the spreading directions but possibly related to flow at depths, e.g., Basin and Range (Figure 12) [*Savage and Silver*, 1993; *Sheehan et al.*, 1997] and Iceland [*Bjarnason et al.*, 1996]. At the Mid-Atlantic rift, it has been suggested that early *P* arrivals in the center of the rift may be caused by vertical axes of symmetry [*Blackman et al.*, 1993], although large corrections of up to 0.5 s made for bathymetry cast some doubt on the argument. Similar measurements in Iceland show generally slow arrivals toward the center of the rift [*Bjarnason et al.*, 1996]. Near-vertical fast axes would be difficult to detect with *SKS* phases, but modeling results from upwelling regions suggest that they may occur [*Chastel et al.*, 1993; *Blackman et al.*, 1993].

3.3.3. Strike-slip regions. Models suggest that the anisotropy in strike-slip regions should be particularly strong because the foliation will be vertical and *a* axis orientation should be near-horizontal and parallel to the strike-slip motion (section 2.2.4). Most measurements in zones with significant strike-slip deformation are consistent with these models: the Moma rift in eastern Siberia [*Vinnik et al.*, 1992]; northern Tibet [*Holt*, 1997], the Alpine Fault in New Zealand [*Gledhill et al.*, 1996; *Audoine et al.*, 1997; *Klosko et al.*, 1997], the Caribbean–North American transform margin [*Russo et al.*, 1996], and the northern Cordillera where there are major transcurrent fault systems [*Bostock and Cassidy*, 1995].

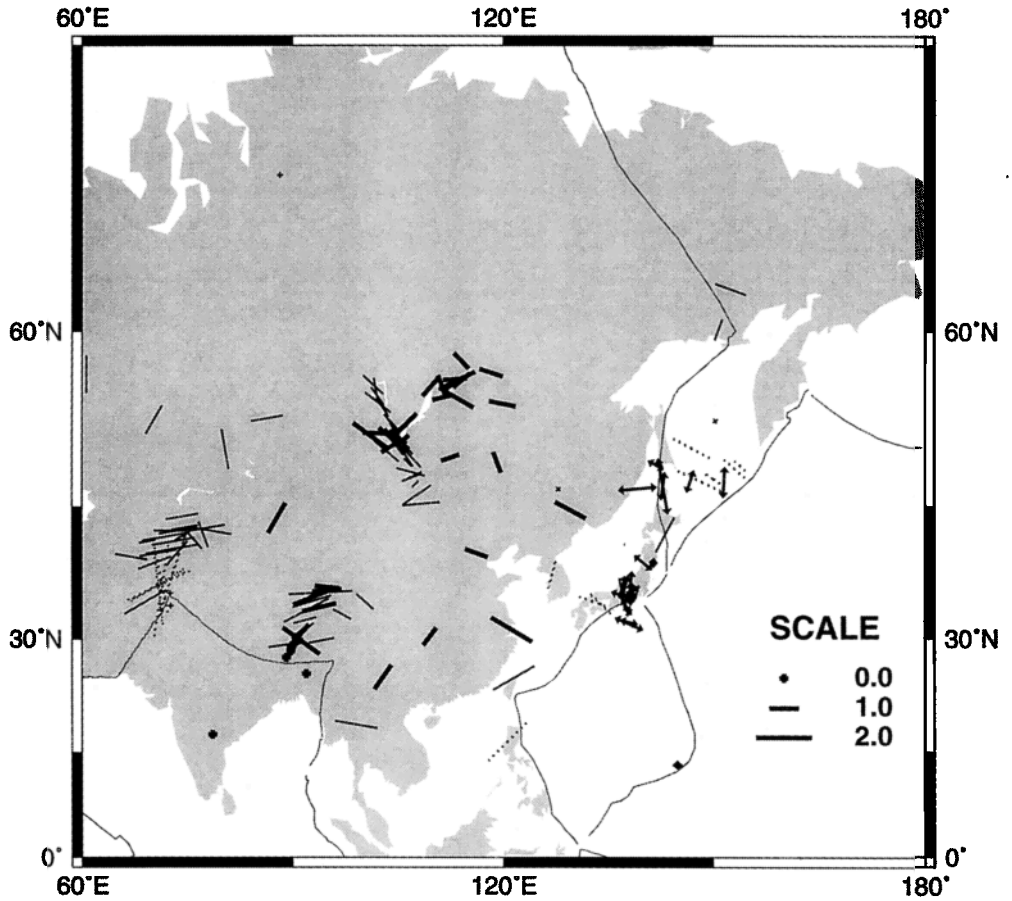

Figure 13c. Same as Figure 13a, except a closeup view of the northwestern Pacific/Eurasia.

An exception is that ANTO, 100 km from the strike-slip North Anatolian fault in Turkey, yielded ϕ not parallel to the fault [*Vinnik et al.*, 1992]. It may be that the transcurrent motion at depth is confined to a region narrower than 100 km. Measurements along the San Andreas Fault are somewhat contradictory, although they are explained well by confining the transcurrent motion to an area <50 km wide and allowing two layers of anisotropy beneath the fault. Individual measurements at stations along the San Andreas Fault from earthquakes with different incoming polarizations yield different results [e.g., *Ansel and Nataf*, 1989; *Vinnik et al.*, 1989a, 1992]. *Savage and Silver* [1993] model these variations by two layers of anisotropy with fast axes at different azimuths (Figure 10). The measured apparent splitting parameters have a period of 90° with incoming polarization; such periodicity is characteristic of double layers and is not seen with orthorhombic symmetry or with dipping layers [*Silver and Savage*, 1994] (Figure 4). The top layer yields a fast direction nearly parallel to the San Andreas Fault and a splitting of 1.0 ± 0.5 s. The lower layer has fast axis oriented E-W, 45° to the fault, with splitting of 1.4 ± 0.5 s [*Savage and Silver*, 1993; *Özalaybey and Savage*, 1994, 1995; *Silver and Savage*, 1994]. The upper 16 km of crust supplies less than 0.2 s of splitting [*Zhang and Schwartz*, 1994]. Phases converted from *P* to *S* at the Moho do not show the patterns on the transverse component expected if a highly anisotropic lower crustal layer were present [*Savage et al.*, 1996a]. Therefore the upper layer of anisotropy is probably in the mantle lithosphere. This pattern disappears between the stations and those 150 km to the east, so the upper layer is at least less than 150 km wide, and probably narrower [*Özalaybey and Savage*, 1995].

Savage and Silver [1993] and *Özalaybey and Savage* [1995] hypothesize that the upper anisotropic layer is caused by the lithospheric strain associated with the San Andreas Fault, while the lower layer is caused by E-W flow in the asthenosphere. A more attractive hypothesis uses recent laboratory results to explain the anisotropy in both layers by the same strike-slip mechanism. Olivine aggregates deformed in simple shear orient with fast axes parallel to the strike-slip direction for strains greater than about 50–75% but parallel to the minimum principal stress and at 45° to the plane of strike-slip deformation for smaller strain [*Zhang and Karato*, 1995]. Thus, if the amount of deformation decreases with depth as the asthenosphere is gradually less coupled to the surface, then the change to E-W in the lower layer is the correct orientation. The two-layer model is thus considered as a simple approximation to a continuous change with depth. This suggestion has the added advantage

that it could explain the E-W fast layer beneath the rest of California and the western Basin and Range (Figure 12) [*Savage and Silver*, 1993; *Özalaybey and Savage*, 1995; *Liu et al.*, 1995] by San-Andreas-Fault-parallel strain less than about 50–75% at mantle depths off the main fault trace. Preliminary evidence in New Zealand, where strain has been acting for a longer time and where the plate is more strongly coupled, yields large, consistent fault-parallel motion across the width of the South Island [*Audoine et al.*, 1997; *Klosko et al.*, 1997].

Plomerovà et al. [1996] invert teleseismic *P* residuals and splitting measurements along the San Andreas for dipping layers and both orthorhombic and hexagonal symmetry and conclude that dipping layers of anisotropy fit the *P* wave data and the *SKS* splitting results. However, they do not model the observed periodicity of the splitting data with incoming polarization direction, and they do not take into account the large effects expected from the heterogeneity of *P* waves coming through the Pacific Plate on one side and the continental United States on the other side.

3.3.4. Subduction zones. Subduction zones provide a wealth of earthquakes with which to study anisotropy but are complicated by the variations of stress, strain, and structure with depth that might produce different amounts and directions of anisotropy (Figure 7). Fast polarizations of *ScS* perpendicular to the trench in Japan and South America [*Ando*, 1984; *Oda and Shimizu*, 1997] are consistent with 200 s Rayleigh waves [*Tanimoto and Anderson*, 1984] and with the slab entrainment model of *Ribe* [1989]. However, *SKS* and *S* results for stations above subduction zones often yield fast polarizations parallel to the plate boundary [e.g., *Milev and Vinnik*, 1991; *Shih et al.*, 1991; *Silver and Chan*, 1991; *Vinnik et al.*, 1992; *Vinnik and Kind*, 1993; *Russo and Silver*, 1994], perpendicular to the expected direction for anisotropy according to models of two-dimensional flow associated with entrainment of lithosphere due to a subducting slab [*Ribe*, 1989]. The most likely source of anisotropy was initially thought to be in the mantle above the slab. Trench-parallel anisotropy was considered evidence of strike-slip deformation and compression in the upper plate. This contributed to the common wisdom that compression yields fast polarizations parallel to the compression direction, either directly through alignment of olivine *b* axes parallel to the direction of maximum compression or through margin-parallel shear associated with convergence [e.g., *Silver and Chan*, 1991; *Vinnik et al.*, 1992].

Other results are more complicated. *Fischer and Yang* [1994] found large spatial variations in splitting parameters estimated from *sS-S* pairs in the Kuril-Kamchatka subduction zone. New studies are beginning to separate contributions from the crust, mantle wedge, slab, and subslab mantle and are changing our interpretations.

Above subduction zones, anisotropy as high as 4% (0.2 s splitting) for paths confined to the crust above 11 km has been observed and interpreted as caused by near-surface, vertical, parallel, aligned cracks [e.g., *Gledhill and Stuart*, 1996]. Some investigators have suggested that water- or melt-filled cracks in the crust and mantle above subduction zones may cause splitting of 0.35–0.5 s and anisotropy up to 2.3% in regions as deep as 50 km [*Cassidy and Bostock*, 1996] or even 50–150 km depth [*Iidaka and Obara*, 1995]. Other studies suggest only small amounts of anisotropy in the crust; there is less than 1% anisotropy measured from the crust in the northwest Pacific [*Fouch and Fischer*, 1996], less than 0.1 s of splitting from the combined effects of the crust and mantle above 120 km in Colombia [*Savage et al.*, 1989; *Shih et al.*, 1991], and less than 0.5% anisotropy in the uppermost 100 km of crust and mantle wedge beneath Peru [*Kaneshima and Silver*, 1995].

Both the strength and orientation of anisotropy in the mantle wedge vary between subduction zones and possibly with depth. The strength of anisotropy for vertically traveling *S* waves varies from nearly isotropic (less than 0.1 s in the upper 120 km beneath Colombia [*Shih et al.*, 1991], 0.5% in upper 100 km beneath Peru [*Kaneshima and Silver*, 1995]) to intermediate anisotropic strengths (0.5% to 1.1% in back arc regions of the northwest Pacific subduction zones [*Fouch and Fischer*, 1996], 1% in the Aleutians [*Yang et al.*, 1995], 1.5% in a region west of the volcanic front above Japan [*Okada et al.*, 1995]), to higher values (2% in the wedge between 100 and 180 km depth beneath Colombia [*Shih et al.*, 1991], 3% in a region east of the volcanic front in Japan [*Okada et al.*, 1995]). The fast polarizations also vary, from roughly parallel to the strike of the trench (Japan [*Ando et al.*, 1983; *Hiramatsu and Ando*, 1996; *Fouch and Fischer*, 1996], east of the volcanic front in Japan [*Okada et al.*, 1995; *Sandvol and Ni*, 1997], Fiji [*Bowman and Ando*, 1987], Colombia [*Shih et al.*, 1991], Aleutians [*Yang et al.*, 1995], Alaska and northern Canada [*Silver and Chan*, 1991; *Bostock and Cassidy*, 1995], and New Zealand [*Marson-Pidgeon and Savage*, 1997]) to subparallel to back arc extension directions (Kuril Basin [*Fischer and Yang*, 1994], Fiji [*Bowman and Ando*, 1987; *Fischer and Wiens*, 1996], Marianas [*Xie*, 1992], Tonga and Izu-Bonin [*Bowman and Ando*, 1987; *Fischer and Wiens*, 1996; *Fouch and Fischer*, 1996]), to parallel to convergence or slab dip direction (west of the volcanic front in Japan [*Okada et al.*, 1995; *Sandvol and Ni*, 1997], Kuril Islands [*Fischer and Yang*, 1994; *Su and Park*, 1994], Tonga [*Bowman and Ando*, 1987]), to parallel to strikes of major shear systems (northern Canada [*Bostock and Cassidy*, 1995] and northern Japan Sea and Sakhalin Island [*Fouch and Fischer*, 1996; *Sandvol and Ni*, 1997]. Some areas fit several of these possibilities.

These results diminish the argument that fast axes parallel to present plate boundaries are caused by coherent deformation of the lithospheric mantle. While there is a tendency for fast axes in environments of oblique convergence to be subparallel to the slab strike and for fast axes in back arc extension areas to be parallel to the extension, these angles are not always

consistent [e.g., *Fischer and Wiens*, 1996]. The variability between subduction regions suggests lithospheric strain or asthenospheric flow that depend upon local effects [*Fouch and Fischer*, 1996].

Fast polarizations of *SKS* phases measured above the Juan de Fuca Plate are nearly perpendicular to those from shallow crustal anisotropy in the region and are attributed to strong convergence-parallel anisotropy caused by mantle flow parallel to the subduction of the Juan de Fuca Plate [*Bostock and Cassidy*, 1995; *Cassidy and Bostock*, 1996]. This is one of the few areas where the expected corner flow around subducting slabs [*Ribe*, 1989] can explain the observed *SKS* fast polarizations.

Lack of accurate earthquake depths and of knowledge of slab structure limits determinations of within-slab anisotropy, but it has been examined in some regions. In the Hikurangi margin at New Zealand, anisotropy within the slab approaches 1.4% and is similar in direction to the anisotropy below the trench [*Gledhill and Stuart*, 1996]. Anisotropy in the slab beneath Peru is estimated to be small because the slab is thin and because anisotropy from combined effects of slab and lower mantle does not show patterns expected from two layers [*Kaneshima and Silver*, 1995]. In Japan, anisotropy has been confined to the slab by comparing splitting of *ScS* phases from deep earthquakes at different depths with *S* wave splitting from deep events [*Hiramatsu and Ando*, 1996; *Hiramatsu et al.*, 1997]. Events above 400 km yield fast polarizations below the events that are parallel to the fossil spreading within the slab. Events deeper than 400 km yield fast polarizations parallel to current plate motion and parallel to pressure axes from centroid moment tensor (CMT) solutions. They suggest that stress accompanying the phase transition from olivine (α phase) to modified β spinel reorients the fast direction below the transition. Anisotropy in the slab is estimated to be 5%, based on a splitting of 1.0 s and a slab thickness of 100 km [*Hiramatsu et al.*, 1997].

Much of the trench-parallel anisotropy observed at subduction zones appears to be in the subslab asthenosphere rather than in the lithosphere above the slab (e.g., New Zealand [*Yu and Park*, 1994; *Gledhill and Stuart*, 1996; *Gledhill and Gubbins*, 1996], South America [*Vinnik et al.*, 1992; *Russo and Silver*, 1994; *Kaneshima and Silver*, 1995], Tonga [*Yu and Park*, 1994]. (Japan and New Zealand may have trench-parallel anisotropy both above and below the slab [*Marson*, 1997; *Fouch and Fischer*, 1996; *Vinnik and Kind*, 1993].) This agreement suggests that the model of slabs acting as barriers to asthenospheric flow is plausible. The anisotropy below the slab may also be variable, however. Consistent fast polarizations and anisotropy of 1.4% determined for local earthquakes recorded in New Zealand [*Gledhill and Stuart*, 1996] contrast with variable polarizations and splitting of from 0.8 to 4.0 s for teleseismically recorded earthquakes originating in the South American slab [*Russo and Silver*, 1994]. A poor correlation between depth and delay time does not allow an average anisotropy to be determined for South America, but if it is assumed the anisotropy lies between the earthquakes and a depth of 400 km, then the values published by *Russo and Silver* [1994] yield anisotropy of between 0.4% and 13.5%, decreasing to 0.2% to 4.5% if the anisotropy reaches to 600 km depth.

New evidence of frequency dependence at one station above a subduction zone suggests that these arguments may need to be revisited [*Marson-Pidgeon and Savage*, 1997]. If high frequencies give smaller splitting than low frequencies, then the small amount of anisotropy reported for the mantle wedge in many regions may simply occur because only high-frequency, local events have been used to measure the anisotropy. Then the corrections of teleseismic arrivals for the local structure may be too small, and inferred high anisotropy beneath the slabs may be in error. However, studies such as those of *Russo and Silver* [1994] and *Schoenecker et al.* [1997] that use teleseismic arrivals from events in the slab will not be affected by these concerns (e.g., Figure 7), although they are still affected by the problems of removing receiver-side anisotropy.

3.3.5. Anisotropy beneath continents. *Silver* [1996] gives a comprehensive review of continental anisotropy. Some of the most outstanding features are presented here.

The collision between the Indian and Eurasian Plates occurring in Tibet is the only widespread present continent-continent collision region. Shear wave splitting results of *McNamara et al.* [1994] are nearly identical in azimuth to the shear flow component of a horizontal strain field calculated from an inversion of earthquake moment release and Quaternary fault slip rates [*Holt et al.*, 1995; *Holt*, 1997]. They are also broadly consistent with orientations of maximum horizontal elongations in the finite strain calculated for a model of indentation of Asian lithosphere by India [*Davis et al.*, 1997]. Other splitting results near this region are also consistent with the Holt et al. model [*Makeyeva et al.*, 1992; *Zheng and Gao*, 1994; *Hirn et al.*, 1995; *Guilbert et al.*, 1996; *Lavé et al.*, 1996], although surface waves suggest some variability [*Yu et al.*, 1995; *Griot et al.*, 1995] and little splitting is observed in the southwestern part of the region [*Sandvol et al.*, 1997] (Figure 13). The coherence of splitting with crustal strain supports the coherent lithospheric deformation model for modern continental collisions. Delay times are variable in the region, ranging from less than 0.6 s to 2.4 s in the region near Tibet. To the northwest, in the Pakistan Himalayas, little splitting of *SKS* phases is measured [*Sandvol et al.*, 1994]. However, only 100 km away, source-side splitting of 2.5–3.5 s for earthquakes of about 100 km depth and 2.5 s for earthquakes of about 200 km depth is interpreted as being caused by complicated mantle strain beneath and between the Hindu Kush and Pamir slabs [*Schoenecker et al.*, 1997].

In other continental regions where present tectonic activity is taking place, there are also complications. In much of the western United States, ϕ appears unrelated

to the surface tectonic features of the past or present [e.g., *Savage and Silver*, 1993; *Özalaybey and Savage*, 1995; *Sheehan et al.*, 1997] (Figure 12). In southern Europe, many interpretations consider anisotropy to be controlled by past geologic events or plate boundary activities [*Vauchez and Barruol*, 1996; *Barruol and Souriau*, 1995; *Margheriti et al.*, 1996], but others consider absolute plate motion [*Vinnik et al.*, 1992] or more complicated flow patterns to dominate [*Díaz et al.*, 1996] (Figure 13).

In the study of continental cratons, there is a current debate about whether anisotropy is parallel to past geologic features and caused by anisotropy in the lithosphere that has remained frozen since the Archean [*Silver and Chan*, 1991; *Silver*, 1996] or whether it is parallel to present absolute plate motion and caused by asthenospheric flow [*Vinnik et al.*, 1992, 1995b, 1996]. *Silver and Chan* [1991] and *Silver* [1996] argue convincingly that much of the anisotropy measured above older continental regions gives fast axes parallel to surface structural features, suggesting that the anisotropy may have been formed at the same time as those features. They argue that the anisotropy is too large to be caused by the crust alone and therefore that lithospheric coherent deformation from past orogenic episodes best explains the measurements. The argument supports the idea of a "tectosphere" (a chemical boundary layer that is stable and does not deform) beneath the continents [*Jordan*, 1978]. However, *Vinnik et al.* [1992] point out that if anisotropy frozen into the lithosphere disappears at depths below that of the 900° isotherm, then shear wave anisotropy of 5% in the lithosphere would be required to explain the splitting data with current models of isotherm depth. Hexagonal symmetry with a horizontal symmetry axis would cause anisotropy of 5–10% in *Pn* that should have been observed in long-range refraction profiling but was not. Anisotropy from surface waves at depths of 300 km is larger beneath continents than beneath oceans [*Montagner*, 1994]. Measurements in subduction zones suggest that anisotropy extends well below 200 km and includes values lower than 4% (sections 3.1.3 and 3.3.4). These arguments suggest that there may be anisotropy present beneath continents at depths usually associated with the asthenosphere.

Gaherty and Jordan [1995] constrain the anisotropy for a radially anisotropic model for a corridor across Australia to be less than 300 km. They propose that a stable tectosphere exists down to >300 km beneath the Australian craton. In this model, regions at high temperatures >900°C do not necessarily imply a resetting of mantle anisotropy because the tectosphere is stable and does not deform easily. The parallelism with structure is explained as transcurrent deformation following arguments of *Vauchez and Nicolas* [1991] and is consistent with data in Tibet for continent-continent collisions [*Holt et al.*, 1995; *Holt*, 1997]. In much of North America and South Africa the geologic structures also tend to be parallel to present absolute plate motion directions, in contrast to South America, where the fast polarizations are parallel to geologic features rather than to the absolute plate motion [*James and Assumpção*, 1996]. Shear wave splitting around the northern Atlantic is explained well by frozen anisotropy from episodes occurring before the opening of the Atlantic [*Barruol et al.*, 1997]. This, and the rapid variation of anisotropy in short spatial scales in many mantle regions and across past tectonic boundaries [e.g., *Babuška et al.*, 1993; *Silver*, 1996], suggests that absolute plate motion cannot be the only factor explaining anisotropy beneath cratons.

If it is so difficult to determine whether lithospheric deformation or asthenospheric deformation causes splitting, then perhaps they are both a cause and perhaps asthenospheric flow is being channeled along the topography at the base of the lithosphere. This was suggested as an explanation for anisotropy in central Europe [*Bormann et al.*, 1996] and is consistent with the new evidence of flow channeling around subduction zones.

3.4. What Are the Big Questions Left to Be Answered?

3.4.1. Where is anisotropy really occurring? Initially, it appeared that splitting observed in teleseismic phases is caused mainly by anisotropy in the upper mantle above the Lehmann discontinuity. Recent results suggest that in some subduction zones, anisotropy extends at least to the olivine-spinel transition at 400 km. Tantalizing evidence of anisotropy in the transition zone, in the D″ layer, and possibly large anisotropy in the crust should be evaluated more fully. Particularly areas with ϕ paralleling crustal shear zones should be evaluated carefully to rule out any contribution from the crust. Investigation of phases converted at the Lehmann discontinuity might resolve some of the controversy about whether it is a boundary between isotropic and anisotropic structures, related to a change of deformation mechanism, or whether it represents a change in anisotropic structure, possibly as a boundary between frozen-in past anisotropy and present strain.

3.4.2. What causes the observed variations of splitting parameters? In a number of regions, varied results are obtained for measurements at different back azimuths or for closely spaced stations or both. Are discrepancies due to lateral variation in anisotropy, to complicated symmetry systems such as dipping layers, multiple layers of anisotropy, or all of the above? Certainly, a rapid variation of parameters seen between stations suggests that an understanding of how lateral variations in anisotropy affect splitting measurements will be necessary. A thorough mapping of splitting at a small scale may help to resolve some of the discrepancies between closely spaced stations, such as in the Basin and Range [*Sheehan et al.*, 1997] and NARS_NL array (a portable digital broadband array) in western Europe

[*Alsina and Snieder*, 1995], and the Baltic Shield [*Plomerovà et al.*, 1996]. Unfortunately, the limitation of earthquake sources to certain active areas in the Earth suggests that even with closely spaced stations recording for a long time, we may need to look at combining other methods such as using phases converted at other discontinuities, correcting for phases outside the *shear wave window* (e.g., using methods by *Tsvankin and Chesnokov* [1990]), and correcting *ScS* phases for the phase changes at the core-mantle boundary. Also, combining splitting with tomographic studies using *Pn*, teleseismic *P* and *S*, and surface waves could enhance understanding of anisotropy. However, understanding anisotropy may also help to explain some of the tomographic results, perhaps leading to simpler tectonic models [e.g., *Babuška et al.*, 1993; *Plomerovà et al.*, 1996]. These methods can help to answer the question, does shear on vertical, horizontal, or dipping planes (or all three) cause the most anisotropy?

3.4.3. Is anisotropy telling us about mantle flow or lithospheric deformation, or both (or neither)? Shear wave splitting studies usually rely on comparison of the average fast polarizations with other directions, such as absolute or relative plate motions, stress, or geologic fabric, often by plotting the directions on a map and "eyeballing" the fit. However, in any given region, there are many possible orientations to consider, and geologic or geophysical reasoning must be invoked to narrow the possibilities. Second, the three-dimensional nature of anisotropy is usually ignored. Third, the scatter in the splitting fast polarizations often yields a wide range of azimuths that could be considered to be parallel or subparallel to some other direction. This problem is similar to a problem with focal mechanism studies, in which *Frohlich and Willemann* [1987] showed that with two nodal planes and random mainshock-aftershock distributions, the average event would align "close to" one of the nodal planes. Using rigorous statistical analysis to compare measured fast polarizations from large data sets with proposed orientations from physical models could help to overcome these problems. Also, statistics of orientation data, such as the Rayleigh test and Fisher statistics, should be applied when calculating averages and comparisons with other directions [e.g., *Mardia*, 1972].

The rapidly increasing volume of anisotropy data may soon be large enough to apply averaging and comparison techniques on a worldwide scale, such as those used in examining stress [*Zoback*, 1992; *Bird and Li*, 1996]. The principal stress directions from the World Stress Map are readily available [*Zoback*, 1992]. Absolute plate motions at any spot can be calculated from plate motion parameters [*Gripp and Gordon*, 1990]. Independent databases of the dominant structural grain in each continental region and of fossil seafloor spreading directions in oceanic regions could be used for global interpretations of structural data as well as for comparison with anisotropy. The method of *Holt et al.* [1995], in which the shear flow component of a horizontal strain field is calculated from an inversion of earthquake moment release and Quaternary fault slip rates, provides a means of quantitatively comparing shear wave splitting with crustal strain in seismically active regions.

3.4.4. What is the role of more sophisticated techniques for examining anisotropy? This study has concentrated mainly on observations of anisotropy. However, new techniques in computing synthetic seismograms in general anisotropic media are being developed that will help to model observations. Some examples are methods for using body wave ray tracing [*Kendall and Thomson*, 1989] and Maslov synthetics [*Kendall and Thomson*, 1993; *Martin and Thomson*, 1997] and methods of calculating waveforms singularities [*Rumpker et al.*, 1997]. Such improvements will allow workers to develop connections between seismic data and realistic synthetic seismograms for heterogeneous anisotropic Earth models.

3.4.5. What tectonic problems remain to be answered? Fundamental questions to address with shear wave splitting are as follows: What is the role of the mantle in orogenesis, how does the mantle at cratons or the tectosphere evolve, and how does convection take place in the lithosphere and asthenosphere? Focused investigations in interesting tectonic regions will provide data to address these questions. To allow for complexity, data from a wide variety of back azimuths are needed, and stations used for shear wave splitting should be in place for at least 6 months, preferably for a year or more.

Some detailed questions are as follows:

1. How does convection take place at subduction zones? The wealth of local earthquakes at subduction zones should allow the best characterization of anisotropy as a function of depth. Already much progress is being made in this area (sections 3.1.3 and 3.3.4), but large scatter suggests that more short-term, broadband experiments will be needed for a complete characterization of subduction zones. Possible frequency dependence must be examined and explained.

2. How does mantle deformation change as the boundary changes from subduction or spreading to transcurrent motion? California, Oregon, New Zealand, and Mexico are excellent places to look at this problem.

3. How wide are strike-slip zones at depth? The variation in anisotropy across fault regions must be characterized in other places to supplement the studies done in California and New Zealand (section 3.3.3).

4. How does convection take place at oceanic spreading centers and continental rifts? Several rifts have been characterized [e.g., *Davis et al.*, 1997], but varied results suggest more measurements are needed.

5. What is the pattern of mantle flow at hotspots? The few measurements so far (Iceland [*Bjarnason et al.*, 1996] and Hawaii [*Wolfe and Silver*, 1998]) do not yield the expected radial flow.

4. CONCLUSIONS

The high-resolution of *S* wave splitting measurements yield much more information than was available from global averages of *S* waves or from *Pn* and detailed surface wave studies. Anisotropy of up to 4% is prevalent throughout the upper 200 km of the mantle and is highly variable in orientation, and possibly in magnitude. Transcurrent deformation in the lithosphere causes strong splitting with fast polarizations parallel to the faulting. Orientation of foliation planes parallel to the plate boundaries and near-horizontal lineation of olivine explain these observations well.

Other conventional models of mantle dynamics are challenged by shear wave splitting measurements, with three particularly important examples: (1) Fast polarizations assumed to originate from mantle anisotropy are parallel to the structural fabric of the crust, suggesting that deformation has been coherent throughout the lithosphere. Such parallelism between the crust and mantle in Archean cratons has further been interpreted as evidence that the mantle, down to at least 200 km, like the crust, has remained undeformed since the Archean. (2) In some subduction zones, fast polarizations for shear waves with paths beneath and above the slab are parallel rather than perpendicular to the strike of the subduction zone. This suggests that rather than the slab entraining the mantle surrounding it and pulling it downward in the direction of plate motion as has been previously assumed, the slabs may instead be acting as a barrier so that the asthenosphere flows parallel to the slab. Other possible explanations are that strain in the bending lithospheric plate may be causing the observed anisotropy or that three-dimensional anisotropic structure is being mismapped into the horizontal dimension [*Babuška et al.*, 1993]. (3) In spreading centers, fast polarizations do not always have a simple relation to the spreading direction. Simple models of mantle flow may need to be rethought to incorporate three-dimensional patterns of flow. These differences are important in understanding the tectonics of rifting, subduction, and mountain building, as well as in providing constraints for modeling of asthenospheric flow and mantle convection.

There are still many questions that need to be resolved. Frequency dependence has been largely ignored. Lateral variations in anisotropy appear to be ubiquitous, and techniques for incorporating those variations in shear wave splitting studies as well as in tomographic modeling need to be more widely developed and applied. Complexity from anisotropy such as orthorhombic symmetry and dipping axes of symmetry also needs to be addressed [e.g., *Plomerovà et al.*, 1996]. Lack of vertical resolution leaves unresolved the source of the anisotropy. Initial interpretations that anisotropy in the mantle is confined to the upper 200 km are being challenged by measurements in subduction zones, which suggest that anisotropy extends into the transition zone in some regions, and by measurements of anisotropy in the D″ layer at the base of the mantle. While the fast polarizations are reasonably robust and are most likely related to the horizontal components of either mantle strain or flow, the dip is not well resolved. Examining variations in splitting parameters with back azimuth and between stations and comparing with other measures of velocity should help to separate effects of depth and lateral variations and the orientation of the strain ellipsoid.

APPENDIX: ANISOTROPY MINITUTORIAL

Perhaps the most straightforward manifestation of anisotropy occurs when measurements of wave speed carried out at different azimuths yield different results. This is often called azimuthal anisotropy. Early observations were for azimuthal anisotropy of oceanic *Pn* waves, i.e., waves that refract and travel along the top of the mantle just below the crust-mantle boundary, the Moho [*Hess*, 1964] (Figure 2). Surface waves measured along different azimuths can also characterize azimuthal anisotropy [e.g., *Forsyth*, 1975; *Schlue and Knopoff*, 1977; *Montagner and Tanimoto*, 1991]. The depth distribution of anisotropy can be found by examining surface wave anisotropy as a function of period and by examining *Pn* anisotropy at varying distance ranges. The vertical resolution of azimuthal anisotropy measurements is exploited in areas such as the oceanic floor that are believed to have slowly varying seismic properties over a wide region. For studies of azimuthal anisotropy, there are trade-offs between the effects of isotropic lateral heterogeneity and anisotropy. For instance, strong lateral heterogeneity in the crust could be misidentified as azimuthal anisotropy in the mantle [*Babuška and Cara*, 1991; *Montagner*, 1994]. A recent example is the ongoing debate about the anisotropy in the mantle lid beneath the Basin and Range in the western United States. *Beghoul and Barazangi* [1990, 1995] use earthquake arrival times to determine *Pn* fast directions parallel to the present spreading direction. *Zhao* [1993, 1995] explains a similar data set by lateral variations of isotropic material. *Hearn* [1996] explains it by a combination of anisotropy and lateral variation. While *Hearn*'s [1996] study compares favorably in some areas with published *SKS* results, it does not agree in many other areas. At this point, none of the models seems to be most compelling.

Polarization anisotropy occurs when phases of different polarization travel with different speeds. Examples are (1) horizontally polarized surface waves (Love waves) that are faster than surface waves polarized in a vertical plane (Rayleigh waves) [e.g., *Anderson*, 1961], (2) global average travel times of *SH* phases that are faster than *SV* [e.g., *Shearer*, 1991; *Earle and Shearer*, 1994], and (3) shear wave splitting. Compared to azimuthal anisotropy, polarization anisotropy is less sensitive to heterogeneous isotropic structure.

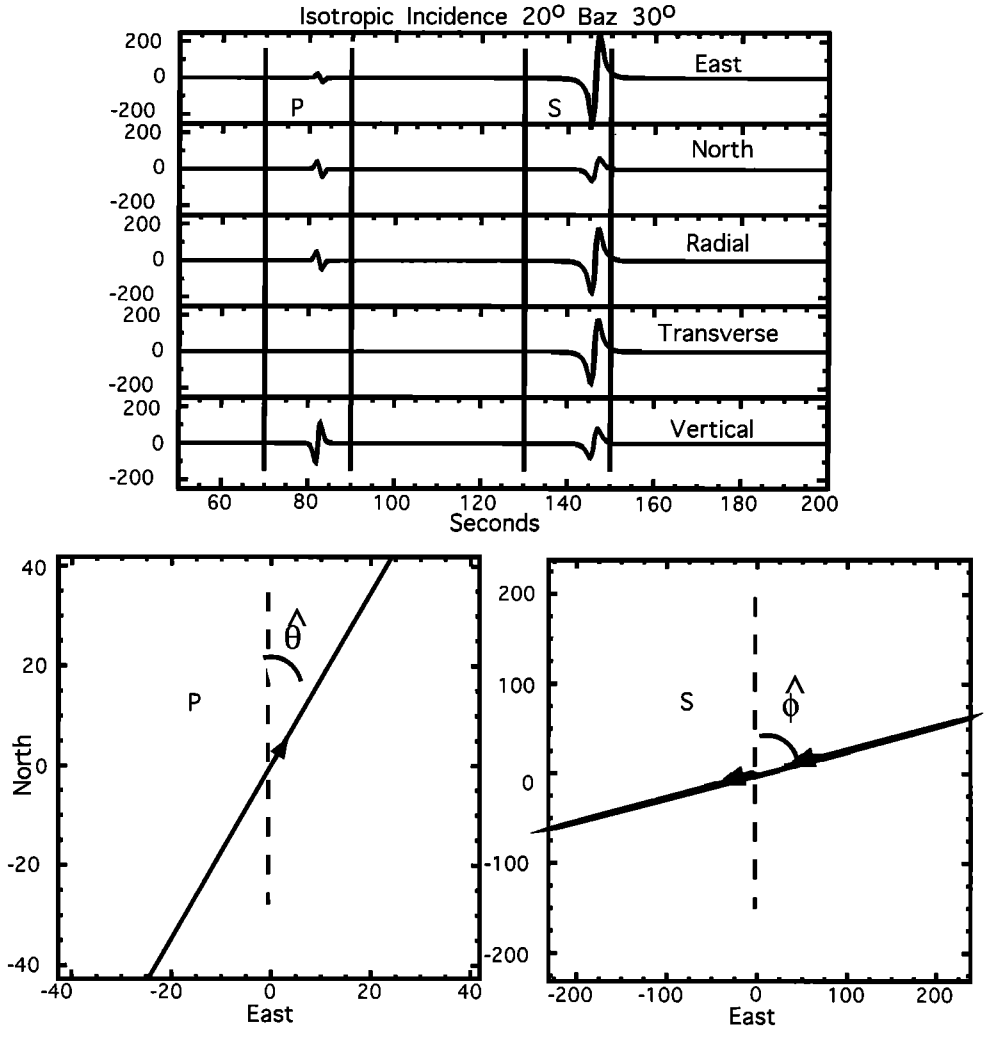

Figure A1. Synthetic seismogram for isotropic propagation at a 20° incidence angle from the vertical, with back azimuth 30°. (top) Seismogram rotated into east, north, radial, transverse, and vertical components. Note the lack of *P* wave energy on the transverse component. (bottom) Particle motion in the N/E plane for *P* and *S* time windows shown at top. Arrows show direction of increasing time; $\hat{\theta}$ is *P* wave particle motion polarization; $\hat{\phi}$ is *S* wave particle motion polarization.

A1. Explanation of Shear Wave Splitting

Shear wave splitting is a fundamental property of anisotropic media, and its analysis allows us to circumvent the problem of the trade-off between lateral variations and anisotropy. First, it is useful to review isotropic wave propagation.

In an isotropic elastic medium, the *P* and *S* waves propagate with mutually orthogonal polarizations and with different phase velocities (Figure 1). While the longitudinal *P* wave particle motion is set by the propagation direction, the transverse *S* polarization can be in any direction in the plane perpendicular to the propagation direction. For earthquake sources, the *S* wave polarization depends on the focal mechanism [e.g., *Aki and Richards*, 1980]. The plane that joins the source and receiver along a great circle through the center of the Earth is often called the *sagittal plane*. In an isotropic Earth with wave speeds varying only with depth, the ray propagation, or direction of energy transport, is within the sagittal plane. The component of *S* motion in the plane of propagation is termed the *SV* phase, and the orthogonal component is the horizontally polarized *SH* phase. Horizontal seismograms are often rotated into *radial*, parallel to the earthquake-station back azimuth and transverse, perpendicular to the radial. For an isotropic medium varying only with depth, the vertical and radial components each record both *P* and *SV* waves, while the transverse component measures only *SH* waves. A general *S* wave in an isotropic medium has both an *SV* and an *SH* component; the amplitude of each component depends upon the polarization direction (Figures 1 and A1).

In addition to seismograms, which plot the particle motion as a function of time, seismologists may examine *polarization diagrams*, which plot the components of motion against each other (Figure A1). Polarization

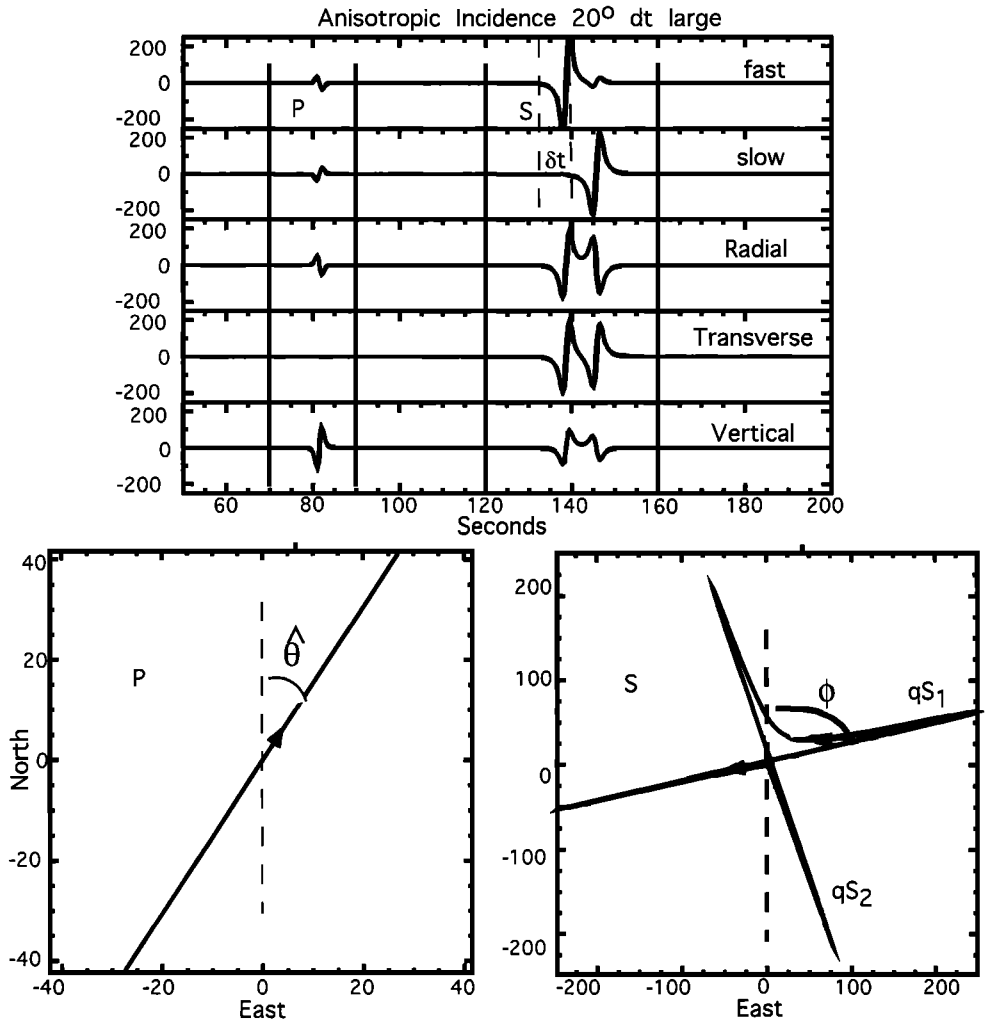

Figure A2. (top) Synthetic seismogram as in Figure A1, but for anisotropic propagation with δt large compared to the period, rotated into fast, slow, radial, transverse, and vertical components. Note the small energy on the transverse component for *P* wave energy and the complex *S* waveform that is simpler when rotated into fast and slow directions, with a time separation δt between the fast and slow waveform. (bottom) Particle motion in the N-E plane for *P* and *S* windows shown at top. The cruciform shape is diagnostic of *S* wave splitting; $\hat{\theta}$ is *P* wave particle motion; ϕ is fast polarization.

diagrams have been called by other names such as *hodograms*, or the familiar lissajous figures of electronic applications. Each point in the polarization diagram represents a single point in time and represents the amplitudes of two components of a seismogram at that time. Often arrows on the diagrams show the direction of increasing time. The polarization diagram of a *P* wave should be a line, and the particle motion is linear; in a N-E diagram, the angle between the north axis and the line is equal to the *P* wave particle motion direction, which should be the earthquake-station back azimuth with a 180° ambiguity. The *S* wave particle motion for an isotropic medium should also be linear. However, for *S* waves the angle between north and the line depends upon the polarization of the *S* wave, which is controlled by the geometry of the earthquake faulting (the focal mechanism), except for special cases such as for phases converted from *P* to *S* at a boundary, as discussed in section A2.

In an anisotropic medium, wave propagation is more complicated. There are three plane waves that propagate with three different speeds and with mutually perpendicular polarizations (Figures 1 and A2). These polarizations are no longer strictly parallel or perpendicular to the direction of energy propagation. However, for most rocks the particle motion is no more than 10° away from parallel and perpendicular to the propagation direction. Because of this near parallelism, the three waves are often referred to as the quasi-*P* and quasi-*S* waves, and sometimes the qualifier "quasi" is dropped. Typically, the fastest shear wave is called the quasi-*S*1 and the slow the quasi-*S*2 wave; quasi-*SV* and quasi-*SH* are occasionally used instead for the polarizations that are closest to being in and out of the sagittal

plane, respectively. These waves all depend upon the anisotropic model in consideration.

The polarizations and speeds of the two quasi-*S* waves are determined by both the properties of the medium and the propagation direction through the medium. In addition to the separation between the quasi-*P* and quasi-*S* waves, there is a time delay (δt) between the two quasi-*S* waves, which depends on both the path length in the anisotropic material and the difference in speed between the two quasi-*S* waves. Analogous to *S* minus *P* travel times, we find

$$\delta t = L(1/V_{S1} - 1/V_{S2}), \quad (1)$$

where V_{S1} and V_{S2} represent the speeds of the two quasi-shear waves given the direction of propagation and the material properties and L is the length of the anisotropic path traversed. The differences between V_{S1} and V_{S2} are often reported as a percent anisotropy k_S, calculated as

$$k_S = 200(V_{S1} - V_{S2})/(V_{S2} + V_{S1}).$$

However, this anisotropy should be distinguished from the *intrinsic anisotropy* of the material, which is defined as the percent difference between the maximum and minimum velocities [*Birch*, 1961]. In general, the intrinsic anisotropy is higher than k_S because these values vary depending on propagation direction. Shear wave splitting measurements can only give information on $(1/V_{S1} - 1/V_{S2})$ (equation (1)) for nearly vertically traveling *S* waves. Therefore values of anisotropy quoted in this paper refer to differences between V_{S1} and V_{S2} rather than to the intrinsic anisotropy. Other papers quote the anisotropy parameter $\xi = N/L$ [e.g., *Montagner and Kennett*, 1996], where N and L are the Love parameters [e.g., *Babuška and Cara*, 1991]. For simple radial anisotropy with propagation within the plane of symmetry, ξ is related to the percent anisotropy defined above as

$$k_S = \frac{200(\sqrt{\xi} - 1)}{(\sqrt{\xi} + 1)}.$$

A shear wave that traverses an anisotropic layer is split according to equation (1). The splitting is preserved if the shear wave then subsequently traverses an isotropic layer and the polarization of the first shear wave (ϕ) and δt can be determined. The separation between the two components is called shear wave splitting, birefringence, or *double refraction*, and ϕ and δt are often called the shear wave splitting parameters, or simply the splitting parameters. If the ray has passed through a single anisotropic layer with homogeneous properties, the splitting parameters can be measured no matter what form of anisotropy has been traversed. Even when multiple layers of anisotropy have been traversed, waveforms appear similar to those passing through a single layer of anisotropy, and "apparent" single-layer splitting parameters can be measured [*Silver and Savage*, 1994].

The amplitude of the fast and slow shear waves is directly proportional to the amplitude of the initial *S* wave in the fast and slow directions, respectively (the *S* wave polarization). If an initial source is polarized parallel to either the fast or slow direction of anisotropy, then no splitting is observed because only the fast shear wave (for a fast initial polarization) or the slow shear wave (for a slow initial polarization) occurs. Measurements with no splitting are often referred to as "*nulls*" and suggest that if anisotropy is present, the fast direction is either parallel or perpendicular to the polarization of the shear wave. When nulls are measured at a wide variety of azimuths for nearly vertically traveling shear waves, the usual interpretation is that the medium is either effectively isotropic or transversely isotropic with a vertical symmetry axis.

When viewed on particle motion diagrams, the *P* wave, after passing through a single anisotropic layer and entering an isotropic layer, has the same linear particle motion as before, but the *S* wave has a characteristic shape that depends on δt compared to the period (Figures A2 and A3). For large splitting or short periods the two split shear waves may be entirely separated from each other. Then polarization diagrams take on a cruciform appearance with the initial polarization from the fast quasi-*S* wave and a following, perpendicular, one from the slow quasi-*S* wave [e.g., *Keith and Crampin*, 1977]. For smaller splitting or longer periods the two split waves are separated by only a fraction of a period. The initial portion of the particle motion is linear and polarized in the fast direction, but the majority of the waveform has elliptical particle motion (Figure A3).

The beauty of shear wave splitting is the wealth of information that can be gleaned from a simple measurement. With assumptions about the type and degree of anisotropy, ϕ determines the orientation of the anisotropic symmetry system, and δt gives the thickness of the anisotropic layer. Furthermore, if the relationship between the orientation of the system and the strain is known, then we can infer the orientation and magnitude of the strain. Thus a single earthquake recorded at one station can measure the strain along the path. Lateral resolution is limited only by the station spacing and the wavelengths examined. High lateral resolution trades off against poor vertical resolution because a single basic splitting measurement cannot determine along which part of the path the splitting was formed.

A2. Phases Used to Measure *S* Wave Splitting

In principal, *S* wave splitting can be measured from any type of shear wave if appropriate care is taken to avoid pitfalls. One major consideration is the angle of incidence of the shear wave at the surface. If it is greater than the critical angle of about 35° from the vertical (the exact value depends on the Poisson's ratio of the medium and the curvature of the wave front), the "post-critical" *S*-to-*P* reflection at the surface distorts both the amplitude and phase of the recorded wave, yielding nonlinear particle motion [*Nuttli*, 1961; *Nuttli and Whit-*

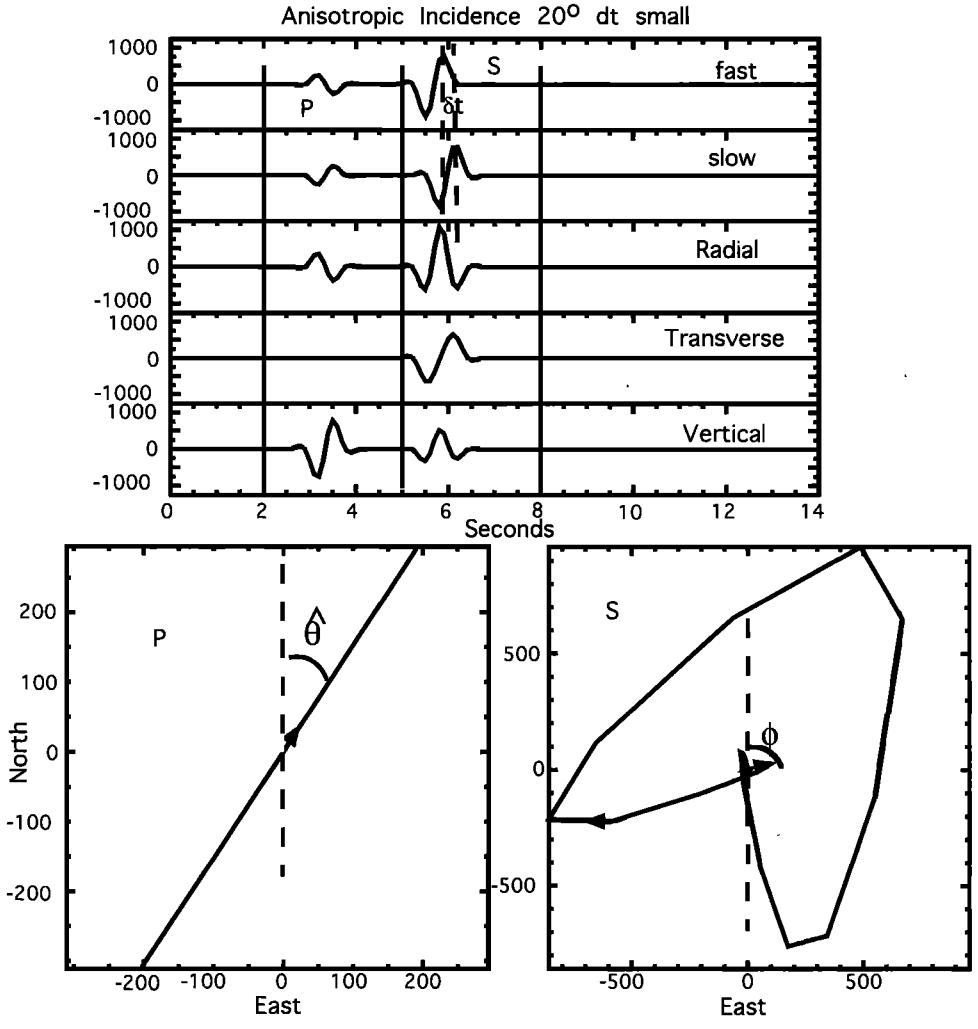

Figure A3. Same as Figure A2, but for δt small compared to the period. Note the elliptical particle motion of most of the *S* waveform.

more, 1962; *Okal*, 1992]. The cone of angles smaller than the critical angle is often termed the shear wave window. While near-surface low-velocity layers tend to refract even relatively low-angle arrivals to near-vertical, the same phase differences may sometimes occur from transitions between high- and low-velocity layers, causing an "internal" shear wave window that needs to be avoided even if the arrival angle at the surface is within the shear wave window [*Rowlands et al.*, 1993]. Therefore studies of shear wave splitting are often limited to those phases with incidence angles of less than 35°, although a slightly larger range of angles is often allowed because of the effects of refraction (Figure 6).

Direct *S* phases at stations above subcrustal earthquakes can determine mantle anisotropy [e.g., *Ando and Ishikawa*, 1982; *Savage et al.*, 1989; *Shih et al.*, 1991; *Gledhill and Stuart*, 1996; *Fouch and Fischer*, 1996] (Figures 6 and 7). Teleseismic *S* phases from distances of greater than about 60° arrive with near-vertical incidence angles and can also be used, although difficulties arise in knowing the position along the path where the anisotropy occurs. Direct *S* phases may be used to examine receiver-side anisotropy [e.g., *Savage et al.*, 1990b; *Sandvol et al.*, 1994] or source-side anisotropy if the receiver-side anisotropy is known and corrections applied [e.g., *Kaneshima and Silver*, 1992, 1995; *Vinnik and Kind*, 1993; *Russo and Silver*, 1994; *Schoenecker et al.*, 1997].

SKS phases are popular because of their prominence and ease of interpretation. These waves begin as *S* waves, are converted to *P* waves at the liquid outer core, and are converted back to *S* waves when they pass back into the mantle. Since *P* waves have only longitudinal motion and therefore only one direction of particle motion, any splitting from the source side of the path is destroyed on entering the outer core and simply complicates the *P* waveform. Thus any splitting on the waveform must have occurred on the path between the core-mantle boundary and the surface, and any anisotropy from the source side is lost. The anomalous region at base of the mantle, known as the D″ region, is believed to be characterized by either isotropy or radial anisot-

ropy of varying magnitudes [e.g., *Matzel et al.*, 1996; this paper, section 3.1.5]. These characteristics imply that when the *P* wave converts back into an *S* wave on its exit from the core, it can impart only energy in the plane of its motion, and the converted *S* wave is a radially polarized *SV* phase. Thus the polarization of the *S* wave is known and is independent of the earthquake focal mechanism. Other phases with almost the same properties that have been used to examine anisotropy above the core are *PKS*, which travel as *P* in both the downward leg of the mantle path and in the core and *SKKS* and *PKKS*, which bounce once from the underside of the core-mantle boundary (Figure 6).

Station and earthquake distributions limit studies using direct *S* and *SKS* phases, requiring other phases to fill in gaps. Deep sources of *ScS* phases, which are *S* waves reflected from the core-mantle boundary, can be used if the arrival angle at the core is less than about 35°, the angle required to avoid problems with phase shifts at the reflection from the core [*Furumoto*, 1962; *Ando and Ishikawa*, 1982; *Fukao*, 1984; *Ando*, 1984]. Phases bouncing from the surface help to characterize the area under the bounce points, allowing anisotropy to be examined in regions where there are neither earthquakes nor stations (e.g., *PS* [*Su and Park*, 1994], *sS* [*Fischer and Yang*, 1994], and *SS* [*Yang and Fischer*, 1994; *Wolfe and Silver*, 1998]). However, these studies are difficult because of the need to correct for source-side or receiver-side anisotropy of *SS* phases. Some studies do not attempt such corrections [e.g., *Yang and Fischer*, 1994], and even when the correction is made, the extra processing steps make the anisotropy more difficult to constrain, and such results should be interpreted with caution. Another method examines splitting in multiple ScS_n phases. However, the published method assumes that the splitting operator commutes, that is, that splitting in one layer followed by splitting in another layer is identical to reversing the procedure [*Farra and Vinnik*, 1994]. This is false, as shown with examples from synthetic seismograms [*Silver and Savage*, 1994]. Therefore, if such a method is used in the future, it must be modified to take into account the noncommutativity of the shear wave splitting operator.

A3. Anisotropic Symmetry Systems

Most theoretical studies of anisotropy consider wave slowness, which in isotropic media is the reciprocal of the wave speed. The concepts of slowness surfaces and their relation to symmetry systems are presented and reviewed in the theoretical anisotropy literature and can give a more thorough grounding in understanding anisotropy [e.g., *Anderson*, 1989; *Garmany*, 1989]. However, we concentrate here on understanding phase velocities and their relation to the shear wave splitting observations.

An anisotropic elastic system can be characterized by its elastic tensor, which relates the stress to the strain and is intimately related to the seismic velocities. The general form of Hooke's law in a homogeneous system is $\sigma_{ij} = c_{ijkl}\varepsilon_{kl}$, where σ_{ij} is the stress tensor for the system, ε_{kl} is the strain tensor, and c_{ijkl} is a fourth-order stiffness tensor, and the summation convention has been used [e.g., *Auld*, 1990; *Babuška and Cara*, 1991]. The symmetries of stress and deformation tensors lead to the symmetries $c_{ijkl} = c_{jikl} = c_{ijlk} = c_{klij}$; therefore the 81 possible components of a fourth-order tensor are reduced to 21 elastic constants for a general anisotropic medium, described as *monoclinic* symmetry.

Additional symmetry can further reduce the number of independent elastic constants required. While a number of symmetry systems exist, most studies of anisotropy to date have concentrated on two types; hexagonal symmetry and orthorhombic symmetry. The elastic tensor of the orthorhombic, hexagonal and isotropic materials, with Love identifiers, are as follows:

General orthorhombic

$$\begin{matrix} a & b & c & 0 & 0 & \\ b & d & e & 0 & 0 & 0 \\ c & e & f & 0 & 0 & 0 \\ 0 & 0 & 0 & g & 0 & 0 \\ 0 & 0 & 0 & 0 & h & 0 \\ 0 & 0 & 0 & 0 & 0 & i \end{matrix}$$

Hexagonal

$$\begin{matrix} A & A\text{-}2N & F & 0 & 0 & 0 \\ A\text{-}2N & A & F & 0 & 0 & 0 \\ F & F & C & 0 & 0 & 0 \\ 0 & 0 & 0 & L & 0 & 0 \\ 0 & 0 & 0 & 0 & L & 0 \\ 0 & 0 & 0 & 0 & 0 & N \end{matrix}$$

Isotropic

$$\begin{matrix} \lambda + 2\mu & \lambda & \lambda & 0 & 0 & 0 \\ \lambda & \lambda + 2\mu & \lambda & 0 & 0 & 0 \\ \lambda & \lambda & \lambda + 2\mu & 0 & 0 & 0 \\ 0 & 0 & 0 & \mu & 0 & 0 \\ 0 & 0 & 0 & 0 & \mu & 0 \\ 0 & 0 & 0 & 0 & 0 & \mu \end{matrix}$$

The 6 × 6 symmetric matrices represent the 21 elastic constants of the tensor; *a* through *i* represent the following tensor elements: $a = c_{1111}$; $b = c_{1122}$; $c = c_{1133}$; $d = c_{2222}$; $e = c_{2233}$; $f = c_{3333}$; $g = c_{2323}$; $h = c_{1313}$; $i = c_{1212}$. Orthorhombic systems have three perpendicular axes of symmetry, with nine independent elastic constants. Hexagonal symmetry systems have five independent elastic constants and may be referred to as transverse anisotropy, *transverse isotropy* or TI. The term radial anisotropy is used here for hexagonal anisotropy with a vertical symmetry axis. The elastic properties of hexagonal symmetry systems are identical to those of cylindrical symmetry around a single axis, and the two terms are often used interchangeably. In these systems,

properties vary in only one direction. For example, the P wave speed along the axis of symmetry differs from that perpendicular to the axis of symmetry, while the speed for waves propagating in any direction in the plane perpendicular to the axis of symmetry is constant. Often the problem is made even simpler by considering the symmetry axis to be either vertical or horizontal. Isotropic systems have only two independent elastic parameters, usually referred to as Lame's constants, λ and μ.

A schematic example of splitting for propagation along three principal axes of an orthorhombic material is shown in Figure 3. The phase velocities and wave polarizations for propagation along an arbitrary direction $\hat{n}$ are found from the eigenvalues and eigenvectors of the Christoffel matrix. The elements of the Christoffel matrix m_{il} are $m_{il} = c_{ijkl}n_j n_k/\rho$, where ρ is the density and n_j and n_k are two of the three components of $\hat{n}$, and the summation convention applies. The three eigenvalues of the Christoffel matrix give the three wave speeds, and the eigenvector corresponding to each eigenvalue gives the polarization of the wave that travels at each wave speed. For these simple systems, it is relatively easy to solve the Christoffel matrix analytically for propagation along an axis of symmetry [*Stonely*, 1949]. The example of *Babuška and Cara* [1991] for a hexagonally anisotropic medium is easily extended to an orthorhombic system. For plane P wave propagation along the $x1$, $x2$, and $x3$ directions in an orthorhombic system, the speeds are given by $\sqrt{(a/\rho)}$, $\sqrt{(d/\rho)}$, and $\sqrt{(f/\rho)}$, respectively, and the wave is polarized parallel to the $x1$, $x2$, and $x3$ axes, respectively. However, for plane S wave propagation the speed depends not only on the polarization but also on the propagation direction. Examples from the theoretical specimen are above and for a real specimen are below:

Example values for Nunuvak [*Ji et al.*, 1994] (units in GPa; density is 3260 kg/m^3)

224.44	67.27	70.71	−0.28	−0.33	−0.94
67.27	193.13	68.69	0.29	0.19	−0.88
70.71	68.69	210.52	0.57	−0.25	−0.25
−0.28	0.29	0.57	65.52	−0.65	0.00
−0.33	0.19	−0.25	−0.65	73.03	−0.05
−0.94	−0.88	−0.25	0.00	−0.05	68.65

For propagation along $x1$, an S wave is polarized parallel to the $x3$ direction traveling with speed $\sqrt{(h/\rho)}$ (4.73 km/s), and another is parallel to the $x2$ direction traveling with speed $\sqrt{(i/\rho)}$ (4.59 km/s). For propagation along $x2$, one S wave is polarized parallel to $x1$ and travels with speed $\sqrt{(i/\rho)}$ (4.59 km/s), while the S wave polarized parallel to $x3$ travels with speed $\sqrt{(g/\rho)}$ (4.48 km/s). Finally, for propagation along $x3$, one S wave is polarized parallel to $x2$ with speed $\sqrt{(g/\rho)}$ (4.48 km/s), and the other is parallel to $x1$ with speed $\sqrt{(h/\rho)}$ (4.73 km/s). Thus, for our real example the wave polarized in the $x3$ direction is slowest for propagation along $x2$ (4.48 km/s) and fastest for propagation along $x1$ (4.73 km/s). Maximum splitting occurs for propagation along $x3$, which corresponds to the Y direction of *Ji et al.* [1994], or parallel to foliation but perpendicular to lineation. Direction $x2$ corresponds to Z, and $x1$ corresponds to X, or the lineation direction (Figure 3).

Hexagonal symmetry can be considered as a special case of orthorhombic symmetry in which two of the axes have identical speeds (Figure 3). For propagation along the axis of symmetry, the P wave is polarized along the axis, and two orthogonal S waves can have any polarization in the plane perpendicular to the axis of symmetry and do not split. They travel with the speed given by the eigenvalue corresponding to the axis of symmetry, fast if the axis of symmetry is fast (e.g., aligned olivine) or slow if the axis of symmetry is slow (e.g., cracked solids). For propagation in the plane of symmetry the S wave splits in two, with one wave polarized parallel to the axis of symmetry and one orthogonal to it. For propagation in other directions the Christoffel matrix must be solved for each specific case. The largest or smallest splitting or S wave speeds are not necessarily along a structural axis or an axis of symmetry (e.g., values reported by *Keith and Crampin* [1977] and *Mainprice and Silver* [1993]) (Figure 4). Radial anisotropy explains Love-Rayleigh polarization anisotropy and the differences between SH and SV arrivals of teleseisms [e.g., *Anderson*, 1961; *Shearer*, 1991].

Examples of orthorhombic symmetry systems include the mantle minerals olivine and pyroxene and many mantle xenoliths. Hexagonal systems include mica minerals, sedimentary layering, and aligned, parallel cracks [e.g., *Babuška and Cara*, 1991].

The elastic coefficients of materials, with Love identifiers, are as follows:

A4. Effect of Symmetry System on Splitting Parameters

Shear wave splitting occurs in all types of anisotropic media, whether they are weakly or highly anisotropic and no matter what the symmetry system. However, the shear wave splitting parameters ϕ and δt vary with propagation direction, depending on the type of symmetry and dip of the symmetry axes (Figure 4) [e.g., *Booth et al.*, 1985; *Crampin and Booth*, 1985; *Babuška and Cara*, 1991; *Šílený and Plomerová*, 1996; *Plomerová et al.*, 1996].

For example, for typical mantle aggregates, hexagonal anisotropy with a horizontal symmetry axis yields no variation in polarization azimuth and variation up to a factor of 2 in δt for incidence angles within the shear wave window (Figure 4) but with smaller variation for incidence angles less than 15°, as is usual in the typical SKS study. For both hexagonal and orthorhombic symmetry, arrivals within the shear wave window yield ϕ parallel or subparallel to the fast axis when it is not near vertical, but large variations in δt can occur at dips of 45° or more. Radial anisotropy (Figure 4a, 90°) yields no splitting at all for vertically traveling waves, and only small amounts of splitting for waves within the shear wave window; variation in ϕ is rapid only because δt is

small. In contrast, orthorhombic symmetry yields splitting for propagation along any axis. For the cases shown in Figure 4 the orthorhombic symmetry has less variation in δt with back azimuth than does the hexagonal symmetry.

A5. How to Measure ϕ and δt

Much past work in anisotropic systems has been focused on weakly anisotropic systems with hexagonal anisotropy, with a horizontal or vertical symmetry axis [e.g., *Crampin*, 1981; *Silver*, 1996]. Unfortunately, some of the descriptions of the methods have been confused as to what aspects of shear wave splitting are a consequence of general anisotropy and what are a consequence of the hexagonal symmetry system and of weakly anisotropic media.

A5.1. Methods valid at short or long periods. When the anisotropy and path length are both large or the frequency is high, δt may be greater than the pulse duration, and the two split phases may be completely separated (Figure A2). This happens often with high-frequency S waves from local microearthquakes, but it is also important in mantle studies of subduction areas where there are high-frequency sources of local earthquakes [e.g., *Ando et al.*, 1983]. One direct method is to rotate the horizontal seismograms to various azimuths [e.g., *Ando et al.*, 1983]. When the seismograms have been rotated to fast and slow directions, the first shear arrival is seen entirely on the fast component, and the second shear arrival follows on the slow component at a time δt after the first arrival (Figure A2). Polarization diagrams yield ϕ from the polarization of the first shear phase and δt from the time between the first phase and the onset of elliptical or cruciform motion. *Bowman and Ando* [1987] use polarization diagrams to determine the polarization of the fast shear wave, then rotate the seismograms to fast and slow direction, and perform a cross correlation between the fast and slow components to determine the time separation as the time that gives the maximum cross correlation. Other methods have automated both the process of determining the initial fast polarization and the time separation and are used in the time domain [*Shih et al.*, 1989] or frequency domain [e.g., *Majer et al.*, 1988; *Aster et al.*, 1990]. Polarization diagrams and plots of fast and slow components are used as diagnostics to assure that ϕ and δt have been correctly identified.

A5.2. Methods valid only at long periods. For most splitting studies involving the mantle, only longer periods are available because the teleseismic phases used to sample the mantle have lost their short-period energy due to attenuation. The shear wave particle motion is elliptical (Figure A3). Two of the most popular methods [*Vinnik et al.*, 1989b; *Silver and Chan*, 1991] were originally derived for *SKS* phases and are essentially equivalent. These methods use a grid search to find the values of ϕ and δt that most nearly remove the splitting.

For long-period phases converted from P to SV at a boundary between two isotropic media, such as the core-mantle boundary, the 660- or 410-km discontinuities or the Moho, the S phase is radially polarized, and thus there is no transverse component. If the SV phase is later split by a fraction of a period due to passage through an anisotropic medium, the transverse component is the time derivative of the radial component [*Vinnik et al.*, 1988; *Silver and Chan*, 1988]. *Vinnik et al.* [1989b] use this observation directly by modeling the expected transverse component from the observed radial component, assuming parameters of ϕ and δt. They find the values that best reproduce the observed transverse component, but they do not present formal error bars. *Silver and Chan* [1991] use assumed values of ϕ and δt to "unsplit" the seismogram and create corrected radial and transverse components. The energy on the corrected transverse component is contoured; the minimum energy corresponds to the preferred values of ϕ and δt, and the error bars are based on energy contours (Figure A4).

Šílený and Plomerová [1996] extend the *Silver and Chan* [1991] method to examine splitting in out-of-the-horizontal planes. *Aster et al.* [1990] also evaluate out-of-plane motion for crustal earthquake analysis. However, the difference between the horizontal and the plane perpendicular to the ray path is small for the near-vertical incidence phases, and therefore horizontal axes are sufficient for studies of *SKS* phases. For S phases, near-surface low-velocity layers often rotate the arrivals to be nearly vertical. However, the possibility that they pass through anisotropic material at lower incidence angles should be taken into account.

If the isotropic polarization vector of a teleseismic S phase is known through published focal mechanisms, the *SKS* methods can determine splitting in direct S; the problem is reposed with "radial" replaced by "parallel to incoming polarization direction" and "transverse" replaced by "perpendicular to incoming polarization direction" [e.g., *Özalaybey and Savage*, 1994]. If the polarization is unknown, then the S waveforms can be inverted simultaneously using grid search techniques to find the incoming polarization direction and the splitting parameters by maximizing the *aspect ratio* as in the work by *Shih et al.* [1989] or, equivalently, by solving for the minimum eigenvalue of the covariance matrix as in the work by *Silver and Chan* [1991].

Initially, the methods of *Vinnik et al.* [1989b] and *Silver and Chan* [1991] were advertised as being designed to study transverse anisotropy with horizontal symmetry axes. However, they actually measure splitting parameters in any symmetry system, as long as the S arrivals are mainly in the horizontal plane. When extended to three components such as by *Šílený and Plomerová* [1996] and *Aster et al.* [1990], this restriction is removed. The horizontal approximation should be valid for determining ϕ and δt for shear waves traveling nearly vertically through most common anisotropic media.

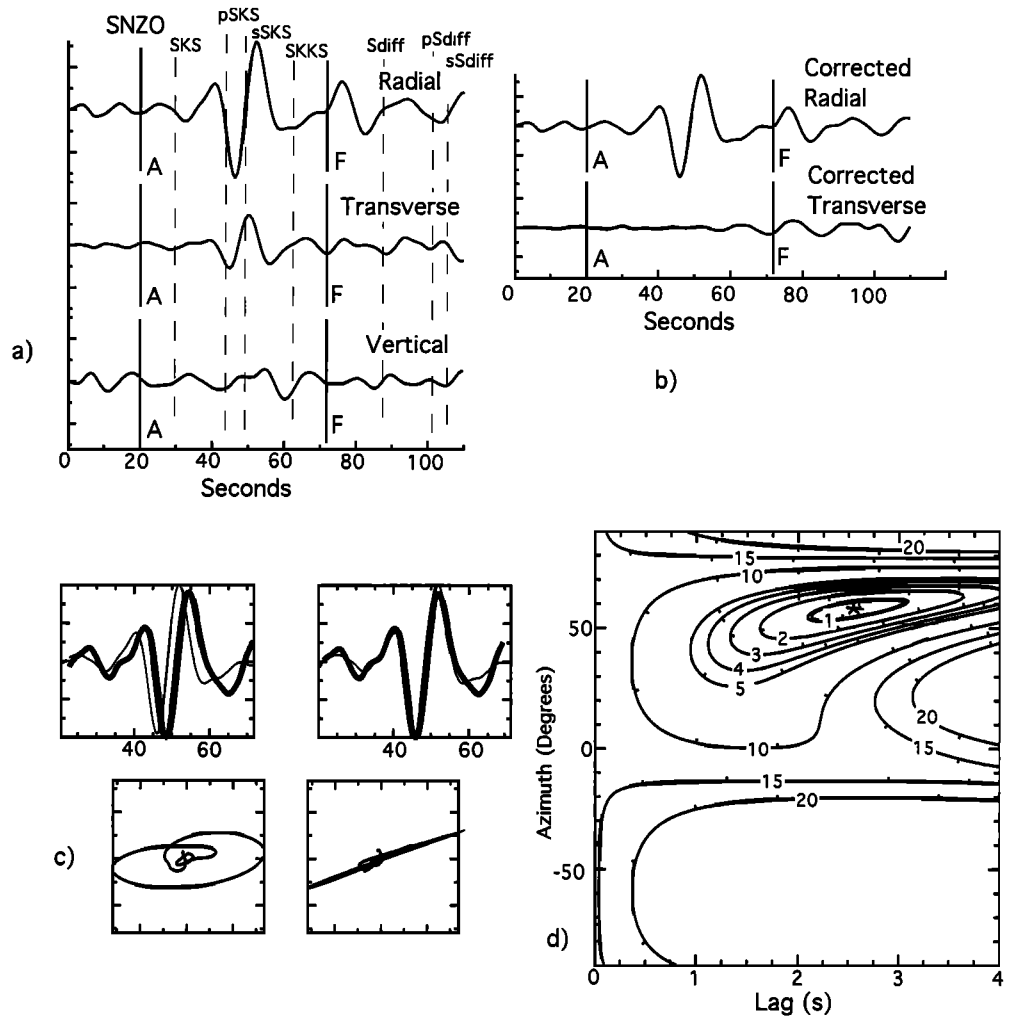

Figure A4. Example of a good shear wave splitting measurement using the method of *Silver and Chan* [1991] along with the diagnostic plots from station SNZO, New Zealand [*Marson-Pidgeon and Savage*, 1997]. (a) Original (filtered) radial, transverse, and vertical component seismograms, with scale set by the radial component amplitude. Predicted phase arrivals are displayed along with the time interval (between A and F) used to make the measurements. (b) Corrected radial and transverse components. Note that the corrected transverse component has been minimized. (c) (top) superposition of fast and slow (bold) components uncorrected (left) and corrected (right). Note the similarity of the pulse shapes. (bottom) Corresponding particle motion diagrams. Note that the elliptical particle motion becomes linear when corrected. (d) Contour plot of the energy on the corrected transverse component showing the minimum value (star) along with the 95% confidence region (double contour) and multiples of that contour interval.

While anisotropy can be measured on many types of instruments, broadband sensors provide the most unambiguous measurements. The derivations of *Silver and Chan* [1991] show that the transverse component is the time derivative of the radial component if the splitting is small compared to the period. In practice, splitting is difficult to measure unless sufficient energy is available on the transverse waveform. This leads to a suggestion that waveforms should contain energy at periods of less than 10 times the delay time [*Silver and Chan*, 1991; *Wolfe and Silver*, 1998]. When narrow band, short-period sensors are used, or if heavy filtering is used, "cycle skipping" can occur, whereby several maxima occur at δt separated by one-half period.

Vinnik et al. [1989b] and *Wolfe and Silver* [1998] invert observations simultaneously from many different locations, angles of incidence, and back azimuth to find the best single fast direction and time delay that explain all of the data. This increases the signal to noise ratio in simple anisotropic symmetry systems and yields average splitting parameters. However, the validity of the average depends on the variability of the parameters for the symmetry system. If a symmetry system has a small range of ϕ and δt for the range of back azimuths and incidence angles in the data, then these averaging methods yield good results. However, the single-observation methods are best to determine if azimuthal variations are caused by dipping symmetry axes or by heterogeneous anisotropic properties.

A5.3. Distinguishing splitting from other processes. Some of the secondary characteristics of shear wave splitting can be mimicked by other phenomena. For example, conversions from S to P near the station might be observed on the radial component and initially be confused with early arriving S waves; the higher energy on the vertical component should help to distinguish them. Nonlinear particle motion occurs if a phase shift between components is caused by some other phenomenon, for example, if arrivals are outside the shear wave window. Energy on the transverse component for phases that are expected to appear only on the radial component could be caused by anisotropy or by scattering. The scattered energy usually has linear particle motion, but sometimes scattered waveforms might interfere with an initial arrival, creating an apparent phase shift. However, second arrivals are not, in general, orthogonal to the original arrival, and therefore the slow waveforms should appear different from the fast one unless true splitting has occurred. Comparing the split waveforms with each other and reconstructing the initial waveform by a process of "unsplitting" is the best way to ensure that splitting rather than scattering has caused the observation [e.g., *Aster et al.*, 1990]. This is performed during the waveform inversion techniques [*Vinnik et al.*, 1989b; *Silver and Chan*, 1991]. Theoretical waveforms from scattering in a random medium are often nonlinear but are rarely mistaken for splitting when one of the whole waveform techniques is used [*Alsina and Snieder*, 1995]. *Vinnik et al.* [1989a, 1992] further argue that using long-period waves allows the indirect effect of splitting to be sufficiently strong to observe, whereas the effects of lateral heterogeneity are relatively weak.

Diagnostic plots associated with the method of *Silver and Chan* [1991] help to eliminate "false" splitting measurements (Figure A4). Energy on the vertical component and a mismatch in waveform between the fast and slow components may indicate scattering. Small transverse energy on original waveforms, energy contours elongate in the δt direction, and ϕ within 10–15° of the incoming polarization direction indicate *null measurements* even though formal minima may yield apparently large δt (Figure A5). Occasionally, when a waveform is examined in a relatively narrow time window, microseismic noise on the transverse component may mimic splitting, causing beautiful looking error contour plots and possibly even good waveform matches but results that do not match those from nearby earthquakes. This situation can be spotted when the reconstructed transverse component is much smaller in amplitude than the surrounding noise.

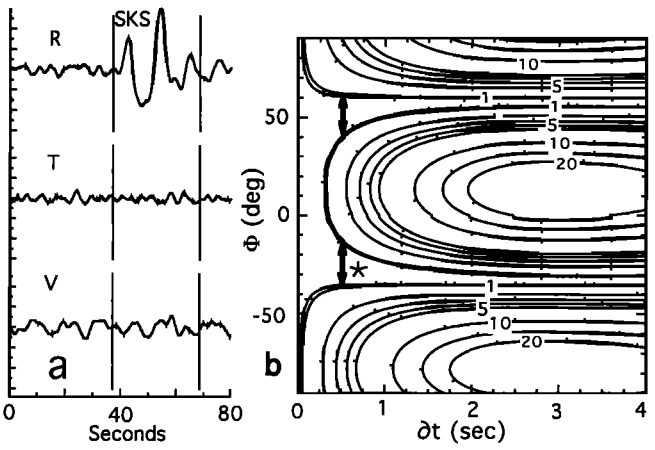

Figure A5. Example of a null measurement at station CCY in the Rocky Mountains [after *Savage et al.*, 1996b]. (a) Seismograms rotated to (top) radial, (middle) tangential, and (bottom) vertical orientations. The *SKS* phase used in the measurement lies between the solid lines. (b) Contour plot of the energy on the tangential component for seismograms corrected to the given azimuths of ϕ or lag δt. The 95% confidence interval is the double contour, with multiples of this interval labeled. The elongate 95% confidence region is typical of a null measurement, in which any amount of splitting is allowed, provided that the fast axis occurs at azimuths equal to the back azimuth or the back azimuth minus 90°. Arrows show the allowed azimuth ranges of fast axes of anisotropy at 0.5 s splitting.

A6. Causes of Anisotropy

Three candidate processes for anisotropy are (1) thin layers of otherwise isotropic material with different velocities, or aligned heterogeneities, (2) aligned, fluid-filled fractures or cracks, and (3) aligned anisotropic minerals. *Babuška and Cara* [1991] give a thorough overview of the causes of crustal and mantle anisotropy. *Crampin* [1994] discusses some crustal hypotheses, and *Silver* [1996] discusses a number of hypotheses for mantle anisotropy. We present a brief review and discuss some of the more recent ideas.

Seismic techniques view every system through the wavelength used to probe it. Systems that appear merely heterogeneous at short wavelengths can be anisotropic at long wavelengths. One example is finely layered material with differing elastic properties in the otherwise isotropic layers. For wavelengths longer than the thicknesses of the material, these layers appear anisotropic [*Backus*, 1962]. Propagation along bedding planes allows the P waves to refract around the slow layers and travel mainly in the fast layers. Conversely, propagation perpendicular to the planes requires P waves to go through both media, thus decreasing the average velocity of the waves.

Usually, thin layers are horizontal. Such layers yield radial anisotropy with a slow (vertical) symmetry axis. For propagation along the horizontal plane in such a system, SH phases are fast and SV phases are slow, but for vertical incidence angles, there is no splitting. Vertically intruded dikes in host rocks of higher or lower speeds could cause anisotropy from alternate layers of fast and slow material with a horizontal symmetry axis. If horizontal or vertical layers are later tilted by tectonic forces, they can yield hexagonal symmetry with nonhorizontal and nonvertical symmetry axes.

Such arguments can be extended to more general material with aligned heterogeneities. *Grechka and McMechan* [1995] do so for a simple form of heterogeneity that allows for analytic solution. Such systems would be characterized by frequency-dependent splitting measurements. A recent study in New Zealand suggests that frequency dependence in splitting may be related to these processes [*Marson-Pidgeon and Savage*, 1997]. If so, the way we view anisotropy may need to be rethought.

Parallel, aligned, fluid-filled cracks and microcracks can cause anisotropy and may be sensitive indicators of stress. Differential stress preferentially closes cracks perpendicular to the maximum principal stress [e.g., *Christensen*, 1966a; *Nur and Simmons*, 1969; *Nur*, 1971]. The remaining open cracks are aligned with the maximum principal stress, which is often horizontal. These vertical cracks yield anisotropy with hexagonal symmetry and a (slow) horizontal symmetry axis, perpendicular to the planes of the cracks. Thus, for vertically traveling S waves, ϕ is parallel to the cracks and to the maximum principal stress direction. The fast wave speeds in such a medium are identical to those in the uncracked medium (the fast waves do not "see" the cracks.) Similar properties are expected for vertically aligned disks of melt-filled cracks in the mantle beneath mid-oceanic ridges [e.g., *Blackman and Kendall*, 1997; *Mainprice*, 1997].

Sometimes two natural phenomena that normally each cause hexagonal symmetry combine to form other symmetry systems, for example, cracks in sedimentary rocks or two sets of cracks. If the two axes of symmetry are parallel, then the effect is additive. If they are perpendicular, the resulting anisotropy is orthorhombic. If they are at any other angle, the symmetry may be monoclinic (i.e., full, general anisotropy with 21 elastic constants).

Most minerals composing the crust and mantle are anisotropic. If they are randomly oriented, then the bulk material appears isotropic, but if there is a preferred orientation, the bulk material appears anisotropic. Measured anisotropic properties are usually close to those calculated by averaging the elastic tensors of the crystals composing the medium in proportion to the mineral abundance and orientation [e.g., *Crosson and Lin*, 1971; *Mainprice and Humbert*, 1994]. However, *Kern et al.* [1996] give an example in which calculations based on preferred orientations yield different results from measurements of real rocks. They attribute the differences to neglect of some important mantle minerals and to grain boundary effects such as retrogressive reactions, interstitial glass, and incomplete crack closure.

Most common rock-forming minerals in the crust are anisotropic (e.g., quartz has V_P anisotropy of 26% and V_S anisotropy of 40% [*Babuška and Cara*, 1991]). However, rocks formed of aggregates of these minerals are, in general, much less anisotropic than the individual crystals. Gneisses, schists, and amphibolites containing amphibole, biotite, and other phylosilicates are the most strongly anisotropic rocks. This is because deformation tends to orient the velocity extremes of amphibole, biotite, and other phylosilicates most strongly [e.g., *Babuška and Cara*, 1991; *Barruol and Mainprice*, 1993; *Ji et al.*, 1993]. Phylosilicates oriented via flow in the lower crust have been invoked to explain lower crustal anisotropy observed in phases converted from P to S at the Moho [e.g., *McNamara and Owens*, 1993]. In fault zones the extreme grain size reduction of mylonites could contribute significantly to anisotropy at short periods [e.g., *Kern and Wenk*, 1990; *Kern*, 1993b], but mylonites are usually narrow and may not, therefore, cause much splitting of teleseismic phases.

The common mantle minerals are olivine, garnet, and pyroxene [e.g., *Babuška and Cara*, 1991; *Ji et al.*, 1994]. *Birch* [1960] was the first to point out that the high anisotropy in the mantle rock dunite was caused by preferred orientation of olivine. Garnet is isotropic. Olivine and orthopyroxene have orthorhombic symmetry, and clinopyroxene is monoclinic. Pyroxenes are anisotropic, but compared to olivine, they have somewhat smaller anisotropy and are usually found to be less strongly oriented [e.g., *Nicolas and Poirier*, 1976; *Babuška and Cara*, 1991; *Mainprice and Silver*, 1993; *Ji et al.*, 1994]. Thus preferred orientation of olivine is thought to be the dominant source of anisotropy in the upper mantle. For P waves, olivine a axes (100) are fast, b axes (010) are slow, and c axes (001) are intermediate.

The lower mantle is thought to be composed mainly of Mg-perovskite and wüstite, which are anisotropic. Most studies suggest they do not develop preferred orientation [e.g., *Meade and Jeanloz*, 1990; *Karato and Li*, 1992; *Meade et al.*, 1995] and that splitting does not occur in the transition zone or below [e.g., *Kaneshima and Silver*, 1995]. However, anisotropy in the transition zone may be present in some areas [e.g., *Fouch and Fischer*, 1996; *Vinnik and Montagner*, 1996] due to the preferred orientation of β spinel, an abundant transition zone phase with strong crystal anisotropy [*Sawamoto et al.*, 1984] that orients significantly under uniaxial strain [*Fujimura*, 1984, 1989; *Sharp et al.*, 1994; *Fouch and Fischer*, 1996]. The D″ layer between the lower mantle and core may be anisotropic (section 3.1.5), but there is no consensus as to the cause of the anisotropy.

Velocity measurements in xenoliths are often made with respect to the *structural frame* of the sample, that is, the foliation and lineation directions (Figure 3). The orientation of the structural frame in its natural environment is important, for it controls the orientation of the anisotropic symmetry system and therefore the pattern of splitting that is observed. For both crustal and mantle samples the strongest splitting is for propagation within the foliation plane. For crustal rocks, lineation direction has little effect, but for mantle rocks, olivine a axes are oriented parallel to lineations, and the maximum splitting occurs for propagation within the foliation plane and perpendicular to the lineation, conditions common in transcurrent deformation [e.g., *Kern and Wenk*, 1990; *Barruol and Mainprice*, 1993; *Kern*, 1993a, b; *Mainprice and Silver*, 1993; *Ji et al.*, 1994]. Thus, for nearly vertically

arriving phases, splitting is smallest in regions for which the foliation plane is oriented horizontally.

GLOSSARY

Aspect ratio: The ratio of the longest to the shortest axis of an ellipse. It may characterize crack geometry, or the linearity of particle motion on a polarization diagram.

Azimuthal anisotropy: The variation of speed for a given wave type as a function of the azimuth of the propagation direction.

Back azimuth: The angle measured between north and the direction to the source.

Birefringence: The phenomenon by which one component of a transverse wave travels through an anisotropic medium faster than the orthogonal component. When observed for acoustic (seismic shear) waves, it is commonly called shear wave splitting.

D″: The layer, roughly 250 km thick at the base of the mantle, just above the core.

Delay time: δt, Time separation between fast and slow components of split shear waves.

Diffusion creep: Deformation caused by diffusive mass transport across the crystal lattice or along grain boundaries [*Nicolas*, 1984]. It results in an isotropic rock fabric.

Dislocation creep: Deformation caused by the motion of crystalline dislocations within grains, which results in preferred mineral orientation. The deformation rate is controlled by atomic diffusion [*Nicolas*, 1984; *Takeuchi*, 1989].

Double refraction: Birefringence.

Fast direction: (1) The direction in a medium which results in the fastest velocity for a given wave type or fastest polarizations of the S wave, or (2) the horizontal component of the fast direction. With some symmetry systems the fast directions will differ for P and S waves [e.g., *Keith and Crampin*, 1977; *Kern*, 1993a].

Fresnel zone: The region surrounding the ray path in which the material properties of the region affect the waveform. The Fresnel zone is dependent upon the period and length of the ray path.

Hexagonal symmetry: Symmetry with a single axis of sixfold rotation. The seismic properties of hexagonally symmetric systems are identical to those of cylindrical symmetry, in which properties in the plane perpendicular to the symmetry axis are independent of direction.

Hodogram: Polarization diagram.

Homogeneous: Constant, not varying.

Intrinsic anisotropy: The difference between the maximum and minimum velocities in a medium.

Lehmann discontinuity: A seismic discontinuity at about 200 km depth that is seen in many localities.

Love wave: Horizontally polarized surface wave.

Moho: The Mohorovicic discontinuity in seismic wave velocities, usually interpreted as the boundary between the crust and mantle.

Monoclinic: Adjective for material with full, general anisotropy with 21 elastic constants.

Null measurement: A measurement that detects no splitting on a shear wave. Such measurements suggest either that the medium is isotropic or that the initial polarization was parallel to the fast or slow direction of anisotropy for that propagation direction.

Percent anisotropy: Values of anisotropy reported in this paper refer to differences between the two quasi-S waves in a given propagation direction, not to the intrinsic anisotropy of a material.

Polarization: Direction of particle motion in a wave, where $\hat{\phi}$ is polarization of initial P and S waves before entering anisotropic media, and ϕ is fast polarization after passing through an anisotropic medium; ϕ is usually measured in the horizontal plane.

Polarization anisotropy: The property that wave speed differs for shear or surface waves of different polarization traveling along the same direction.

Polarization diagram: A two-dimensional diagram in which two components of a seismogram are plotted against each other, as in the X-Y "lissajous" figure of an oscilloscope. As time increases, the figure traces out a pattern that is linear if there is no phase shift between the two components (no splitting) and elliptical if a phase shift exists.

Radial anisotropy: Hexagonal anisotropy with a vertical symmetry axis.

Radial component: A horizontal component, rotated to being parallel to the earthquake-station back azimuth.

Rayleigh waves: Surface waves polarized in a vertical plane.

Sagittal plane: The vertical plane containing an observing station and a seismic source.

***SH* wave:** A shear wave vibrating in the horizontal plane.

Shear wave splitting: Acoustic birefringence.

Shear wave window: The cone of incidence angles that are sufficiently close to vertical so that particle motion for an isotropic Earth is expected to be linear.

Structural frame: Usually used in describing mineral orientations or velocity measurements in rock samples; it is defined by the foliation plane and lineation direction.

Surface wave: A seismic wave that propagates along the Earth's surface.

***SV* wave:** A shear wave vibrating in the sagittal plane.

Transverse anisotropy: Anisotropy with hexagonal symmetry.

Transverse component: The horizontal component that is perpendicular to the radial component.

Transverse isotropy: Transverse anisotropy. Often reserved for cases in which the symmetry axis is vertical.

ACKNOWLEDGMENTS. Ken Gledhill, Peter Molnar, Barb Dutrow, Jaroslava Plomerovà, Jeff Park, Karen Fischer, Serdar Ozalaybey, and Cecily Wolfe made suggestions on the manuscript. The work was partially supported by U.S. NSF grant 93-19007 and New Zealand Marsden Fund grant VUW601. The waveform in Figure A4 came from the IRIS data management center, as did a large fraction of the original data used to calculate the splitting parameters.

Roel Snieder was the Editor responsible for this paper. He acknowledges the technical reviews of Cecily Wolfe and Jarka Plomerovà, and the cross-disciplinary review of Barb Dutrow.

REFERENCES

Aki, K., and P. G. Richards, *Quantitative Seismology: Theory and Methods*, 932 pp., W. H. Freeman, New York, 1980.

Alsina, D., and R. Snieder, Small-scale sublithospheric continental mantle deformation: Constraints from *SKS* splitting observations, *Geophys. J. Int.*, *123*, 431–448, 1995.

Alvarez, W., Geological evidence for the geographical pattern of mantle return flow and the driving mechanism of plate tectonics, *J. Geophys. Res.*, *87*, 6697–6710, 1982.

Anderson, D. L., Elastic wave propagation in layered anisotropic media, *J. Geophys. Res.*, *66*, 2953–2963, 1961.

Anderson, D. L., *Theory of the Earth*, Blackwell Sci., Cambridge, Mass., 1989.

Ando, M., *ScS* polarization anisotropy around the Pacific Ocean, *J. Phys. Earth*, *32*, 179–196, 1984.

Ando, M., and Y. Ishikawa, Observations of shear-wave velocity polarization anisotropy beneath Honshu, Japan: Two masses with different polarization in the upper mantle, *J. Phys. Earth*, *30*, 191–199, 1982.

Ando, M., Y. Ishikawa, and F. Yamazaki, Shear waves polarization anisotropy in the upper mantle beneath Honshu, Japan, *J. Geophys. Res.*, *88*, 5850–5864, 1983.

Ansel, V., and H.-C. Nataf, Anisotropy beneath 9 stations of the geoscope broadband network as deduced from shear-wave splitting, *Geophys. Res. Lett.*, *16*, 409–412, 1989.

Aster, R. C., P. M. Shearer, and J. Berger, Quantitative measurements of shear wave polarizations at the Anza seismic network, southern California: Implications for shear wave splitting and earthquake prediction, *J. Geophys. Res.*, *95*, 12,449–12,473, 1990.

Audoine, E., M. Savage, and K. Gledhill, Mantle deformation and seismic anisotropy of the South Island, New Zealand (abstract), *Geol. Soc. N. Z. Misc. Publ.*, *95A*, 10, 1997.

Auld, B. A., *Acoustic Fields and Waves in Solids*, vol. I, 435 pp., Krieger, Melbourne, Fla., 1990.

Babuška, V., and M. Cara, *Seismic Anisotropy in the Earth*, 217 pp., Kluwer Acad., Norwell, Mass., 1991.

Babuška, V., J. Plomerovà, and J. Šílený, Large-scale oriented structures in the subcrustal lithosphere of central Europe, *Ann. Geophys.*, *2*, 649–662, 1984.

Babuška, V., J. Plomerovà, and J. Šílený, Models of seismic anisotropy in the deep continental lithosphere, *Phys. Earth Planet. Inter.*, *78*, 167–191, 1993.

Backus, G. E., Long-wave elastic anisotropy produced by horizontal layering, *J. Geophys. Res.*, *67*, 4427–4440, 1962.

Barruol, G., and H. Kern, Seismic anisotropy and shear-wave splitting in lower-crustal and upper-mantle rocks from the Ivrea Zone—Experimental and calculated data, *Phys. Earth Planet. Inter.*, *95*, 175–194, 1996.

Barruol, G., and D. Mainprice, A quantitative evaluation of the contribution of crustal rocks to the shear wave splitting of teleseismic *SKS* measurements, *Phys. Earth Planet. Inter.*, *78*, 281–300, 1993.

Barruol, G., and A. Souriau, Anisotropy beneath the Pyrenees range from teleseismic shear wave splitting: Results from a test experiment, *Geophys. Res. Lett.*, *22*, 493–496, 1995.

Barruol, G., G. Helffrich, and A. Vauchez, Shear wave splitting around the northern Atlantic: Frozen Pangaean lithospheric anisotropy?, *Tectonophysics*, *279*, 135–148, 1997.

Beghoul, N., and M. Barazangi, Azimuthal anisotropy of velocity in the mantle lid beneath the Basin and Range Province, *Nature*, *348*, 536–538, 1990.

Beghoul, N., and M. Barazangi, Comment on "Lateral variations and azimuthal isotropy of *Pn* velocities beneath Basin and Range Province" by Lian-She Zhao, *J. Geophys. Res.*, *100*, 12,459–12,461, 1995.

Birch, F., The velocity of compressional waves in rocks to 10 kilobars, *J. Geophys. Res.*, *65*, 1083–1102, 1960.

Birch, F., The velocity of compressional waves in rocks to 10 kilobars, 2, *J. Geophys. Res.*, *66*, 2199–2224, 1961.

Bird, P., and Y. Li, Interpolation of principal stress directions by nonparametric statistics: Global maps with confidence limits, *J. Geophys. Res.*, *101*, 5435–5443, 1996.

Bjarnason, I. T., C. J. Wolfe, S. C. Solomon, and G. Gudmundsson, Initial results from the ICEMELT experiment: Body-wave delay times and shear-wave splitting across Iceland, *Geophys. Res. Lett.*, *23*, 459–463, 1996. (Correction, *Geophys. Res. Lett.*, *23*, 903, 1996.)

Blackman, D. K., and J. M. Kendall, Sensitivity of teleseismic body waves to mineral texture and melt in the mantle beneath a mid-ocean ridge, *Philos. Trans. R. Soc. London, Ser. A*, *355*, 217–231, 1997.

Blackman, D. K., J. A. Orcutt, D. W. Forsyth, and J. M. Kendall, Seismic anisotropy in the mantle beneath an oceanic spreading centre, *Nature*, *366*, 675–677, 1993. (Correction to Seismic anisotropy in the mantle beneath an oceanic spreading centre, *Nature*, *374*, 824, 1995.)

Blackman, D. K., J. M. Kendall, P. R. Dawson, H. R. Wenk, D. Boyce, and J. P. Morgan, Teleseismic imaging of subaxial flow at mid-ocean ridges: Traveltime effects of anisotropic mineral texture in the mantle, *Geophys. J. Int.*, *127*, 415–426, 1996.

Booth, D. C., S. Crampin, R. Evans, and G. Roberts, Shear-wave polarization near the North Anatolian Fault, I, Evidence for anisotropy-induced shear-wave splitting, *Geophys. J. R. Astron. Soc.*, *83*, 61–73, 1985.

Bormann, P., G. Gruntha, R. Kind, and H. Montag, Upper mantle anisotropy beneath central Europe from *SKS* wave splitting: Effects of absolute plate motion and lithosphere-asthenosphere boundary topography?, *J. Geodyn.*, *22*, 11–32, 1996.

Bostock, M. G., Anisotropic upper-mantle stratigraphy and architecture of the Slave craton, *Nature*, *390*, 392–395, 1997.

Bostock, M. G., and J. F. Cassidy, Variations in *SKS* splitting across western Canada, *Geophys. Res. Lett.*, *22*, 5–8, 1995.

Bowman, J. R., and M. Ando, Shear-wave splitting in the upper-mantle wedge above the Tonga subduction zone, *Geophys. J. R. Astron. Soc.*, *88*, 25–41, 1987.

Bunge, H-P., and M. A. Richards, The origin of large scale structure in mantle convection: Effects of plate motions and viscosity stratification, *Geophys. Res. Lett.*, *23*, 2987–2990, 1996.

Cassidy, J. F., and M. G. Bostock, Shear-wave splitting above the subducting Juan de Fuca plate, *Geophys. Res. Lett.*, *23*, 941–944, 1996.

Chastel, Y. B., P. R. Dawson, H.-R. Wenk, and K. Bennett, Anisotropic convection with implications for the upper mantle, *J. Geophys. Res.*, *98*, 17,757–17,771, 1993.

Christensen, D., C. Searcy, S. Spitzak, and M. Savage, Velocity structure and anisotropy of the crust and upper mantle in the Brooks Range, Alaska from teleseismic observations (abstract), *Eos Trans. AGU*, *72*(44), Fall Meet. Suppl., 296, 1991.

Christensen, N. I., Shear wave velocities in metamorphic rocks at pressures to 10 kilobars, *J. Geophys. Res.*, *71*, 3549–3556, 1966a.

Christensen, N. I., Elasticity of ultrabasic rocks, *J. Geophys. Res.*, *71*, 5921–5931, 1966b.

Christensen, N. I., The magnitude, symmetry and origin of upper mantle anisotropy based on fabric analyses of ultramafic tectonites, *Geophys. J. R. Astron. Soc.*, *76*, 89–111, 1984.

Christensen, N. I., and R. S. Crosson, Seismic anisotropy in the upper mantle: Transverse isotropy of olivine-rich ultramafic rocks, significance for upper mantle anisotropy, *Tectonophysics*, *6*, 93–107, 1968.

Christensen, N. I., and M. H. Salisbury, Seismic anisotropy in the oceanic upper mantle: Evidence from the Bay of Islands ophiolite complex, *J. Geophys. Res.*, *84*, 4601–4610, 1979.

Christoffel, E. B., Uber die Fortpflanzung von Stossen durch elastische feste Korper, *Ann. Mater.*, *8*, 193–243, 1877.

Clitheroe, G., and R. van der Hilst, Complex anisotropy in the Australian lithosphere from shear-wave splitting in broadband *SKS* records, in *Structure and Evolution of the Australian Continent*, *Geodyn. Ser.*, vol. 26, edited by J. Braun et al., pp. 73–78, AGU, Washington, D. C., 1998.

Cooper, R. F., and D. L. Kohlstedt, Rheology and structure of olivine-basalt partial melts, *J. Geophys. Res.*, *91*, 9315–9323, 1986.

Crampin, S., A review of the effects of anisotropy layering on the propagation of seismic waves, *Geophys. J. R. Astron. Soc.*, *45*, 9–27, 1977.

Crampin, S., A review of wave motion in anisotropic and cracked elastic-media, *Wave Motion*, *3*, 343–391, 1981.

Crampin, S., The fracture criticality of crustal rocks, *Geophys. J. Int.*, *118*, 428–438, 1994.

Crampin, S., and D. C. Booth, Shear-wave polarizations near the North Anatolian Fault, II, Interpretations in terms of crack-induced anisotropy, *Geophys. J. R. Astron. Soc.*, *83*, 75–92, 1985.

Crampin, S., and R. McGonigle, The variation of delays in stress-induced anisotropic polarization anomalies, *Geophys. J. R. Astron. Soc.*, *64*, 115–131, 1981.

Crosson, R. S., and J. W. Lin, Voight and Reuss prediction of anisotropic elasticity of dunite, *J. Geophys. Res.*, *76*, 570–578, 1971.

Davidson, C., S. M. Schmid, and L. S. Hollister, Role of melt during deformation in the deep crust, *Terra Nova*, *6*, 133–142, 1994.

Davis, P., P. England, and G. Houseman, Comparison of shear wave splitting and finite strain from the India-Asia collision zone, *J. Geophys. Res.*, *102*, 27,511–27,522, 1997.

Dell'Angelo, L. N., and J. Tullis, Experimental deformation of partially melted granitic aggregates, *J. Metamorph. Geol.*, *6*, 495–515, 1988.

Díaz, J., A. Hirn, J. Gallart, and B. Abalos, Upper-mantle anisotropy in SW Iberia from long-range seismic profiles and teleseismic shear-wave data, *Phys. Earth Planet. Inter.*, *95*, 153–166, 1996.

Dunn, R. A., and D. R. Toomey, Seismological evidence for three-dimensional melt migration beneath the East Pacific Rise, *Nature*, *388*, 259–262, 1997.

Dziewonski, A. M., and D. L. Anderson, Preliminary reference Earth model, *Phys. Earth Planet. Inter.*, *25*, 297–356, 1981.

Earle, P. S., and P. M. Shearer, Characterization of global seismograms using an automatic-picking algorithm, *Bull. Seismol. Soc. Am.*, *84*, 366–376, 1994.

Ellis, R. M., Z. Hajnal, and M. G. Bostock, Seismic studies on the Trans-Hudson orogen of western Canada, *Tectonophysics*, *252*, 35–50, 1997.

Enderle, U., J. Mechie, S. Sobolev, and K. Fuchs, Seismic anisotropy within the uppermost mantle of southern Germany, *Geophys. J. Int.*, *125*, 747–767, 1996.

Estey, L., and B. Douglas, Upper mantle anisotropy: A preliminary model, *J. Geophys. Res.*, *91*, 11,393–11,406, 1986.

Farra, V., and L. Vinnik, Shear wave splitting in the mantle of the Pacific, *Geophys. J. Int.*, *119*, 195–218, 1994.

Farra, V., L. P. Vinnik, B. Romanowicz, G. L. Kosarev, and R. Kind, Inversion of teleseismic *S* particle motion for azimuthal anisotropy in the mantle: A feasibility study, *Geophys. J. Int.*, *106*, 421–431, 1991.

Fischer, K. M., and D. A. Wiens, The depth distribution of mantle anisotropy beneath the Tonga subduction zone, *Earth Planet. Sci. Lett.*, *142*, 253–260, 1996.

Fischer, K. M., and X. Yang, Anisotropy in Kuril-Kamchatka subduction zone structure, *Geophys. Res. Lett.*, *21*, 5–8, 1994.

Forsyth, D. W., The early structural evolution and anisotropy of the oceanic upper mantle, *Geophys. J. R. Astron. Soc.*, *43*, 103–162, 1975.

Forsyth, D. W., S. C. Webb, L. M. Dorman, and Y. Shen, Phase velocities of Rayleigh waves in the MELT experiment on the East Pacific Rise, *Science*, *280*, 1235–1238, 1998.

Fouch, M. J., and K. M. Fischer, Mantle anisotropy beneath northwest Pacific subduction zones, *J. Geophys. Res.*, *101*, 15,987–16,002, 1996.

Francis, T. J. G., Generation of seismic anisotropy in the upper mantle along the mid-ocean ridges, *Nature*, *221*, 162–165, 1969.

Frohlich, C., and R. J. Willemann, Statistical methods for comparing directions to the orientations of focal mechanisms and Wadati-Benioff zones, *Bull. Seismol. Soc. Am.*, *77*, 2135–2142, 1987.

Fujimura, A., Preferred orientation of silicate spinel inferred from experimentally deformed aggregates of trevorite, *J. Phys. Earth*, *32*, 273–297, 1984.

Fujimura, A., Preferred orientation of mantle minerals, in *Rheology of Solids and of the Earth*, edited by S. Karato and M. Toriumi, pp. 263–283, Oxford Univ. Press, New York, 1989.

Fukao, Y., Evidence from core-reflected shear waves for anisotropy in the Earths' mantle, *Nature*, *371*, 149–151, 1984.

Furumoto, A. S., The use of *ScS*-wave data in focal mechanism determinations, *Bull. Seismol. Soc. Am.*, *52*, 551–572, 1962.

Gable, C. W., R. J. O'Connell, and B. J. Travis, Convection in three dimensions with surface plates: Generation of toroidal flow, *J. Geophys. Res.*, *96*, 8391–8405, 1991.

Gaherty, J. B., and T. H. Jordan, Lehmann discontinuity as the base of an anisotropic layer beneath continents, *Science*, *268*, 1468–1471, 1995.

Gaherty, J. B., T. H. Jordan, and L. S. Gee, Seismic structure of the upper mantle in a central Pacific corridor, *J. Geophys. Res.*, *101*, 22,291–22,309, 1996.

Gao, S., P. M. Davis, H. Liu, P. D. Slack, and Y. A. Zorin, Seismic anisotropy and mantle flow beneath the Baikal rift zone, *Nature*, *371*, 149–151, 1994.

Gao, S., P. M. Davis, H. Liu, P. D. Slack, A. W. Rigor, Y. Z. Zorin, V. V. Mordvinova, V. M. Kozhevnikov, and N. A. Logatchev, *SKS* splitting beneath continental rift zones, *J. Geophys. Res.*, *102*, 22,781–22,797, 1997.

Garmany, J., A student's garden of anisotropy, *Annu. Rev. Earth Planet. Sci.*, *17*, 285–308, 1989.

Garnero, E. J., and T. Lay, Lateral variations in lowermost mantle shear wave anisotropy beneath the North Pacific and Alaska, *J. Geophys. Res.*, *102*, 8121–8135, 1997.

Gledhill, K., and D. Gubbins, *SKS* splitting and the seismic anisotropy of the mantle beneath the Hikurangi subduction zone, New Zealand, *Phys. Earth Planet. Inter.*, *95*, 227–236, 1996.

Gledhill, K., and G. Stuart, Seismic anisotropy in the fore-arc region of the Hikurangi subduction zone, New Zealand, *Phys. Earth Planet. Inter.*, *95*, 211–225, 1996.

Gledhill, K., M. Savage, and K. Marson, Shear-wave splitting measurements in the Southern Alps region, South Island, New Zealand (abstract), *Eos Trans. AGU*, *77*(22), West. Pac. Geophys. Meet. Suppl., W84, 1996.

Goetze, C., and D. L. Kohlstedt, Laboratory study of dislocation climb and diffusion in olivine, *J. Geophys. Res.*, *78*, 5961–5971, 1973.

Grechka, V., and G. McMechan, Anisotropy and non-linear polarization of body waves in exponentially heterogeneous media, *Geophys. J. Int.*, *123*, 959–965, 1995.

Griot, D.-A., J.-P. Montagner, and P. Tapponnier, Anisotropic tomography in Central Asia (abstract), *Eos Trans. AGU*, *76*(46), Fall Meet. Suppl., F386, 1995.

Gripp, A. G., and R. G. Gordon, Current plate velocities relative to the hotspots incorporating the NUVEL-1 global plate motion model, *Geophys. Res. Lett.*, *17*, 1109–1112, 1990.

Guilbert, J., G. Poupinet, and J. Mei, A study of azimuthal *P* residuals and shear-wave splitting across the Kunlun range (northern Tibetan Plateau), *Phys. Earth Planet. Inter.*, *95*, 167–174, 1996.

Hadiouche, O., N. Jobert, and J. P. Montagner, Anisotropy of the African continent inferred from surface waves, *Phys. Earth Planet. Inter.*, *58*, 61–81, 1989.

Hager, B. H., and R. J. O'Connell, Kinematic models of large-scale flow in the Earth's mantle, *J. Geophys. Res.*, *84*, 1031–1048, 1979.

Hearn, T. M., Anisotropic P_n tomography in the western United States, *J. Geophys. Res.*, *101*, 8403–8414, 1996.

Helbig, K., Simultaneous observation of seismic waves of different polarization indicates subsurface anisotropy and might help to unravel its cause, *J. Appl. Geophys.*, *30*, 1–24, 1993.

Hess, H. H., Seismic anisotropy of the uppermost mantle under oceans, *Nature*, *203*, 629–631, 1964.

Hiramatsu, Y., and M. Ando, Seismic anisotropy near source region in subductions zones around Japan, *Phys. Earth Planet. Inter.*, *95*, 237–250, 1996.

Hiramatsu, Y., M. Ando, and Y. Ishikawa, *ScS* wave splitting of deep earthquakes around Japan, *Geophys. J. Int.*, *128*, 409–242, 1997.

Hirn, A., M. Jiang, M. Sapin, J. Díaz, A. Nercessian, Q. T. Lu, J. C. Lepine, D. N. Shi, M. Sachpazi, M. R. Pandy, K. Ma, and J. Gallart, Seismic anisotropy as an indicator of mantle flow beneath the Himalayas and Tibet, *Nature*, *375*, 571–574, 1995.

Holt, W., Placing constraints on the crust and mantle deformation field in Asia (abstract), *Eos Trans. AGU*, *78*(46), Fall Meet. Suppl., F699, 1997.

Holt, W. E., M. Li, and A. J. Haines, Earthquake strain rates and instantaneous relative motions within central and eastern Asia, *Geophys. J. Int.*, *122*, 569–593, 1995.

Hrouda, F., Z. Pros, and J. Wohlgemuth, Development of magnetic and elastic anisotropies in slates during progressive deformation, *Phys. Earth Planet. Inter.*, *77*, 251–265, 1993.

Ida, Y., Preferred orientation of olivine and anisotropy of the oceanic lithosphere, *J. Phys. Earth*, *32*, 245–257, 1984.

Iidaka, T., and K. Obara, Shear-wave polarization anisotropy in the mantle wedge above the subducting Pacific Plate, *Tectonophysics*, *249*, 53–68, 1995.

Ishikawa, Y., Anisotropic plate thickening model, *J. Phys. Earth*, *32*, 219–228, 1984.

James, D. E., and M. Assumpção, Tectonic implications of *S*-wave anisotropy beneath SE Brazil, *Geophys. J. Int.*, *126*, 1–10, 1996.

Ji, S., M. Salisbury, and S. Hanmer, Petrofabric, *P*-wave anisotropy and seismic reflectivity of high-grade tectonites, *Tectonophysics*, *222*, 195–226, 1993.

Ji, S., X. Zhao, and D. Francis, Calibration of shear-wave splitting in the subcontinental upper mantle beneath active orogenic belts using ultramafic xenoliths from the Canadian Cordillera and Alaska, *Tectonophysics*, *239*, 1–27, 1994.

Jordan, T. H., Composition and development of the continental tectosphere, *Nature*, *274*, 544–548, 1978.

Kaneshima, S., and P. G. Silver, A search for source side mantle anisotropy, *Geophys. Res. Lett.*, *19*, 1049–1052, 1992.

Kaneshima, S., and P. G. Silver, Anisotropic loci in the mantle beneath central Peru, *Phys. Earth Planet. Inter.*, *88*, 257–272, 1995.

Kaneshima, S., M. Ando, and S. Kimura, Evidence from shear-wave splitting for the restriction of seismic anisotropy to the upper crust, *Nature*, *335*, 627–629, 1988.

Karato, S., Seismic anisotropy due to lattice preferred orientation of minerals: Kinematic or dynamic?, in *High-Pressure Research in Mineral Physics*, *Geophys. Monogr. Ser.*, vol. 39, edited by M. H. Manghnani and S. Syono, pp. 455–471, AGU, Washington, D. C., 1987.

Karato, S., On the Lehmann discontinuity, *Geophys. Res. Lett.*, *19*, 2255–2258, 1992.

Karato, S., and P. Li, Diffusive creep in perovskite: Implications for the rheology of the lower mantle, *Science*, *255*, 1238–1240, 1992.

Karato, S., and P. Wu, Rheology of the upper mantle: A synthesis, *Science*, *260*, 771–778, 1993.

Kawasaki, I., Azimuthally anisotropic model of the oceanic upper mantle, *Phys. Earth Planet. Inter.*, *43*, 1–21, 1986.

Keith, C. M., and S. Crampin, Seismic body waves in anisotropic media: Synthetic seismograms, *Geophys. J. R. Astron. Soc.*, *49*, 225–243, 1977.

Kelvin, Lord (W. Thomson), *Baltimore Lectures*, Cambridge Univ. Press, New York, 1904.

Kendall, J. M., Teleseismic arrivals at a mid-ocean ridge: Effects of mantle melt and anisotropy, *Geophys. Res. Lett.*, *21*, 301–304, 1994.

Kendall, J. M., and P. G. Silver, Constraints from seismic anisotropy on the nature of the lowermost mantle, *Nature*, *381*, 409–413, 1996.

Kendall, J. M., and C. J. Thomson, A comment on the form of the geometrical spreading equations, with some examples of seismic ray tracing in inhomogeneous, anisotropic media, *Geophys. J. Int.*, *99*, 401–413, 1989.

Kendall, J. M., and C. J. Thomson, Maslov ray summation, pseudo-caustics, Lagrangian equivalence and transient seismic waveforms, *Geophys. J. Int.*, *113*, 186–214, 1993.

Kern, H., Laboratory seismic measurements: An aid in the interpretation of seismic field data, *Terra Nova*, *2*, 617–628, 1990.

Kern, H., *P*- and *S*-wave anisotropy and shear wave splitting at pressure and temperature in possible mantle rocks and their relations to the rock fabric, *Phys. Earth Planet. Inter.*, *78*, 245–256, 1993a.

Kern, H., Physical properties of crustal and upper mantle rocks with regards to lithosphere dynamics and high pressure mineralogy, *Phys. Earth Planet. Inter.*, *79*, 113–136, 1993b.

Kern, H., and H. R. Wenk, Fabric-related velocity anisotropy and shear wave splitting in rocks from Santa Rosa mylonite zone, California, *J. Geophys. Res.*, *95*, 11,213–11,223, 1990.

Kern, H., L. Burlini, and I. V. Aschepkov, Fabric-related seismic anisotropy in upper-mantle xenoliths: Evidence from measurements and calculations, *Phys. Earth Planet. Inter.*, *95*, 195–209, 1996.

Klosko, E., F. Wu, H. Anderson, D. Eberhart-Phillips, and T. McEvilly, Shear-wave splitting and seismic anisotropy in the New Zealand region (abstract), *Eos Trans. AGU*, *78*(46), Fall Meet. Suppl., F488, 1997.

Kuo, B.-Y., and D. W. Forsyth, A search for split *SKS* wave-

forms in the North Atlantic, *Geophys. J. Int.*, *108*, 557–574, 1992.

Kuo, B.-Y., D. W. Forsyth, and M. Wysession, Lateral heterogeneity and azimuthal anisotropy in the North Atlantic determined from *SS-S* differential travel times, *J. Geophys. Res.*, *92*, 6421–6436, 1987.

Lavé, J., J. P. Avouac, R. Lacassin, P. Tapponnier, and J. P. Montagner, Seismic anisotropy beneath Tibet: Evidence for eastward extrusion of the Tibetan lithosphere?, *Earth Planet. Sci. Lett.*, *140*, 83–96, 1996.

Lay, T., and D. V. Helmberger, The shear-wave velocity gradient at the base of the mantle, *J. Geophys. Res.*, *88*, 8160–8170, 1983.

Lay, T., and C. J. Young, Analysis of seismic *SV* waves in the core's penumbra, *Geophys. Res. Lett.*, *18*, 1373–1376, 1991.

Lehmann, I., Velocities of longitudinal waves in the upper part of the Earth's mantle, *Ann. Geophys.*, *15*, 93–118, 1959.

Lehmann, I., *S* and the structure of the upper mantle, *Geophys. J. R. Astron. Soc.*, *4*, 124–138. 1961.

Leven, J. N., L. Jackson, and A. E. Ringwood, Upper mantle seismic anisotropy and lithospheric decoupling, *Nature*, *289*, 234–239, 1981.

Levin, V., and J. Park, Crustal anisotropy in the Ural Mountains foredeep from teleseismic receiver functions, *Geophys. Res. Lett.*, *24*, 1283–1286, 1997a.

Levin, V., and J. Park, *P-SH* conversions in a flat-layered medium with anisotropy of arbitrary orientation, *Geophys. J. Int.*, *131*, 253–266, 1997b.

Levin, V., W. Menke, and A. Lerner-Lam, Seismic anisotropy in the north-eastern US as a source of significant teleseismic *P* traveltime anomalies, *Geophys. J. Int.*, *126*, 593–603, 1997.

Liu, H., P. M. Davis, and S. Gao, *SKS* splitting beneath southern California, *Geophys. Res. Lett.*, *22*, 767–770, 1995.

Love, A. E. H., *A Treatise on the Mathematical Theory of Elasticity*, 4th ed., Dover, Mineola, N. Y., 1944.

Mainprice, D., Modeling the anisotropic seismic properties of partially molten rocks found at mid-ocean ridges, *Tectonophysics*, *279*, 161–179, 1997.

Mainprice, D., and M. Humbert, Methods of calculating petrophysical properties from lattice preferred orientation data, *Surv. Geophys.*, *15*, 575–592, 1994.

Mainprice, D., and A. Nicolas, Development of shape and lattice preferred orientations: Applications to the seismic anisotropy of the lower crust, *J. Struct. Geol.*, *11*, 175–189, 1989.

Mainprice, D., and P. G. Silver, Interpretation of *SKS*-waves using samples from the subcontinental lithosphere, *Phys. Earth Planet. Inter.*, *78*, 257–280, 1993.

Majer, E. L., T. V. McEvilly, F. S. Eastwood, and L. R. Myer, Fracture detection using *P* wave and *S* wave vertical seismic profiling at The Geysers, *Geophysics*, *53*, 76–84, 1988.

Makeyeva, L. I., L. P. Vinnik, and S. W. Roecker, Shear-wave splitting and small-scale convection in the continental upper mantle, *Nature*, *358*, 144–146, 1992.

Mardia, K. V., *Statistics of Directional Data*, Academic, San Diego, Calif., 1972.

Margheriti, L., C. Nostro, M. Cocco, and A. Amato, Seismic anisotropy beneath the Northern Apennines (Italy) and its tectonic implications, *Geophys. Res. Lett.*, *23*, 2721–2724, 1996.

Marson, K., Seismic anisotropy beneath the lower half of the North Island, New Zealand, Masters thesis, 72 pp., Victoria Univ. of Wellington, Wellington, New Zealand, 1997.

Marson-Pidgeon, K., and M. Savage, Seismic anisotropy beneath Wellington, New Zealand from shear-wave splitting, *Geophys. Res. Lett.*, *24*, 3297–3300, 1997.

Martin, B. E., and C. J. Thomson, Modeling surface waves in anisotropic structures, II, Examples, *Phys. Earth Planet. Inter.*, *103*, 253–279, 1997.

Matzel, E., M. K. Sen, and S. P. Grand, Evidence for anisotropy in the deep mantle beneath Alaska, *Geophys. Res. Lett.*, *23*, 2417–2420, 1996.

Maupin, V., Partial derivatives of surface wave phase velocities for flat anisotropic models, *Geophys. J. R. Astron. Soc.*, *83*, 379–398, 1985.

Maupin, V., On the possibility of anisotropy in the D″ layer as inferred from the polarization of diffracted *S* waves, *Phys. Earth Planet. Inter.*, *87*, 1–32, 1994.

McKenzie, D., Finite deformation during fluid flow, *Geophys. J. R. Astron. Soc.*, *58*, 687–715, 1979.

McNamara, D. E., and T. J. Owens, Azimuthal shear wave velocity anisotropy in the Basin and Range Province using Moho *Ps* converted phases, *J. Geophys. Res.*, *98*, 12,003–12,017, 1993.

McNamara, D. E., T. J. Owens, P. G. Silver, and F. T. Wu, Shear wave anisotropy beneath the Tibetan Plateau, *J. Geophys. Res.*, *99*, 13,655–13,665, 1994.

Meade, C., and R. Jeanloz, The strength of mantle silicates at high pressures and room temperature: Implications for the viscosity of the mantle, *Nature*, *348*, 533–535, 1990.

Meade, C., P. G. Silver, and S. Kaneshima, Laboratory and seismological observations of lower mantle isotropy, *Geophys. Res. Lett.*, *22*, 1293–1296, 1995.

Menke, W., B. Brandsdottir, P. Einarsson, R. Sethi, R. White, and J. McBride, Seismic structure of the Mid-Atlantic plate boundary in northern Iceland (abstract), *Eos Trans. AGU*, *75*(44), Fall Meet. Suppl., 619, 1994.

Milev, A., and L. P. Vinnik, Deformations in the continental mantle from the data of Global Digital Seismograph network (in Russian), *Dokl. Akad. Nauk SSSR*, *318*, 1132–1136, 1991.

Mjelde, R., and M. A. Sellevoll, Seismic anisotropy inferred from wide-angle reflections off Lofoten, Norway, indicative of shear-aligned minerals in the upper mantle, *Tectonophysics*, *222*, 21–32, 1993.

Montagner, J.-P., Can seismology tell us anything about convection in the mantle?, *Rev. Geophys.*, *32*, 115–137, 1994.

Montagner, J.-P., and B. L. N. Kennett, How to reconcile body-wave and normal-mode reference Earth models, *Geophys. J. Int.*, *125*, 229–248, 1996.

Montagner, J.-P., and T. Tanimoto, Global anisotropy in the upper mantle inferred from the regionalization of the phase velocities, *J. Geophys. Res.*, *95*, 4797–4819, 1990.

Montagner, J.-P., and T. Tanimoto, Global upper mantle tomography of seismic velocities and anisotropies, *J. Geophys. Res.*, *96*, 20,337–20,351, 1991.

Musgrave, M. J. P., Propagation of elastic waves in crystals and anisotropic media, *Rep. Progr. Phys.*, *22*, 74–96, 1959.

Nicolas, A., *Principles of Rock Deformation*, 208 pp., D. Reidel, Norwell, Mass., 1984.

Nicolas, A., Kinematics in magmatic rocks with special reference to gabbros, *J. Petrol.*, *33*, 891–915, 1992.

Nicolas, A., Why fast polarization directions of *SKS* seismic waves are parallel to mountain belts, *Phys. Earth Planet. Inter.*, *78*, 337–342, 1993.

Nicolas, A., and N. I. Christensen, Formation of anisotropy in upper mantle peridotites: A review, in *Composition, Structure and Dynamics of the Lithosphere-Asthenosphere System*, *Geodyn. Ser.*, vol. 16, edited by K. Fuchs and C. Froidevaux, pp. 111–123, AGU, Washington, D. C., 1987.

Nicolas, A., and J. P. Poirier, *Crystalline Plasticity and Solid State Flow in Metamorphic Rocks*, 444 pp., John Wiley, New York, 1976.

Nicolas, A., F. Boudier, and A. M. Boullier, Mechanisms of flow in naturally and experimentally deformed peridotites, *Am. J. Sci.*, *273*, 853–876, 1973.

Nishimura, C. E., and D. W. Forsyth, Rayleigh wave phase velocities in the Pacific with implications for azimuthal anisotropy and lateral heterogeneity, *Geophys. J. R. Astron. Soc.*, *94*, 497–501, 1988.

Nishimura, C. E., and D. W. Forsyth, The anisotropic structure of the upper mantle in the Pacific, *Geophys. J.*, *96*, 203–229, 1989.

Nur, A., Effects of stress on velocity anisotropy in rocks with cracks, *J. Geophys. Res.*, *76*, 2022–2034, 1971.

Nur, A., and G. Simmons, Stress-induced velocity anisotropy in rock: An experimental study, *J. Geophys. Res.*, *74*, 6667–6674, 1969.

Nuttli, O. W., The effect of the Earth's surface on the *S* wave particle motion, *Bull. Seismol. Soc. Am.*, *51*, 237–246, 1961.

Nuttli, O. W., and J. D. Whitmore, On the determination of the polarization angle of the *S* wave, *Bull. Seismol. Soc. Am.*, *52*, 95–107, 1962.

Oda, H., and H. Shimizu, *S* wave splitting observed in southwest Japan, *Tectonophysics*, *270*, 73–82, 1997.

Okada, T., T. Matsuzawa, and A. Hasegawa, Shear-wave polarization anisotropy beneath the north-eastern part of Honshu, Japan, *Geophys. J. Int.*, *123*, 781–797, 1995.

Okal, E. A., A student's guide to teleseismic body wave amplitudes, *Seismol. Res. Lett.*, *63*, 169–180, 1992.

Okaya, D., N. Christensen, D. Stanley, and T. Stern, Crustal anisotropy in the vicinity of the Alpine Fault Zone, *N. Z. J. Geol. Geophys.*, *38*, 579–583, 1995.

Özalaybey, S., and M. K. Savage, Double-layer anisotropy resolved from *S* phases, *Geophys. J. Int.*, *117*, 653–664, 1994.

Özalaybey, S., and M. K. Savage, Shear wave splitting beneath western United States in relation to plate tectonics, *J. Geophys. Res.*, *100*, 18,135–18,149, 1995.

Plomerovà, J., J. Šílený, and V. Babuška, Joint interpretation of upper-mantle anisotropy based on teleseismic *P*-travel time delays and inversion of shear-wave splitting parameters, *Phys. Earth Planet. Inter.*, *95*, 293–310, 1996.

Raitt, R. W., G. G. Shor, T. J. G. Francis, and G. B. Morris, Anisotropy of the Pacific upper mantle, *J. Geophys. Res.*, *74*, 3095–3109, 1969.

Revenaugh, J., and T. H. Jordan, Mantle layering from *ScS* reverberations, 3, The upper mantle, *J. Geophys. Res.*, *96*, 19,781–19,810, 1991.

Ribe, N. M., Seismic anisotropy and mantle flow, *J. Geophys. Res.*, *94*, 4213–4223, 1989.

Ribe, N. M., On the relation between seismic anisotropy and finite strain, *J. Geophys. Res.*, *97*, 8737–8747, 1992.

Ribe, N. M., and Y. Yu, A theory for plastic deformation and textural evolution of olivine polycrystals, *J. Geophys. Res.*, *96*, 8325–8335, 1991.

Rowlands, H. J., D. C. Booth, and J-M. Chiu, Shear-wave splitting from microearthquakes in the New Madrid seismic zone, *Can. J. Expl. Geophys.*, *29*, 352–362, 1993.

Rumpker, G., R. J. Brown, and C. J. Thomson, Shear wave propagation in orthorhombic phenolic: A comparison of numerical and physical modeling, *J. Geophys. Res.*, *101*, 27,765–27,777, 1997.

Ruppert, S. D., Teleseismic shear-wave response of the crust and upper mantle across the southwest margin of the Colorado Plateau, Arizona, Ph.D. thesis, Stanford Univ., Stanford, Calif., 1992.

Russo, R. M., and P. G. Silver, Trench-parallel flow beneath the Nazca plate from seismic anisotropy, *Science*, *263*, 1105–1111, 1994.

Russo, R. M., P. G. Silver, M. Franke, W. B. Ambeh, and D. E. James, Shear-wave splitting in northeast Venezuela, Trinidad, and the eastern Caribbean, *Phys. Earth Planet. Inter.*, *95*, 251–275, 1996.

Sandvol, E., and J. Ni, Deep azimuthal anisotropy in the southern Kurile and Japan subduction zones, *J. Geophys. Res.*, *102*, 9911–9922, 1997.

Sandvol, E., J. Ni, S. Özalaybey, and J. Schlue, Shear-wave splitting in the Rio Grande Rift, *Geophys. Res. Lett.*, *19*, 2337–2340, 1992.

Sandvol, E., J. F. Ni, T. M. Hearn, and S. Roecker, Seismic azimuthal anisotropy beneath the Pakistan Himalayas, *Geophys. Res. Lett.*, *21*, 1635–1638, 1994.

Sandvol, E., J. Ni, R. Kind, and W. Zhao, Seismic anisotropy beneath the southern Himalayas-Tibet collision zone, *J. Geophys. Res.*, *102*, 17,813–17,823, 1997.

Savage, M. K., Lower crustal anisotropy or dipping boundaries? Effects on receiver functions, *J. Geophys. Res.*, *103*, 15,069–15,087, 1998.

Savage, M. K., and P. G. Silver, Mantle deformation and tectonics: Constraints from seismic anisotropy in western United States, *Phys. Earth Planet. Inter.*, *78*, 207–228, 1993.

Savage, M. K., X. R. Shih, R. P. Meyer, and R. C. Aster, Shear-wave anisotropy of active tectonic regions via automated *S*-wave polarization analysis, *Tectonophysics*, *165*, 279–292, 1989.

Savage, M. K., W. A. Peppin, and U. R. Vetter, Shear-wave anisotropy and stress direction in and near Long Valley Caldera, California, 1979–1988, *J. Geophys. Res.*, *95*, 11,165–11,177, 1990a.

Savage, M. K., P. G. Silver, and R. P. Meyer, Observations of teleseismic shear-wave splitting in the Basin and Range from portable and permanent stations, *Geophys. Res. Lett.*, *17*, 21–24, 1990b.

Savage, M. K., K. Gledhill, and K. Marson, A search for lower crustal anisotropy in strike-slip regions, *Eos Trans. AGU*, *77*(22), West. Pac. Geophys. Meet. Suppl., W84, 1996a.

Savage, M. K., A. F. Sheehan, and A. Lerner-Lam, Shear-wave splitting across the Rocky Mountain Front, *Geophys. Res. Lett.*, *23*, 2267–2270, 1996b.

Sawamoto, H., D. J. Weidner, S. Sasaki, and M. Kumazawa, Single-crystal elastic properties of the modified spinel (beta) phase of magnesium orthosilicate, *Science*, *224*, 749–751, 1984.

Schlue, J. W., and L. Knopoff, Shear-wave polarization anisotropy in the Pacific basin, *Geophys. J. R. Astron. Soc.*, *49*, 145–165, 1977.

Schoenecker, S. C., R. M. Russo, and P. G. Silver, Source-side splitting of *S* waves from Hindu Kush-Pamir earthquakes, *Tectonophysics*, *279*, 149–159, 1997.

Schutt, D., E. D. Humphreys, and K. Dueker, Anisotropy of the Yellowstone Hotspot wake, eastern Snake River Plain, Idaho, *Pure Appl. Geophys.*, *151*, 443–462, 1998.

Sharp, T. G., G. Y. A. Bussod, and T. Katsura, Microstructures in $\beta - Mg_{1.8}Fe_{0.2}SiO_4$ experimentally deformed at transition-zone conditions, *Phys. Earth Planet. Inter.*, *86*, 69–83, 1994.

Shearer, P., Imaging global body wave phases by stacking long-period seismograms, *J. Geophys. Res.*, *96*, 20,353–20,364, 1991.

Shearer, P. M., and J. A. Orcutt, Compressional and shear wave anisotropy in the oceanic lithosphere—The Ngendei seismic refraction experiment, *Geophys. J. R. Astron. Soc.*, *87*, 967–1003, 1986.

Sheehan, A. F., and S. C. Solomon, Joint inversion of shear wave travel time residuals, geoid, and depth anomalies along the Mid-Atlantic Ridge for long-wavelength variations in upper mantle temperature and composition, *J. Geophys. Res.*, *96*, 19,981–20,009, 1991.

Sheehan, A. F., C. H. Jones, M. K. Savage, S. Özalaybey, K. G. Dueker, J. M. Schneider, and J. E. Bartsch, Contrasting lithospheric structure between the Colorado Plateau and Great Basin: Initial results from Colorado Plateau–Great

Basin PASSCAL experiment, *Geophys. Res. Lett.*, *24*, 2609–2612, 1997.

Shih, X. R., R. P. Meyer, and J. F. Schneider, An automated, analytic method to determine shear-wave anisotropy, *Tectonophysics*, *165*, 271–278, 1989.

Shih, X. R., R. P. Meyer, and J. F. Schneider, Seismic anisotropy above a subducting plate, *Geology*, *19*, 807–810, 1991.

Šílený, J., and J. Plomerovà, Inversion of shear-wave splitting parameters to retrieve three-dimensional orientation of anisotropy in continental lithosphere, *Phys. Earth Planet. Inter.*, *95*, 277–292, 1996.

Silver, P. G., Seismic anisotropy beneath the continents: Probing the depths of Geology, *Annu. Rev. Earth Planet. Sci.*, *24*, 385–432, 1996.

Silver, P. G., and W. W. Chan, Implications for continental structure and evolution from seismic anisotropy, *Nature*, *335*, 34–39, 1988.

Silver, P. G., and W. W. Chan, Shear-wave splitting and subcontinental mantle deformation, *J. Geophys. Res.*, *96*, 16,429–16,454, 1991.

Silver, P. G., and M. K. Savage, The interpretation of shear-wave splitting parameters in the presence of two anisotropic layers, *Geophys. J. Int.*, *119*, 949–963, 1994.

Smith, M. L., and F. A. Dahlen, The azimuthal dependence of Love and Rayleigh wave propagation in a slightly anisotropic medium, *J. Geophys. Res.*, *78*, 3321–3333, 1973.

Stonely, R., The seismological implications of aelotropy in continental structure, *Mon. Not. R. Astron. Soc., Geophys. Suppl.*, *5*, 222–232, 1949.

Su, L., and J. Park, Anisotropy and the splitting of *PS* waves, *Phys. Earth Planet. Inter.*, *86*, 263–276, 1994.

Takeuchi, S., Motion of dislocations: Characteristics of high-temperature deformation, in *Rheology of Solids and of the Earth*, edited by S.-I. Karato and M. Toriumi, pp. 1–14, Oxford Univ. Press, New York, 1989.

Tanimoto, T., and D. L. Anderson, Mapping mantle convection, *Geophys. Res. Lett.*, *11*, 287–290, 1984.

Taylor, D. B., Double contour integration for transmission from point sources through anisotropic layers as used in ROCPAC software, *Geophys. J. R. Astron. Soc.*, *91*, 373–381, 1987.

Tommasi, A., A. Vauchez, and R. Russo, Seismic anisotropy in ocean basins: Resistive drag of the sublithospheric mantle?, *Geophys. Res. Lett.*, *23*, 2991–2994, 1996.

Tong, C., O. Gudmundsson, and B. L. N. Kennett, Shear wave splitting in refracted waves returned from the upper mantle transition zone beneath northern Australia, *J. Geophys. Res.*, *99*, 15,783–15,797, 1994.

Toriumi, M., Preferred orientation of olivine in mantle-derived peridotites and stress in the lithosphere, *J. Phys. Earth*, *32*, 259–271, 1984.

Tsvankin, I., and E. Chesnokov, Synthetic waveforms and polarizations at the free surface of an anisotropic halfspace, *Geophys. J. Int.*, *101*, 497–505, 1990.

Van der Molen, I., and M. S. Paterson, Experimental deformation of partially-melted granite, *Contrib. Mineral. Petrol.*, *70*, 299–318, 1979.

Vauchez, A., and G. Barruol, Shear-wave splitting in the Appalachians and the Pyrenees: Importance of the inherited tectonic fabric of the lithosphere, *Phys. Earth Planet. Inter.*, *95*, 127–138, 1996.

Vauchez, A., and A. Nicolas, Mountain building: Strike-parallel motion and mantle anisotropy, *Tectonophysics*, *185*, 183–191, 1991.

Vinnik, L., and R. Kind, Ellipticity of teleseismic *S*-particle motion, *Geophys. J. Int.*, *113*, 165–174, 1993.

Vinnik, L., and J.-P. Montagner, Shear wave splitting in the mantle *Ps* phases, *Geophys. Res. Lett.*, *23*, 2449–2452, 1996.

Vinnik, L. P., G. L. Kosarev, and L. I. Makeyeva, Azimuthal anisotropy of the lithosphere from observations of long period converted waves (in Russian), in *Structure and Dynamics of the Lithosphere According to Seismic Data*, edited by I. L. Nercesov, pp. 62–107, Nauka, Moscow, 1988.

Vinnik, L. P., V. Farra, and B. Romanowicz, Azimuthal anisotropy in the Earth from observations of *SKS* at Geoscope and NARS broadband stations, *Bull. Seismol. Soc. Am.*, *79*, 1542–1558, 1989a.

Vinnik, L. P., R. Kind, G. L. Kosarev, and L. I. Makeyeva, Azimuthal anisotropy in the lithosphere from observations of long-period *S*-waves, *Geophys. J. Int.*, *99*, 549–559, 1989b.

Vinnik, L. P., L. I. Makeyeva, A. Milev, and A. Yu. Usenko, Global patterns of azimuthal anisotropy and deformations in the continental mantle, *Geophys. J. Int.*, *111*, 433–447, 1992.

Vinnik, L. P., V. G. Krishna, R. Kind, P. Bormann, and K. Stammler, Shear wave splitting in the records of the German Regional Seismic Network, *Geophys. Res. Lett.*, *21*, 457–460, 1994.

Vinnik, L., B. Romanowicz, Y. Le Stunff, and L. Makeyeva, Seismic anisotropy in the D″ layer, *Geophys. Res. Lett.*, *22*, 1657–1660, 1995a.

Vinnik, L. P., R. W. E. Green, and L. O. Nicolaysen, Recent deformations of the deep continental root beneath southern Africa, *Nature*, *375*, 50–52, 1995b.

Vinnik, L. P., R. W. E. Green, and L. O. Nicolaysen, Seismic constraints on dynamics of the mantle of the Kaapvaal craton, *Phys. Earth Planet. Inter.*, *95*, 139–151, 1996.

Wenk, H.-R., and J. M. Christie, Review paper: Comments on the interpretation of deformation textures in rocks, *J. Struct. Geol.*, *13*, 1091–1110, 1991.

Wenk, H.-R., G. Canova, A. Molinari, and U. F. Kocks, Viscoplastic modeling of texture development in quartzite, *J. Geophys. Res.*, *94*, 17,895–17,906, 1989.

Wenk, H.-R., K. Bennett, G. R. Canova, and A. Molinari, Modeling plastic deformation of peridotite with the self-consistent theory, *J. Geophys. Res.*, *96*, 8337–8349, 1991.

Wolfe, C. J., and P. G. Silver, Seismic anisotropy of oceanic upper mantle: Shear-wave splitting methodologies and observations, *J. Geophys. Res.*, *103*, 749–771, 1998.

Wolfe, C. J., and S. C. Solomon, Shear-wave splitting and implications for mantle flow beneath the MELT region of the East Pacific Rise, *Science*, *280*, 1230–1232, 1998.

Wolfe, C. J., S. C. Solomon, D. R. Toomey, and D. W. Forsyth, Upper mantle anisotropy beneath the MELT region of the East Pacific Rise: Initial shear-wave splitting measurements, *Eos Trans. AGU*, *77*(46), Fall Meet. Suppl., F653, 1996.

Woodward, R. L., and G. Masters, Global upper mantle structure from long-period differential travel-times, *J. Geophys. Res.*, *96*, 6351–6377, 1991.

Xie, J., Shear-wave splitting near Guam, *Phys. Earth Planet. Inter.*, *72*, 211–219, 1992.

Yang, X., and K. M. Fischer, Constraints on North Atlantic upper mantle anisotropy from *S* and *SS* phases, *Geophys. Res. Lett.*, *21*, 309–312, 1994.

Yang, X., K. M. Fischer, and G. A. Abers, Seismic anisotropy beneath the Shumagin Islands segment of the Aleutian-Alaska subduction zone, *J. Geophys. Res.*, *100*, 18,165–18,178, 1995.

Yardley, G. S., and S. Crampin, Extensive-dilatancy anisotropy: Relative information in VSPs and reflection surveys, *Geophys. Prospect.*, *39*, 337–355, 1991.

Yu, Y., and J. Park, Hunting for upper mantle anisotropy beneath the Pacific Ocean region, *J. Geophys. Res.*, *99*, 15,399–15,421, 1994.

Yu, Y., J. Park, and F. Wu, Mantle anisotropy beneath the Tibetan Plateau: Evidence from long-period surface waves, *Phys. Earth Planet. Inter.*, *87*, 231–246, 1995.

Zhang, S., and S.-I. Karato, Lattice preferred orientation of olivine aggregates deformed in simple shear, *Nature*, *375*, 774–777, 1995.

Zhang, Z., and S. Y. Schwartz, Seismic anisotropy in the shallow crust of the Loma Prieta segment of the San Andreas fault system, central Coast Ranges, California, *J. Geophys. Res.*, *99*, 9651–9661, 1994.

Zhao, L., Lateral variations and azimuthal isotropy of *Pn* velocities beneath Basin and Range Province, *J. Geophys. Res.*, *98*, 22,109–22,122, 1993.

Zhao, L., Reply, *J. Geophys. Res.*, *100*, 12,463–12,464, 1995.

Zheng, S.-H., and Y. Gao, Azimuthal anisotropy in lithosphere on the Chinese mainland from observations of *SKS* at CDSN, *Acta Seismol. Sin.*, *7*, 177–186, 1994.

Zoback, M. L., First- and second-order patterns of stress in the lithosphere: The World Stress Map Project, *J. Geophys. Res.*, *97*, 11,703–11,728, 1992.

M. S. Savage, Institute of Geophysics, Victoria University of Wellington, Box 600, Wellington, New Zealand. (martha.savage@vuw.ac.nz)